

APPLICATION OF CHEMOSTRATIGRAPHY OF SLACKWATER DEPOSITS TO
ENHANCE PALEOFLOOD RECONSTRUCTION, RIO SALADO, ANTOFAGASTA REGION,
CHILE

A thesis presented to the faculty of the Graduate School of Western Carolina University
in partial fulfillment of the requirements for the degree of Master of Science in Chemistry

By

Danvey C. Walsh

Director: Dr. Jerry R. Miller
Whitmire Professor of Environmental Science
Department of Geosciences & Natural Resources Department

Committee Members: Dr. Cynthia A. Atterholt, Chemistry and Physics
Dr. Mark L. Lord, Geosciences and Natural Resources
Dr. Arthur L. Salido, Chemistry and Physics

March 2016

ACKNOWLEDGEMENTS

I would like to thank my committee members and director for their assistance and encouragement. In particular, I thank Dr. Jerry Miller, whose patience and guidance during this process will always be remembered and appreciated. I also would like to thank Dr. Mark Lord for the many thought-provoking conversations which have been so formative in my scientific understanding. I sincerely thank the many individuals in both the Chemistry and Geoscience departments who offered their time and advice in helping me accomplish my goals. Lastly, I offer my warmest regards and thanks to my parents and family for their continued support

TABLE OF CONTENTS

Table of Figures	v
List of Tables	vii
Abstract	iix
Chapter One: Introduction and Research Objectives	1
Introduction	1
Objectives	7
Chapter Two: Study Area	9
Chapter Three: Materials and Methods	15
Field Methods	15
Topographic Surveys	15
Sedimentological Methods	16
Radiocarbon Dating	16
Determination of Elemental Concentration	17
Sample Preparation and Digestion	17
Sample Analysis	18
Chemostratigraphic Analysis and Unit Correlation	19
Hydraulic Modeling	21
Flood Frequency Analysis	25
Chapter Four: Results	30
Study Area	30
Puente Diablo Reach	31
PD1	31
Depositional environment	31
Stratigraphy	31
Radiocarbon Dating	32
Elemental Analysis	32
PD2	33
Depositional Environment	33
Stratigraphy	34
Radiocarbon Dating	35
Elemental Analysis	35
Correlation of PD1 and PD2	36
Hydraulic Analysis for Reach PD	36
PD Reach Flood Frequency Analysis	38
Rio Salado Reach	38
RS1	38
Depositional Environment	38
Stratigraphy	39
Radiocarbon Dating	39
Elemental Analysis	40
RS2	41
Depositional Environment	41

Stratigraphy	41
Radiocarbon Dating.....	42
Elemental Analysis	42
Correlation of PD reach with RS reach	44
Hydraulic Analysis	44
Correlation of RS1 and RS2	45
RS Reach Flood Frequency Analysis	45
Chapter Five: Discussion	86
Utilization of Chemostratigraphic Methods.....	86
Rio Salado Paleoflood History.....	93
Chapter Six: Conclusion.....	97
Future Work	98
Bibliography	99

TABLE OF FIGURES

Figure 1. Regional location map.....	8
Figure 2. Map of Puente Diablo and Rio Salado reaches.....	10
Figure 3. Narrow bedrock slot canyon with flood debris lodged near the canyon rim....	11
Figure 4. Broad portion of the PD reach with a narrow constriction downstream	12
Figure 5. Pool and riffle type sequence observed in Rio Salado	13
Figure 6. The RS reach has a much more consistent width (~50 m) compared to the PD reach.	14
Figure 7. Outline of the work flow and methods used for the study.....	28
Figure 8. Annual peak discharge at the El Sifon gaging station near Ayquina, Chile.	29
Figure 9. PD1 stratigraphic sections 1-4	49
Figure 10. PD1 Flood deposits.	51
Figure 11. Scatterplot matrix of selected elemental concentrations for PD1.	54
Figure 12. Concentration-depth profile of selected elements for PD1 samples.....	55
Figure 13. PD1 linear discriminant analysis results for PD1 samples.	56
Figure 14. Stratigraphic section at PD2.....	57
Figure 15. Flood deposits at PD2.....	59
Figure 16. PD2 scatterplot matrix.....	61
Figure 17. The concentration depth profile of PD2 deposits.....	62
Figure 18. Similarities of As concentrations for the lower portions of the stratigraphic sections at PD1 and PD2	63
Figure 19. Water surface profile for PD reach.....	64
Figure 20. Flood deposit units and location of radiocarbon dating samples.....	66
Figure 21. RS1 inset stratigraphy.....	67
Figure 22. RS1 scatter plot matrix.....	69
Figure 23. Concentration-depth profile for RS1.....	70
Figure 24. Alcove of RS2. Inset of flood deposits units at RS2.....	71
Figure 25. Flood deposit units at RS2.....	73
Figure 26. RS2 scatterplot matrix.....	75
Figure 27. Concentration depth profile for RS2.....	76
Figure 28. RS2 LDA classification.....	77
Figure 29. RS2 and RS1-FD3 LDA classification.....	78
Figure 30. Mouth of the drainage between the PD reach and RS reach	79
Figure 31. PCA analysis of elemental concentrations for selected elements for each of the individual sites.....	80
Figure 32. Rating curve for the cross section at RS1	81
Figure 33. Water surface profiles for RS reach for varying discharge.....	82
Figure 34. The computed elevation of the water surface profile for a discharge.....	83
Figure 35. Flood frequency analysis results using the gaged record vs paleoflood and gaged record.....	84
Figure 36. Partial cross section of computed water surface elevations for the 50-year recurrence interval (RI) and 100-year RI flood	85

Figure 37. The interception of the radiocarbon age with multiple points along the calibration curve.....96

LIST OF TABLES

Table 1. Description of Flood Deposit (FD) units at PD1.....	50
Table 2. Sample ID, section number, depth, and flood deposit ID for PD1 samples.	52
Table 3. Description of Flood Deposit (FD) units at PD2.....	58
Table 4. PD2 Chemical samples	60
Table 5. Description of Flood Deposit (FD) units at RS1.....	65
Table 6. Radiocarbon age dating	67
Table 7. RS1 sample ID, section, depth, and Flood Deposit unit	68
Table 8. Description of Flood Deposit (FD) units at RS2.....	72
Table 9. Chemical sample ID, section, depth, and flood deposit unit for RS2.	74

LIST OF APPENDICES

<u>Appendix</u>	<u>Page</u>
Appendices	102
Appendix A: ICP-OES readings	102
Appendix B: Radiocarbon dating results	106

ABSTRACT

APPLICATION OF CHEMOSTRATIGRAPHY OF SLACKWATER DEPOSITS TO ENHANCE PALEOFLOOD RECONSTRUCTION, RIO SALADO, ANTOFAGASTA REGION, CHILE

Danvey Walsh M.S.

Western Carolina University (March 2016)

Director: Dr. Jerry R. Miller

This thesis reports a study of novel chemostratigraphic methods applied to flood deposit identification/correlation and subsequent paleoflood hydrology and flood frequency analysis in the Rio Salado, Chile. Flood deposit identification at 4 stratigraphic sections and inter-reach correlations are made on the basis of stratigraphic analysis, radiocarbon dating, concentration-depth profile evaluation of trace elements, and discriminant function analysis of trace elements. Concentrations of trace metals were determined by Inductively Coupled Plasma Optical Emission Spectrometry (ICP-OES). Inherent uncertainty and limitations of radiocarbon dating make unit correlation difficult by this method alone. Chemostratigraphic methods including a multivariate statistical approach show promise for improving the delineation and correlation of slackwater flood deposits in the Rio Salado. Flood deposit correlation by these methods is used to determine the discharge that produced a geologically defined water surface profile employing step-backwater methods. Paleoflood analysis is used to extend the time scale of a short systematically measured gaging record (25 years) in order to better characterize flood magnitude-frequency relationships. Analysis is performed on a well preserved record of

10 floods with discharges ranging from 240 to 515 m³s⁻¹. The oldest of these floods dates to the early 1600's AD. Using only gaging data, the 100 year flood event has a discharge of 856 m³s⁻¹. The gaging data plus paleoflood data indicates the discharge of the 100 year flood event is 429 m³s⁻¹, a reduction of about 50 %. The recurrence interval of the 2001 flood changes from ~40 years based on gaging data only to ~100 years using the gaging data plus the paleoflood data. A comparison to studies for the well documented and widely destructive 2001 Atacama flood indicates floods of this magnitude have a shorter recurrence interval than previously suggested.

CHAPTER ONE: INTRODUCTION AND RESEARCH OBJECTIVES

Introduction

Between latitudes 30°S and 20°S, the hyperarid Atacama Desert stretches from the west flank of the Andes Mountains to the Pacific coast of South America. With an annual average precipitation of ~20 to 50 mm per year, the Atacama is widely recognized as one of the driest places on Earth and likely has been for much of past 10-15 million years (Houston and Hartley, 2003). The hyper-aridity of the Atacama is driven by several factors (Houston, 2006): (1) it is located within the subtropical high-pressure belt where stable air associated with Hadley circulation reduces convection and therefore precipitation, (2) the cold Peruvian Current upwells along the Pacific coast and limits the moisture capacity of westward blowing onshore winds while producing an inversion layer that persistently traps Pacific moisture along the coast at an elevation below ~800 m; and (3) the high Andes inhibit the advection of moisture from the east, creating a rain shadow.

The extreme climatic conditions in this geographic setting are currently exacerbated by the occurrence of El Niños and La Niñas (i.e., the El Niño South Oscillation). Significant flooding across the Atacama is linked to the magnitude of the El Niño-Southern Oscillation (Magilligan et al., 2008). During the El Niño phase, the strength of the Bolivian high decreases and shifts southward, weakening easterly winds that transport moisture onto the Altiplano. Thus, the western cordillera and the western flank of the Andes are characterized by relatively dry conditions during El Niño events. However, rainfall from Pacific frontal storms may penetrate inland, producing flooding within both higher elevation axial drainages (Magilligan et al., 2008), and low- to

moderate-elevation ephemeral tributaries. In contrast, large rainfall events occur during La Nina episodes over the Altiplano and the western flank of the Andes, causes large scale flooding along westward draining, axial channels. Lower elevation channel systems are not affected by these precipitation events. Given these spatial differences in rainfall distribution, Magilligan et al. (2008) argued that paleoflood records for the past 20k years within the main stream and tributary sections of the Rio Moquegua, located along the northern fringes of the Atacama, differed because the tributaries recorded only El Niño events whereas the axial channels recorded both El Nino and La Nina events. Temporally, the stratigraphic records showed that there was an increase in the frequency and magnitude of large floods between 700 and 1610 AD as compared to 160 BCE to 700 AD. These ‘mega-niños’ significantly impacted channels within the Rio Moquegua basin, while floods associated with more recent El Niños did not (Magilligan et al., 2008). The point is that differences in the response and recovery of the channels may not only reflect differences in the drivers of flooding within the basin, but larger-scale temporal variations in the magnitude and frequency of the events.

Despite its extreme aridity, the Atacama is traversed by the Rio Loa, a perennial river whose sources are located at high elevations (>4000m) on the west slopes of the Andes. One of two major tributaries to the Rio Loa is the Rio Salado, which is formed from several branches emerging from the El Tatio geyser basin and discharge from springs that form at the base of the Quaternary volcanic rocks. The Rio Salado joins the Rio Loa near the village of Chiu Chiu, Chile (Figure 1).

Waters of the Rio Loa are an important source of domestic water for the city of Calama (population: ~138,000 as of 2002), agriculture, and the mining industry. Nearby

Chuquicamata is one of the world's largest copper mines and produces an estimated 366,000 metric tons of fine copper per year. Concentrations of trace metals and metalloids are high in the Rio Loa, with arsenic (As) concentrations exceeding the World Health Organization (WHO) guidelines for drinking water by 1,000 to 10,000 percent (WHO, 2011; Wilson, 2011). These elevated concentrations are thought to be due to the influence of mining and smelting debris to the river as well as natural sources. The introduction of As, antimony (Sb), mercury (Hg), cadmium (Cd), and other metals/metalloids from El Tatio are particularly important as the concentrations of metals from the geyser basin are elevated in comparison to average crustal concentrations. Previous work also indicates that concentrations of Cd, lead (Pb), copper (Cu), and zinc (Zn) are elevated in channel bed sediments and suggests these concentrations are likely several times higher in floodplain and terrace deposits.

Regional geology, which is dominated by volcanic rocks enriched in sulfide minerals, contributes to high background concentrations of metals in water and sediments. This has made it difficult to quantify how much of the contamination in the Rio Loa is attributable to historic discharge of mining effluent and runoff from impoundments during high magnitude flooding events. For other basins in arid regions, sediment transport and redeposition appears to be dominated by extreme events (Baker, 1977). Extreme temperature and rainfall regimes of arid environments may also exacerbate the movement of high concentration metal-contaminated sediments (Taylor and Hudson-Edwards, 2008).

Flood flows through the Rio Loa and Rio Salado drainage network is dominated by surface runoff which produces high magnitude floods that inundate large areas of the

valley floor including much of Calama. Enormous quantities of sediment are transported from headwater areas and redeposited downstream during these events. A flood in 2001 reached a calculated peak discharge of $310 \text{ m}^3 \text{ s}^{-1}$ at the Ayquina gaging station and was estimated by Houston et al. (2006) to have a recurrence interval (R.I.) of 100-200 years. The 2001 flood resulted in the deposition of up to 1 m of fine-grained sediment over areas exceeding hundreds of square kilometers in the basin (Houston, 2006). Smaller, more frequent events, such as those that occurred in 1977, 1997, and 1999 (R.I. > a few decades), have also been shown to inundate large areas and transport large quantities of sediment. However, not all floods are produced by rainfall in the Andes. Flooding may occur in response to north-easterly moving frontal storms sourced in the Pacific, which contribute about 30 to 40 percent of the rainfall below 2300 m (Houston, 2006; Rech et al., 2006). Thus, flooding at lower elevations in the basin may be disconnected from runoff at higher elevations. Deposits within the drainage system which persist through time are a kind of geochemical archive of flood events in the region.

Data on flood frequency and magnitude are generally derived from regular measurements at gaging stations. The time period over which these measurements have been made is often much less than 100 years and is not of a sufficient length to accurately estimate the recurrence intervals of very large floods (Greenbaum et al., 2014). Paleoflood analysis can extend the flood record to more accurately estimate the frequency and magnitude of sediment transporting and geomorphically important events.

During fieldwork conducted during November 2009, Miller et al. (unpublished data) observed the presence of slackwater deposits in the Rio Loa. Slackwater deposits are typically suspended fine grained sand- and silt-sized sediments that accumulate during major floods in protected areas where stream flow is diminished, such as channel expansions, high alcoves in bedrock gorges, and downstream of bedrock spurs (Baker et. al., 1983). Due to the likelihood slackwater deposits will not be eroded during large flood events, they are often the best paleostage indicators. Layered sequences of slackwater deposits represent a record of individual floods which numerous studies have shown can be analyzed to determine both the magnitude, and if datable, the frequency of paleoflood events (Kochel et al., 1982; Baker, 2008; Greenbaum et al., 2014).

By assuming the elevation of the slackwater deposits represent the high water mark during flooding, they can be used to begin to approximate discharge during high magnitude flood events using hydraulic modeling. Information on the age and magnitude of extreme flood events is then incorporated in flood frequency analysis. This approach is particularly useful in estimating flood frequency curves beyond the range of 100-500 years (Fenske, 2003).

Stratigraphic correlation of flood units at different locations along the river is important in determining the accuracy and elevation of the water surface profile for step-backwater hydraulic modeling. Age dating of deposits has been the most widely used method of stratigraphic correlation in paleoflood analysis studies. However, both radiocarbon dating and Optically Stimulated Luminescence (OSL) dating have inherent sources of error which limit their effectiveness in dating recently deposited sediments

(within the past 200 – 300 years) and deposits which are temporally close to each other but have been deposited by different floods. A potential, but untested, method of improving flood deposit correlation is the use of chemostratigraphy.

Chemostratigraphy makes use of subtle variations in elemental compositions of sediments to characterize and correlate sediment. A chemostratigraphic study aims to identify packages of strata which have unique chemical signatures. These packages can then be identified in a stratigraphic sequence by the relative changes in chemical composition throughout the section (Ratcliffe et al., 2014). Although this technique has been widely used to define stratigraphic correlations in marine and lacustrine sediments and lithified rock, much less work has been done which relates chemical stratigraphy to physical correlations in fluvial systems. However, a few publications do exist which demonstrate the potential of applying chemostratigraphic analysis to recent alluvial sediments (Chillrud et al., 2003; Jones et al., 2012)

Preliminary geochemical data from the nearby Rio Loa are characterized by large variations in elemental concentrations between lithostratified units and similar geochemical signatures of sediments for a single flood event indicating that chemostratigraphic analysis is likely an effective correlation tool for fluvial sediments within the Rio Salado (Wilson, 2011). Another condition which favors the use of chemostratigraphic analysis is that few tributaries join the Rio Salado which would potentially alter the streamwise geochemical signal of discrete fluvial sediment packages.

Objectives

The primary objective of this study is to quantify the magnitude and frequency of large flood events which have occurred within the Rio Salado Basin using slackwater deposits. Inherent in the objective is an analysis of whether chemostratigraphic methods can be used to enhance the correlation of individual paleoflood units between sites. The analysis rests on the hypothesis that if sediments are moving primarily during large flood events, a unique geochemical signature for each flood deposit will allow for accurate reconstruction of paleoflood hydrology and assist in assessing the mobilization potential of sediments during future large magnitude floods.

Specific tasks conducted during this investigation were to determine the timing (age), chemical composition (trace metals/metalloids), and spatial distribution of slackwater flood deposits, and to use the data to reconstruct a record of the magnitude and frequency paleofloods within the basin.

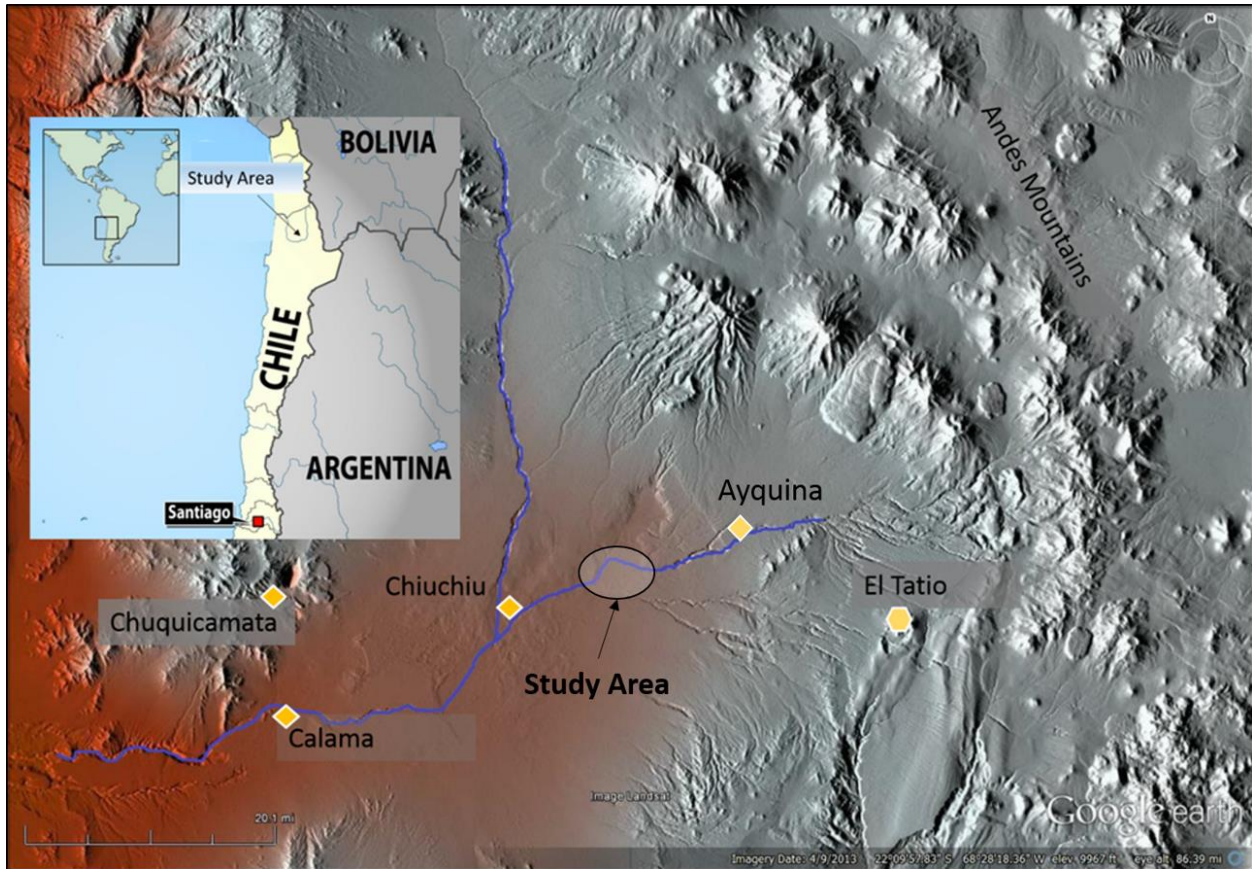


Figure 1. Regional location map with the Rio Salado and Rio Loa represented by the blue line. The study area is the shaded oval.

CHAPTER TWO: STUDY AREA

A large portion of the Rio Salado basin is covered by late Tertiary and early Quaternary ignimbrites, underlain by Paleozoic marine sediments and Mesozoic breccias. Many conspicuous, parallel canyons form in these ignimbrites above 3100 m. The region is tectonically active and several NW–SE normal faults control aspects of local hydrology (Latorre et al., 2006).

Two reaches of the Rio Salado between Chiu Chiu and El Tatio are the focus of this study (Figure 2). The westernmost study reach is approximately 1.4 km in length and is in the vicinity of a feature referred to as Puente del Diablo. At Puente del Diablo a small, stone bridge crosses the Rio Salado at a point where the confining canyon is only 1 to 2 m wide. A large portion of this reach is best described as a bedrock slot canyon which in some sections is ~1 m wide and incised ~7 m below the valley floor (Figure 3). A smaller portion of the Puente Diablo (PD) reach is composed of wider depositional sub-reaches which, at the deepest point, are similar in depth to the slot canyons, but may be up to ~50 m in width (Figure 4). A pool and riffle sequence within the channel contains pools which were measured to be up to 7.5 m deep. (Figure 5).

The Rio Salado (RS) reach is the easternmost study reach, and is located 6.5 km downstream of Puente Diablo, and is 0.31 km in length (Figure 2). From top of canyon rim to top of canyon rim, RS has an average width of 50 m (Figure 6). The average depth from the top of the canyon rim to the water surface is 18 m in RS. Two sets of slackwater deposits are located within the RS reach; one positioned at the far upstream end of the reach and one at the far downstream.

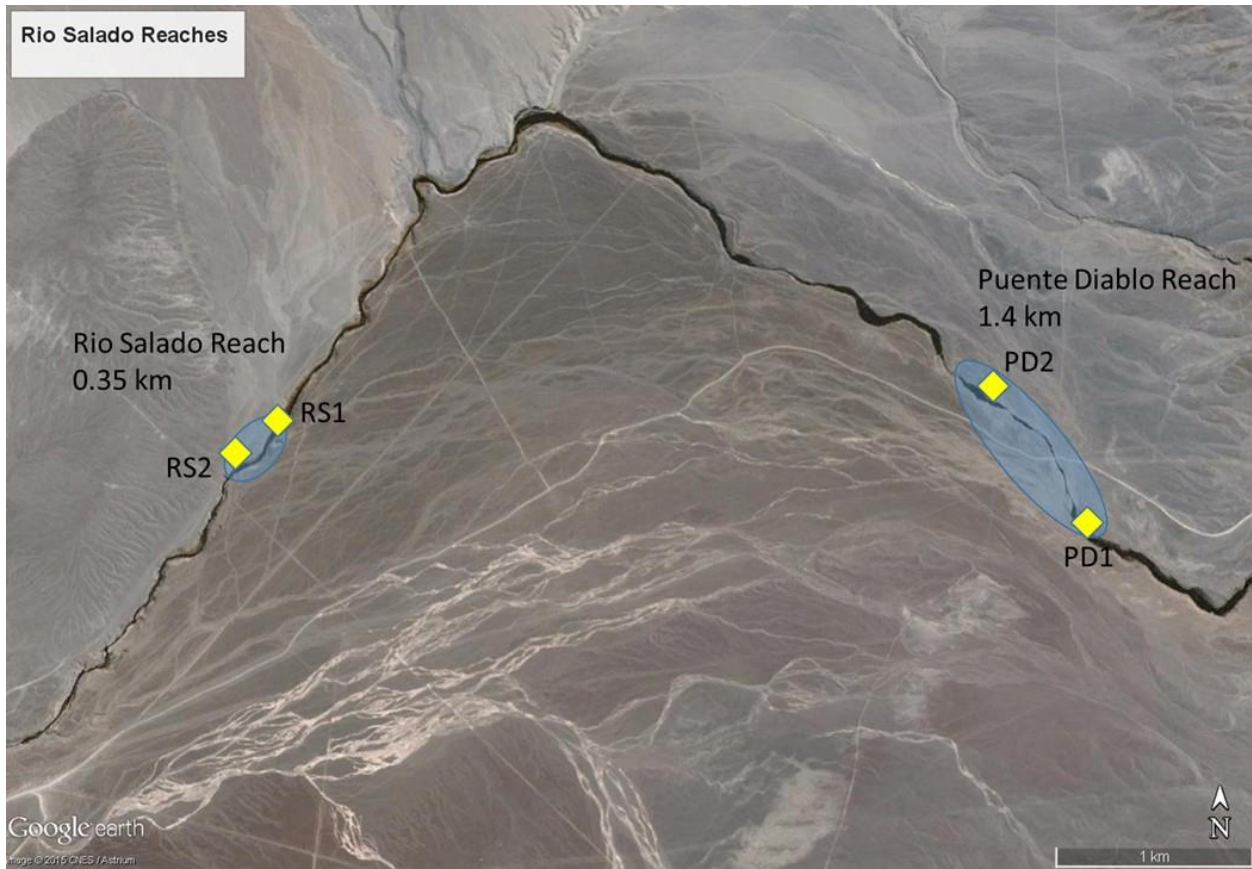


Figure 2. Map of Puente Diablo and Rio Salado reaches (light blue ovals). Sites with slackwater deposits, labeled PD1, PD2, RS1, and RS2, are represented by yellow diamonds. Note overbank channels eroded in desert pavement that originate upstream of the narrow bedrock canyon immediately downstream of PD1 indicating that flow has exceeded the capacity of the channel in the past.

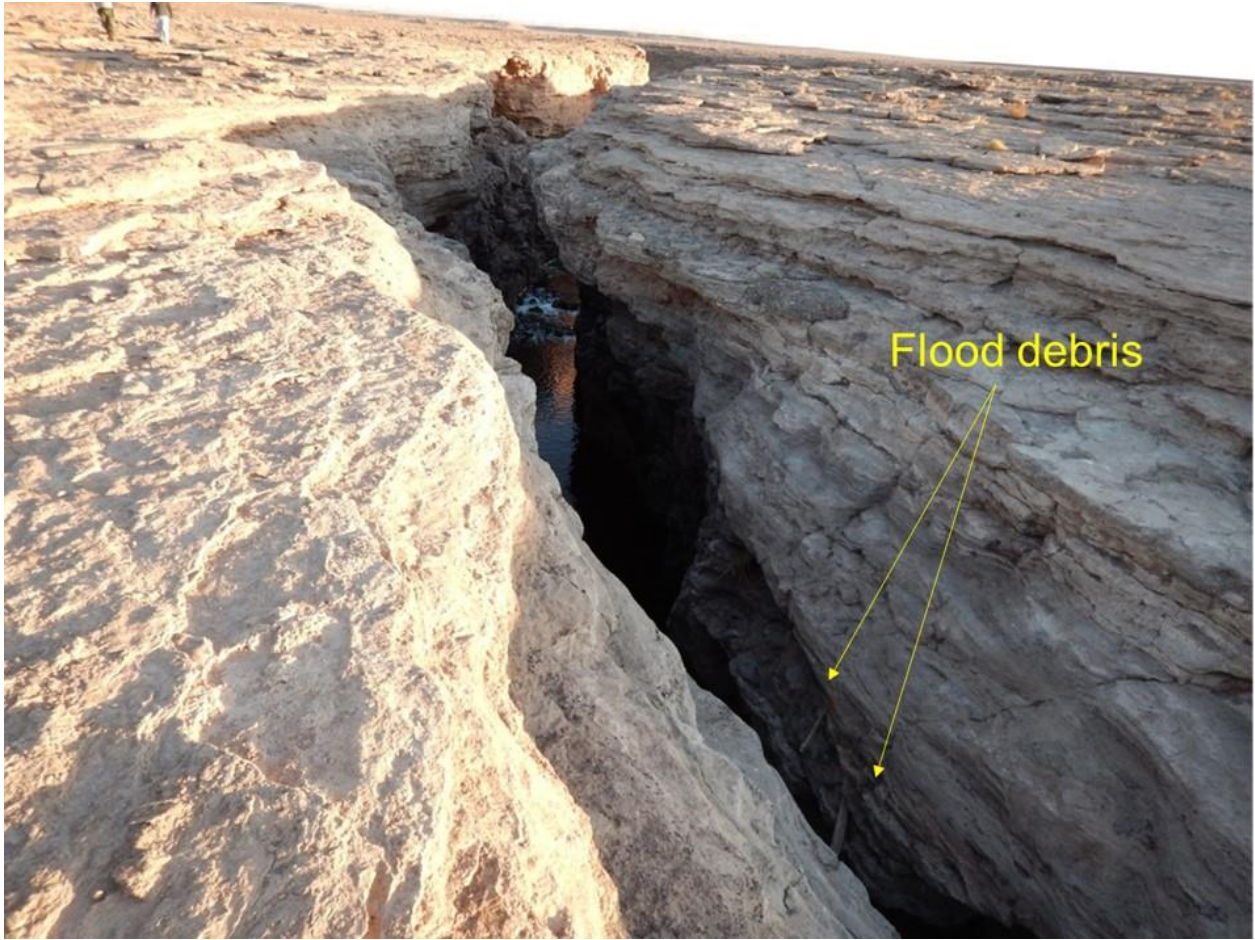


Figure 3. Narrow bedrock slot canyon with flood debris lodged near the canyon rim. This flood debris is believed to be from the 2001 flood event.



Figure 4. Broad portion of the PD reach with a narrow constriction downstream which becomes the narrow slot canyon seen in Figure 3 further downstream.



Figure 5. Pool and riffle type sequence observed in Rio Salado. Some of the pools measured ~7.5 m deep.



Figure 6. The RS reach has a much more consistent width (~50 m) compared to the PD reach. An alcove type feature can be observed to the middle-right of the photograph.

CHAPTER THREE: MATERIALS AND METHODS

Field Methods

A multistep procedure for data collection and analysis was necessary for this study. Methods can be broadly categorized into field methods, laboratory methods, and modeling methods followed by a synthesis of results. An outline of the workflow and methods used are present in Figure 7.

Topographic Surveys

The latitude, longitude, and vertical elevation of the top of slackwater deposits were surveyed using a total station with a laser rangefinder. In order to characterize channel dimensions and shape, a total of 18 cross sections were generated, 12 for the Puente Diablo reach and 6 for the RS reach. Channel cross sections were surveyed at intervals which reflect the complexity of the channel geometry. Cross section measurements were made using two methods depending on the accessibility into the canyon. In accessible areas, the total station was setup and geolocated using a GPS accurate to ± 3 m. All coordinates were recorded using the WGS 84 datum and the UTM coordinate system. High resolution aerial imagery was also used to improve the accuracy of georeferencing the cross section end points. In areas where the canyon was not accessible, channel width and distance to the bottom of the canyon were determined using a laser range finder. Additionally, the distance from the water surface to the bottom of the channel was measured using a weighted tape measure in these inaccessible areas. The end points of these cross sections were geolocated by the same method detailed earlier. This approach is assumed to provide reasonable cross

sectional data given the relatively simple rectangular geometry of the slot canyons in which these cross sections are located.

Sedimentological Methods

Between October 11 and October 14, 2014, a total of 106 sediment samples were collected from the most stratigraphically complete deposits within the study site. For each site pits up to 175cm deep were dug in the flood deposits down to or near the bedrock or the colluvium surface. The pits were dug close to each other with some vertical overlap that enabled a staircase exposure of the entire stratigraphic section. Deposits exposed in each pit were separated into sedimentary units associated with flood events using sedimentological criteria such as grain size and size distribution, color, and erosional surfaces (Kochel and Baker, 1988).

Sediment samples were collected from each flood for geochemical analysis using a plastic trowel. All samples were placed in polyethylene bottles and shipped to Western Carolina University for analysis. Organic matter consisting of partially decomposed plant material also was collected from 8 units at RS1 and RS2.

Radiocarbon Dating

The organic matter sampled for radiocarbon age dating occurred within discontinuous units of fine grained laminae which made it difficult to collect. Radiocarbon dating is the standard absolute dating tool employed in paleohydrologic work (National Research Council, 1988). A conventional radiocarbon date is derived from laboratory determination of the remaining present day ^{14}C activity in an appropriate type of organic material (Faure, 1986). This activity is then compared to an atmospheric ^{14}C level that is assumed to have been constant in the past. Analysis was performed by

accelerator mass spectrometry (AMS). The samples were analyzed at the Beta Analytic radiocarbon dating laboratory in Miami, FL.

Determination of Elemental Concentration

Sample Preparation and Digestion

Sample preparation and digestion were performed according to a standard method adapted from the University of Wisconsin, Madison Soil and Plant Analysis Laboratory's standard operating procedure for the analysis of major, minor, and trace elements in soil and sediment samples by inductively coupled plasma optical emission spectrometry (ICP-OES). Results using this method are the concentrations of leachable components and are not directly comparable to X-ray fluorescence (XRF) concentrations or neutron activation analysis (NAA) concentrations which are true total concentrations.

Because a wide range of elements were analyzed simultaneously, there is an inherently wide range of associated concentrations. To achieve sufficiently high concentrations of those elements which are of the most value in geochemical fingerprinting (minor and trace elements), samples were sieved using a plastic screen mesh which was cleaned between samples. Every sediment sample was sieved to remove particles larger than the clay size fraction ($<0.63 \mu\text{m}$). Trace metals are most likely to be attached to particles in the clay size range (Liebens, 2001; Miller et al., 1998; Taylor and Hudson-Edwards, 2008). The remaining sample was dried for 24 hours at 100°C , weighed into splits of $0.5 \pm 0.01 \text{ g}$ and then placed into nitric acid washed glass Erlenmeyer flasks. Samples were subsequently spiked with 0.04 mL of yttrium as an internal reference standard. To prevent the calcareous samples from foaming over on

the addition of concentrated nitric acid, a few drops of 20-30% nitric acid were used to first moisten the samples. After the samples were moistened with the diluted nitric acid, 5ml of concentrated (~68%) trace metal grade nitric acid was added for digestion. Sample containers were then covered with parafilm and placed on a hot plate at a temperature of 130 °C for 14 to 16 hours. Afterwards, samples were allowed to cool and 1 ml of 30% hydrogen peroxide was added to each sample for the removal of organics. Samples were brought to volume with ultra-pure deionized water (18.2 MΩ) to achieve a 200 fold dilution.

Sample Analysis

After digestion, sediment samples were analyzed for major elements (e.g., Al, Ca, Fe, Mg, Mn, Si) and trace metals and metalloids (e.g., As, Cd, Co, Cr, Cu, Ni, Pb, Sr, Zn) using Inductively Coupled Plasma Optical Emission Spectroscopy (ICP-OES), specifically the Perkin Elmer Optima 4100DV ICP-OES on the campus of Western Carolina University.

When possible, the wavelength selection for each element followed the United States Environmental Protection Agency (EPA) Method 200.7 recommendations. Calibration was performed using a set of working standards made from a primary standard with National Institute of Standards and Technology (NIST) traceability. Reagent blanks and analyte concentrations for the working standards were plotted against blank-subtracted integrated peak areas. A regression line was fitted to the calibration points and the equation of the line was used to quantify unknown sample concentrations. Each calibration curve was linear in nature. Deviation of standards from the regression line was used to estimate analytical accuracy. A method detection limit

(MDL) was established from repeated blank concentrations analyzed over the course of several runs. Use of an internal reference standard (yttrium) provided a check against instrument drift.

Chemostratigraphic Analysis and Unit Correlation

In addition to using radiocarbon dating of slackwater sediments as a correlation tool, chemostratigraphic methods were also employed for this purpose. Elements which were consistently below detection limits were removed from the dataset. Further reduction of the number of elements used in chemostratigraphic analyses were made by identifying those elements that were most likely to be associated with the clay size fraction of the slackwater sediments and that were therefore most valuable in correlation (Miller et al., 2015). The final group of elements used in the analyses consisted of As, Cd, Co, Cr, Cu, Ni, Pb, Sr, and Zn.

Concentration with depth profiles were plotted for stratigraphic sections at sites PD1, PD2, RS1, and RS2. This type of plot is useful for identifying and correlating flood deposits which may be geochemically unique due to a difference in upland source or other distinguishing factors. Differentiation between eolian and fluvial deposits is also made easier by concentration-depth profile plots. Bivariate scatterplots of pairwise elemental concentrations were made to determine correlation and collinearity between variables. This is a valuable geochemical technique for establishing relationships between elements. A 9 x 9 cell scatterplot matrix of measured elements for selected slackwater deposits was created in order to rapidly explore and assess these relationships.

Concentrations of the elements selected for analyses vary by over an order of magnitude. For example, cadmium concentrations in a given sample may be in the range of 5 to 25 ppm while Zn concentrations for the same sample are in the range of 250 to 500 ppm. Multivariate analysis methods are sensitive to such issues of scale. To address this sensitivity, scaling and centering of the data are required. For this study, centering of the dataset matrix was achieved by subtracting the column means of the matrix from their corresponding columns. Scaling is performed by dividing the centered columns of the matrix by their standard deviations.

Linear discriminant analysis (LDA) is commonly used in the discrimination and classification of multivariate geochemical data (Drew et al., 2010; Racey et al., 1995; Ramkumar et al., 2010). LDA is often referred to as a “supervised” machine learning technique which uses a priori knowledge of group labels to minimize within group variance and maximize separation between different groups (Kachigan, 1991). For this study, the groups are slackwater flood deposits. Like other multivariate statistical methods, such as principal component analysis (PCA), LDA seeks to reduce dimensionality while preserving the combination of variables which best explain the data (Martinez and Kak, 2001).

Selection of the elements used in the LDA was made by primarily on the minimization of the Wilks’ Lambda value. Wilk’s Lambda is a measure of the discriminatory power of factors. Furthermore, some non-conservative tracer elements (Al, Fe, Mg) were removed (Mukundan et al., 2010). It is recognized that As, Cd, and Pb may have a high mobility potential under both aerobic and flooding conditions. However, the overall discriminatory of the model was improved by including these elements.

Due to the lack of samples within the slackwater flood deposits selected for LDA, assumptions of normality required for proper application are impossible to meet. However, normality tests (Shapiro-Wilks) performed on deposits with a sufficient number of samples indicate elemental concentrations are normally distributed. The best method for correlation using LDA would be to predict the group unlabeled samples fall into. Again, the lack of samples for the slackwater deposits of interest make this impossible. Therefore, correlation was performed by assigning slackwater deposits from a different section into the group label by radiocarbon dating and determining how well those samples group. It is important to recognize that these limitations relegate the results of LDA to being exploratory in nature and supplemental to the stratigraphic correlations determined by radiocarbon dating.

Hydraulic Modeling

Inverse hydraulic modeling methods using paleostage indicators have been shown to be an effective way of estimating discharge in arid environments (Baker, 2008). The most commonly used method of estimating paleoflood discharge from paleostage indicators is the step-backwater method (O'Connor and Webb, 1988; Webb and Jarrett, 2002). Step-backwater estimations of discharge are based on the continuity equation, which in the special case of one dimensional, steady, incompressible flow assumes the form (where subscripts represent successive cross sections along the flow path)

$$Q = V_1A_1 = V_2A_2$$

Where

Q = Discharge
V = Velocity
A = Cross Sectional Area

and the conservation of energy equation (Bernoulli's equation).

$$h_1 + \alpha_1 \frac{V_1^2}{2g} = h_2 + \alpha_2 \frac{V_2^2}{2g} + h_L$$

Where

- h₁ = upstream stage
- h₂ = downstream stage
- α = velocity distribution coefficient
- V = mean velocity
- h_L = head losses due to minor loss and friction at the free water surface and along the channel boundaries

Head losses due to friction are generally accounted for by application of Manning's equation.

$$V = \frac{a}{n} \times R^{2/3} \times S^{1/2}$$

Where:

- V = velocity
- n = Manning's roughness coefficient
- R = hydraulic radius (Area/Wetted Perimeter)
- S = channel slope
- a = a constant which is 1 for metric units and 1.49 for English units

Because the calculations required for this method are cumbersome, the 1 dimensional step-backwater analysis performed in this study were carried out using computational modeling software, specifically the United States Army Corps of Engineers' Hydrologic Engineering River Analysis System (HEC-RAS).

Several (at least three) channel cross sections are required for step-backwater analysis, and the channel should ideally be uniform in geometry between adjacent cross sections. All cross section data collected in the field were entered into HEC-RAS and additional cross sections were interpolated at a maximum interval of 0.026 km. The quality of the interpolated cross sections was enhanced by using a combination of detailed field notes and georeferencing to high resolution aerial imagery.

Of several methods available for use in step-backwater analysis, the standard step method is most commonly used for estimation of water surface profiles in natural channels (Webb and Jarrett, 2002). The standard step method is an iterative method in which channel roughness and geometry are obtained and a value of Q is chosen. The water surface elevation is then computed for the nearest cross section by application of Bernoulli's equation. This process is continued between adjacent cross section pairs until a water surface elevation is determined for the entire reach.

Hydraulic model calibration is typically performed by using the elevations of observed water surfaces and known discharges during flood events of moderate to large magnitude. In the case of this study, however, the lack of these data necessitates model calibration to be performed by an alternative method. In a study of the February 2001 Atacama flood, Houston estimated a peak instantaneous flow of $310 \text{ m}^3 \text{ s}^{-1}$ at the El Sifon automated gaging station near Ayquina (Houston, 2006). Due to the gaging station being destroyed during the event, Houston interpolated this discharge value "based on catchment daily rainfall and calibration against the maximum instantaneous flow (a) recorded prior to destruction and (b) calculated from surveys of maximum flood levels and analyzed using the slope-area method". For the purpose of model calibration, it is assumed this discharge value of $310 \text{ m}^3 \text{ s}^{-1}$ is correct for the El Sifon gaging station during the February 2001 flood event (Figure 8).

During the time of surveying, a ~3 m long chunk of sediment with plant flood debris on top was found wedged ~2 m from the top of the canyon rim at cross section 12. It is assumed that for this cross section, the top of this sediment represents the minimum water surface elevation at the peak discharge during the February 2001 flood

and serves as the known water surface elevation for a known discharge. It is possible this sediment is from an older event, but the state of decomposition of the plant debris on top suggests it is from a relatively recent flood. A lack of large magnitude events occurring after the February 2001 flood suggests it is unlikely this sediment and flood debris is the result of a flood occurring after the 2001 event.

Because the study reach is located ~16 km downstream of the El Sifon gaging station, it has a larger drainage area. An adjustment was made to the peak discharge at the calibration cross section based on a standard methodology (Cudworth Jr., 1989) in which it is assumed the ratio of Q_1/Q_2 at the two locations is equal to the square root of their respective drainage areas $A_1^{0.5}/A_2^{0.5}$. The difference between the two drainage areas is 830 km², an increase of 48 percent. As a result of applying this adjustment, a discharge value of 443 m³ s⁻¹ at the study site was used for model calibration.

Abrupt constrictions and expansions in channel geometry occur regularly along the Rio Salado. Rapid changes in the channel bed gradient are the result of a riffle-pool sequence which results in water depth varying from a few centimeters to nearly 10 meters over a longitudinal distance of 10 to 20 m. Due to these channel characteristics, it was anticipated that flood flow in the narrow bedrock canyon would be mostly subcritical with a few locations of supercritical flow (Tinkler and Wohl, 1998). Thus, the mixed-flow mode of HEC-RAS was selected for all model runs. Additionally, the default expansion and contraction values of 0.1 and 0.3 were used for all model runs.

Of particular importance in Manning's equation is the selection of the roughness coefficient, Manning's n . Discharge estimations may be affected by selecting an inaccurate Manning's n value. However, studies of uncertainty in flood estimates

associated with roughness coefficient demonstrate low sensitivity to a range of Manning's n values when calculating very large discharges in narrow, deep bedrock canyons (Wohl, 1998). An initial Manning's n may be estimated from literature and correlation to photographs of existing channels where the value has been established (Chow, 1959). Due to the uncertainty associated with estimating Manning's n , it is a parameter which is commonly varied during model calibration. For this study, a Manning's n values of 0.035 for banks and 0.05 for the channel provided a best fit between the known and calculated elevation of the water surface for a discharge of $310 \text{ m}^3 \text{ s}^{-1}$. Studies in similar settings have reported best fit Manning's n values of 0.035 to 0.045 (Greenbaum et al., 2014; Webb et al., 1988).

Flood Frequency Analysis

Flood frequency analysis is performed to predict floods for sites along a river. By using peak annual flow discharge data, it is possible to calculate statistical information such as mean values and recurrence intervals (Dalrymple, 1960). Flood frequency distributions are constructed from this statistical information. Flood frequency distributions express the likelihood of various discharges as a function of exceedance probability or recurrence interval. Although there are a variety of flood frequency distributions, the United States Interagency Advisory Committee on Water Data (1982) recommends the Log-Pearson Type III distribution (U.S. Water Resources Council, 1982). The Log-Pearson Type III distribution is calculated using the general equation:

$$\log x = \overline{\log x} + K\sigma_{\log x}$$

where x is the flood discharge value of some specified probability, $\overline{\log x}$ is the average of the discharge values, K is a frequency factor, and σ is the standard

deviation of the log x values. The frequency factor K is a function of the skewness coefficient and return period and can be found using a frequency factor table. The flood magnitudes for the various return periods are found by solving the general equation. The mean, variance, and standard deviation of the data can be calculated using the two formulas below.

$$\overline{\log x} = \frac{\sum (\log x_i)}{n}$$

$$\frac{\sum_i^n (\log Q - \text{avg}(\log Q))^2}{n-1}$$

where n is the number of entries, and

$$\sigma_{\log x} = \sqrt{\frac{\sum (\log x - \overline{\log x})^2}{n-1}}$$

The station skewness coefficient C_s can be calculated by the following formula:

$$C_s = \frac{n \sum (\log x - \overline{\log x})^3}{(n-1)(n-2)(\sigma_{\log x})^3}$$

Due to variability of the site skewness coefficient, a weighted average of the station skewness coefficient and a generalized skewness coefficient based on regional data are often used (National Research Council, 1999). This technique is commonly applied in the United States but was not employed here because the needed regional data were unavailable.

The gaged annual peak discharge values from the Chilean General Water Directorate (DGA) from the El Sifon gage near Ayquina and the discharge adjustment method described previously were used to calculate the annual peak flows at the study

site. The gaged record includes 24 years of data extending from 1991 to 2015, excluding the 2001 flood when the gage was destroyed during the largest flood (Figure 2). For 2001, the peak instantaneous discharge value calculated by Houston (2001) and adjusted for increased drainage area was used ($443 \text{ m}^3 \text{ s}^{-1}$). Flow measurement quality is assumed to be good or fair; thus, an uncertainty of $\pm 15\%$ was assigned to the gaging station data. Due to the nature of the calculation of the discharge for the 2001 flood event, an uncertainty of $\pm 25\%$ was assigned to this discharge value.

It is important to note the water surface elevation determined from slackwater deposits is usually lower than the actual stage of the flood during peak discharge (Baker, 1987; Kochel and Baker, 1982). Discharge calculated by hydraulic modeling using slackwater deposits is likely underestimated as a result. Paleoflood discharge estimates were assigned an uncertainty of $+50\%$ because it is possible the discharge is significantly larger than what is suggested by the slackwater water deposit but it is impossible for the discharge to be smaller.

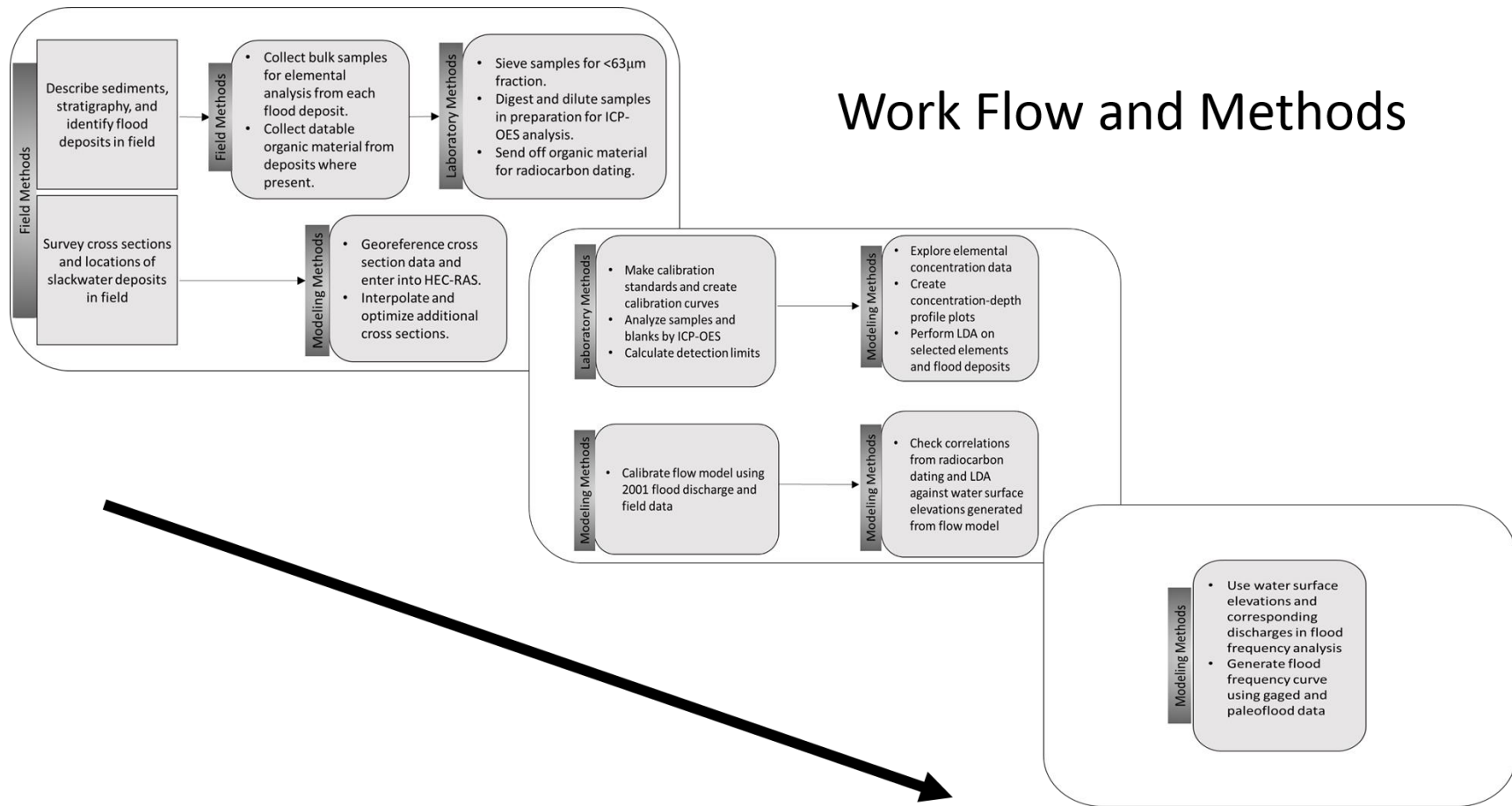


Figure 7. Outline of the work flow and methods used for the study.

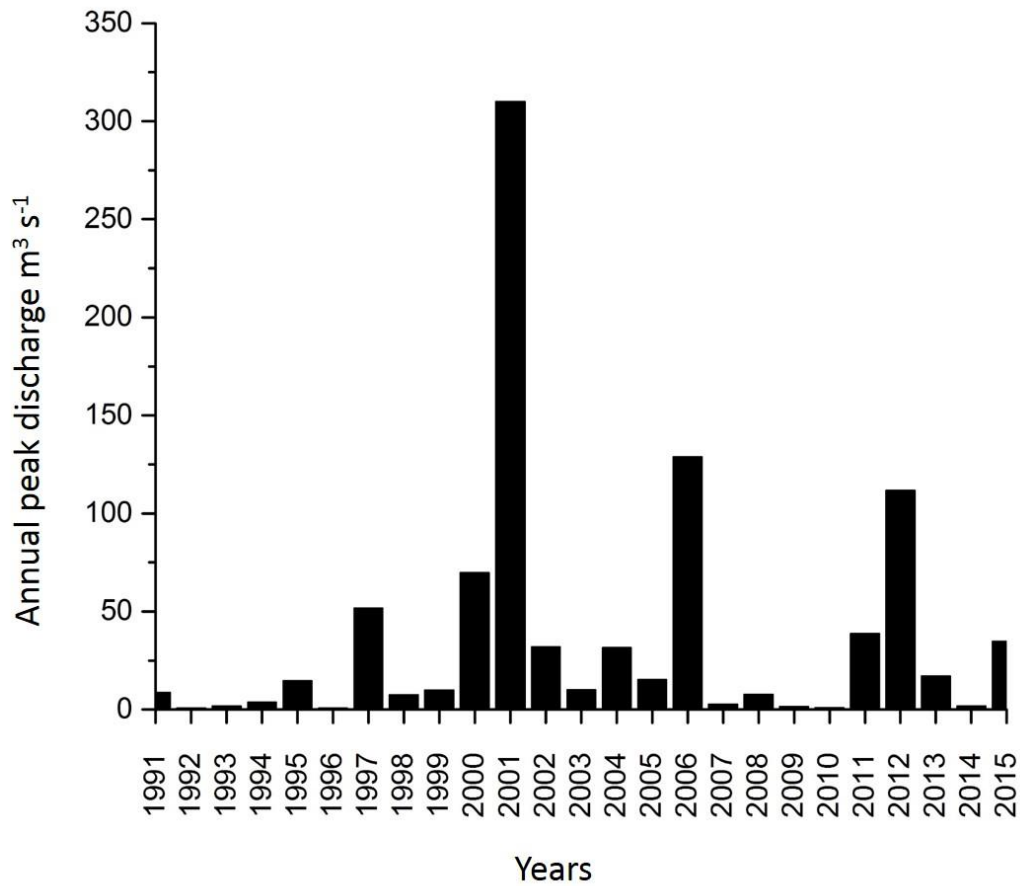


Figure 8. Annual peak discharge at the El Sifon gaging station near Ayquina, Chile. The Chilean government operated gaging station began operating in 1991. The peak discharge value of $310 \text{ m}^3 \text{ s}^{-1}$ for the 2001 flood is taken from Houston's estimate (Houston, 2006). This is necessary because the gaging station was destroyed before the actual peak discharge of the event occurred.

CHAPTER FOUR: RESULTS

Study Area

Two sets of slackwater deposits were examined within the PD reach (Fig. 2). A set of slackwater deposits labeled PD1 is located at 19 K 553828 m E, 7533365 m N, in the upstream portion of the reach. A second set labeled PD2 is located at 19 K 553231 m E, 7533070 m N in the downstream portion of the PD reach.

The Rio Salado (RS) reach, the easternmost study reach, is located 6.5km downstream of Puente Diablo and is 0.34 km in length (Fig. 2). From top of canyon rim to top of canyon rim, RS has an average width of 50 m. The average depth from the top of the canyon rim to the water surface is 18 m in RS.

Two sets of slackwater deposits also are located within the RS reach. The set of slackwater deposits in the upstream portion of the reach is labeled RS1 and is located at 19 K 549394 m E, 7532763.204 m N. The second set of slackwater deposits in the downstream portion of the RS reach is located at 19 K 5549139 m E, 7532618 m N and is labeled RS2. Both sets of slackwater deposits in the RS reach are located in alcoves cut in the bedrock at the mouth of gullies adjacent to the main channel. The mouth of these gullies opens at a low angle in the downstream direction, protecting these deposits from erosion by flow in the main channel. However, these gullies receive significant overland flow which could lead to erosion of the deposits along the gully axes.

Results of the stratigraphy, radiocarbon dating, and geochemical analysis are separately presented for each reach below, followed by the results of unit correlation, hydraulic analysis, and flood frequency modeling.

Puente Diablo Reach

PD1

Depositional environment

Sediments at PD1 (Figures 9 and 10) are located in a relatively broad reach which is approximately 200 m upstream of a 'choke point' where canyon width decreases abruptly. The deposits are inset within the canyon, and extend from 2 to 7 m above the water surface (during base flow on the date of measurement). The surface of the highest deposit is 8 m below the canyon rim. These sediments were deposited at this location as a result of backwater ponding and reduced flow velocities. Thick, rooted vegetation exists at the site which has likely played an important role in the preservation of these sediments during flood events.

Stratigraphy

In general, the stratigraphic section described at PD1 is characterized by an alternating sequence of finer (silt and fine-sand) and coarser (medium to coarse sand) layers (Fig. 10). Each layer was interpreted to represent a distinct flood deposit in a relatively low-energy environment created by the abrupt decrease in canyon width immediately downstream of the site. A total of 15 flood deposits were identified, and a total of 41 samples were collected from the deposits for geochemical analysis. Deposit geometry, lateral continuity, and sedimentologic properties of the deposits are described in more detail in Table 1.

Radiocarbon Dating

While a number of radiocarbon samples were collected from the stratigraphic section at PD1, none of the samples were submitted for radiocarbon dating due financial constraints.

Elemental Analysis

The purpose of the geochemical analysis is to correlate flood deposits from site to site and to provide a better understanding of flood depositional processes. This ultimately provides the context for reconstructing the flow conditions responsible for the deposition of the individual flood units.

Chemical sample names, depths, and corresponding paleoflood units for PD1 are presented in Table 2. As expected, there are differences in elemental concentrations between major and trace elements of up to several orders of magnitude (Table A1 in Appendix A). This further emphasizes the need to address scaling issues by transforming the data as described in the Methods Section. Several of the elements selected for stratigraphic correlation purposes exhibit a high level of covariance with mostly positive correlation (Figure 11). With a correlation coefficient of 0.945, As and Cd have the highest calculated correlation.

There are some interesting and potentially useful spatial patterns contained within the concentration-depth profile (Figure 12). First, deposits which are interpreted as eolian deposits and which are unburied (i.e., at the surface of the section) exhibit high concentrations of As, Cd, Co, Cu, Ni, and Pb, with Cr, Sr, and Zn being the exceptions. At 100 cm in depth, the geochemical signature is characterized by a sharp increase in Sr and Zn accompanied by a sharp decrease in Cr and Pb. Arsenic, Cd, Co,

Cr, Ni, Pb, and Zn concentrations increase sharply at around 230 cm depth. Cadmium, Cr, and Ni concentrations exhibit a lower magnitude increase at a depth of 390 cm. From 420 cm to the bottom of the section (~540 cm), As, Cd, Co, and Zn exhibit a similar concentration trend which is described as being moderately high at 420 cm, dipping to low concentrations at ~440 cm downsection, and steadily increasing toward the bottom of the section. Flood units PD1-FD12 through PD1-FD14 are represented in the bottom portion of the stratigraphic section (Figure 12).

Linear discriminant analysis (LDA) was performed on PD1 chemical samples from flood deposits FD1, FD4, FD9, FD10, FD12, and FD14 in an effort to differentiate flood deposit units on the basis of their geochemical composition (Figure 13). Specifically, the analysis was based on concentrations of As, Cd, Co, Cr, Cu, Ni, Pb, Sr, and Zn. The other deposits were not included because the number of collected and analyzed geochemical samples for the units were limited. The analysis indicates samples cluster into 5 groups, and the samples within 4 of the 5 groups are associated with specific flood deposits (FD1, FD4, FD9, and FD10). Significant overlap between samples from FD12 and FD14 suggests that these flood deposits are composed of sediments from a similar source. Despite this overlap, the LDA which attempts to model differences between classes of data was able to correctly classify 74% of the PD1 samples when cross-validated using a 'leave one out' procedure.

PD2

Depositional Environment

PD2 is located in a reach where the canyon is relatively wide (~50 m in width). Abundant colluvial boulders provide an environment in which slackwater type sediments

may be deposited and trapped. A rock terrace which extends downstream from PD2 also has a thick package of sediments which are covered in dense sagebrush-like vegetation. Approximately 160 m upstream of PD2 the canyon is very narrow (~1 m in width) with vertical bedrock walls which rise 5 m above the water surface at baseflow; the depth of the water in this narrow section was measured at 7.5 m. Downstream of PD2 the canyon narrows to 25 – 30 m in width, with steeply sloped walls (~45°) approximately 6 m high. During baseflow at this location, the river flows through a very narrow (<1 m in width) trench cut deep into a bedrock terrace. Section PD2 is located immediately downstream of the narrow canyon reach. Deposition along this reach is presumed to be associated with the rapid expansion of flow, and a decrease in flow velocities, as water emerges from the canyon. The deposits are located upstream of a protrusion composed of bedrock and colluvial boulders that protects the deposits from erosion.

Stratigraphy

Deposits were located, measured, and described for site PD2, 0.67 km downstream of PD1 (Figure 2). Section PD2 is located between 1 – 3 m above the water surface and the top of the highest deposit is 3 m below the canyon rim (Figure 14). At section PD2, a total of 10 flood deposits were identified (Figure 15). Sedimentology of the deposits is similar to that described at PD1, and individual layers were again interpreted to represent individual floods. Deposit geometry, lateral continuity, and sedimentologic properties are described in Table 3.

Radiocarbon Dating

None of the samples collected for radiocarbon dating within section PD2 reach were analyzed due to financial constraints.

Elemental Analysis

Chemical sample names, depths, and corresponding flood deposit units for PD2 are presented in Table 4. Several of the elements selected for stratigraphic correlation purposes exhibit a high level of covariance with mostly positive correlation (Figure 16). With a value of 0.951, Cd and Zn have the highest calculated correlation coefficient. Arsenic and Cd also exhibit a strong correlation, possessing a correlation coefficient of 0.936.

Concentration-depth profiles for selected elements exhibit a large increase in the concentrations of As, Cd, Co, Cu, Ni, and Zn at 40 cm depth (Figure 17). This corresponds to the PD2-FD3 flood deposits. At 50 cm in depth within section PD2, the geochemical signature is characterized by an increase in Sr accompanied by a sharp decrease in Co, Cr, Ni, Pb, and Zn. This corresponds to the PD2-FD4 flood deposits. From 90 cm to the bottom of the section (200 cm), As, Cd, Co, and Zn exhibit a concentration trend which is described as being moderately high at 90 cm, dipping to low concentrations (similar to those at the top of the section) at ~110 cm downsection, and steadily increasing toward the bottom of the section. Flood units PD2-FD5 through PD2-FD10 are represented in this bottom portion of the stratigraphic section.

Linear discriminant analysis was not performed on the PD2 samples due to an insufficient number of samples from each flood unit.

Correlation of PD1 and PD2

One aspect of this study is to attempt correlation of flood deposits between different sites based on age dating and chemistry. Flood deposits at PD1 and PD2 were not submitted for radiocarbon dating, therefore correlation based on age dating cannot be attempted for these sites. With respect to chemistry, the low number of samples from each flood unit does not allow for correlation to be made on the basis of groupings determined from Linear Discriminant Analysis. However, similarities in the concentration depth profiles between PD1 and PD2 can be examined to identify the potential for correlation between these sites.

PD1-FD8 and PD2-FD3 have similar concentrations and samples are represented graphically by a sharp peak of several elements (As, Cd, Co, Sr, and Zn) within their respective concentration depth profile. PD1-8 and PD2-FD3 may have been deposited during the same flood (Figure 18). It appears PD1-FD1 through FD7 are missing at the PD2 section. A large section (1.2 m) Of PD1, composed of several flood deposits (PD1-FD12 through PD1-FD15) is similar in overall shape and concentration of several elements (As, Cd, Co, Cu, Sr, and Zn) to a large section (also 1.2m) of PD2 (PD2-FD5 through PD2-FD10). Specifically, PD1-FD12 is correlated to PD2-FD5, PD1-FD-13 to PD2-FD9, and PD1-FD14 to PD2-FD10.

Hydraulic Analysis for Reach PD

Hydraulic analysis using the HEC-RAS hydraulic computer model was performed to estimate discharges of paleofloods by generating water surface profiles from which to determine the approximate magnitude of paleofloods responsible for depositing specific flood units. Sharp drops in the water surface profile indicate locations where

supercritical flow occurs (Figure 19). These locations are generally upstream of cataracts and narrow constrictions in the bedrock canyon. As the channel widens downstream of these points, a hydraulic jump occurs (Figure 19). This mechanism explains the large range of variability observed in the water surface profile over short distances for a specific discharge.

Maximum discharge for the PD reach based on the elevations of slackwater deposits at PD1 is approximately $310 \text{ m}^3 \text{ s}^{-1}$ and the corresponding velocity for this discharge is 1.74 m s^{-1} . The peak velocity of 1.91 m s^{-1} corresponds to a lower discharge of $200 \text{ m}^3 \text{ s}^{-1}$. These results are consistent with the interpretation that sediments are deposited at this site during large magnitude floods due to backwater ponding and reduced flow velocities.

At cross section 12 (XS12), where the bedrock canyon is very narrow, sediment is lodged in place ~2 m below the canyon rim (elevation 2655 m a.s.l.), and overbank deposits are observed immediately upstream of the cross section. It is believed this sediment is from the 2001 flood. In addition, flood channels etched in desert pavement on the valley floor are visible on aerial photographs indicating that overbank flows have occurred at this location (Fig. 3). Hydraulic analysis indicates that for a flood discharge of $443 \text{ m}^3 \text{ s}^{-1}$ (the magnitude of the 2001 flood based on Houston's (2006) estimate and corrected for increase drainage area) the elevation of the water surface profile is 2658 m a.s.l.. The elevation of the water surface profile indicates that the 2001 flood stage was sufficiently high enough to emplace the sediment wedged near the top of the canyon.

PD Reach Flood Frequency Analysis

Flood frequency analysis for the PD reach is limited due to the lack of any information on the ages of the flood deposits at PD1 and PD2. Age dating of these deposits would allow for a more detailed flood frequency analysis. However, the data show that multiple floods with a discharge greater than that observed in 2001 have been recorded within the stratigraphic sections.

Rio Salado Reach

RS1

Depositional Environment

Upstream and downstream of RS1, the canyon is approximately 70 m wide and the approximately 20 m high canyon walls are near vertical. Slackwater deposits at RS1 are located on the north facing slope of an alcove at the mouth of a tributary gully situated at an angle of $\sim 60^\circ$ to the direction of flow of the river (SSW). The mouth of this gully is approximately 30 m wide and the alcove is ~ 60 m long along the axis. The slope along the axis of the alcove is significantly less steep than that of the adjacent and opposite canyon walls which are near vertical. Along the sides of the alcove, erosion and colluvial processes acting on the stratified volcanic bedrock have resulted in a stair step series of meter scale bedrock terraces. During large magnitude flood events, the increased cross sectional area afforded by the alcove results in lower flow velocities allowing sediment to be deposited. These sediments are well preserved as they are protected from flow from the main channel; however, flow along the gully which formed the alcove has eroded sediments along its axis.

Stratigraphy

The deposits located downstream in reach RS differ significantly from those along reach PD. These deposits more closely represent slackwater sediments in that they were deposited in alcoves cut within the canyon walls by incoming gully/runoff systems. RS1 deposits are located 6 – 7.5 m above the water surface; the top of the highest deposit is 14 m below the canyon rim. A total of 9 flood deposits were identified at RS1; detailed descriptions of these deposits are provided in Table 5. In general, the deposits are associated where two distinct geomorphic surfaces (terraces) exist within the alcove (Figure 20). The stratigraphic relation between the deposits of the two surfaces is unclear. However, the deposits of the lower surface have been interpreted to be inset into, and therefore younger, than those of the upper surface (Figure 21). The deposits are all dominated by silty, very fine to medium sand that possess abundant quantities of subparallel, horizontally laminated plant fragments. The plant fragments are likely from reeds and other types of vegetation that grow along the channel and that was eroded, degraded, and redeposited during the flood events. Charcoal was also observed within the deposits. A total of 9 flood units were recognized at the site, from which 15 sediment samples were collected for geochemical analysis.

Radiocarbon Dating

Radiocarbon age dating results are presented in Table 6. RS1-C14-3 was collected from flood deposit FD9 at the RS1 site (Figure 20). RS1-C14-5 was collected from flood deposit FD4. FD4 is younger (210 ± 30 RCYBP) than FD9 (390 ± 30 RCYBP) although it is lower in the stratigraphic section. While radiocarbon dating of sample RS1-C14-5 yields several other possible calendar age ranges, none of those ages

indicate the deposit is older than FD9. As a result, the inset relationship described previously in the stratigraphy section (Figure 21) is supported by the radiocarbon ages determined for FD4 and FD9.

Elemental Analysis

Chemical sample names, depths, and corresponding flood units for RS1 are presented in Table 7. Several of the elements selected for stratigraphic correlation purposes exhibit a high level of covariance with mostly positive correlation (Figure 22). With a value of 0.928, As and Cd have the highest calculated correlation coefficient. Cobalt and zinc also have a high correlation coefficient of 0.923.

Concentration-depth profiles for selected elements exhibit relatively high concentrations of As, Cd, and Co, at the top of the stratigraphic section (Figure 23). This corresponds to the RS1 – FD8a flood unit. At ~14 cm in depth, the geochemical signature is characterized by a sharp decrease in As, Cd, Co, Cu, Ni, Sr, and Zn and an increase in Cr. This also corresponds to the RS1 – FD8a flood unit. Another sharp increase in the concentrations of As, Cd, Co, Co, Cu, Ni, Sr, and Zn occurs at 20 cm depth within the profile. Concentrations of As, Cd, Co, Cu, Ni, and Zn increase semi-steadily from 33 cm in depth to the bottom of the section (~60cm in depth). The highest concentrations of all of these elements are located at the bottom of the section.

An independent linear discriminant analysis at RS1 was not performed due to an insufficient number of chemical samples from each flood deposit. However, chemical samples from the RS1– FD9 flood unit were included as part of the linear discriminant analysis for RS2 flood deposits described below.

RS2

Depositional Environment

RS2 is located 0.28 km downstream of RS1. The depositional environment of RS2 is very similar to that of RS1, where slackwater deposits are located in an alcove (Figure 24). Upstream and downstream of RS2, the canyon is approximately 40 m in width and the canyon walls are near vertical and approximately 18 m high. Slackwater deposits at RS2 are located in on the northeastern facing slope of an alcove situated at an angle of $\sim 80^\circ$ to the direction of flow of the river (WSW). The mouth of this alcove is situated between two bedrock spurs and is relatively narrow, measuring approximately 5 – 10 m in width. More circular in geometry than the RS1 alcove, the RS2 alcove is ~ 30 m long along the axis. The slope along the axis of the alcove is significantly less steep than that of the adjacent and opposite canyon walls which are nearly vertical.

Along the sides of the alcove, erosion and colluvial processes acting on the stratified volcanic bedrock have resulted in a stair step series of meter scale bedrock terraces. During large magnitude flood events, the increased cross sectional area afforded by the alcove results in lower flow velocities at this site, allowing sediment to be deposited. These sediments are well preserved as they are protected from flow from the main channel. However, flow along the gully may erode sediments along the alcove axis.

Stratigraphy

Paleoflood deposits at RS2 are located 5 – 7 m above the water surface; the surface of the highest deposit is located 14 m below the canyon rim (Figure 24). A total of 10 flood deposits were identified and described at RS2, from which 16 sediment

samples were collected for geochemical analysis (Table 9 and Figure 25).

Sedimentology of the flood deposits are similar to those observed at RS1. However, a number of the upper layers within the section are separated by loose, well-sorted medium sands that were interpreted to represent eolian sediments. Thus, the section is characterized by alternating sequence of flood deposits separated by eolian sediments.

Radiocarbon Dating

Radiocarbon age dating results are presented in Table 6. RS2-C14-3 was collected from flood deposit FD3 (Figure 25), whereas RS2-C14-2 was collected from flood deposit FD8. FD3 is older (350 ± 30 RCYBP) than FD8 (250 ± 30 RCYBP).

Elemental Analysis

Chemical sample names, depths, and corresponding flood units for RS2 are presented in Table 9. Several of the elements selected for stratigraphic correlation purposes exhibit a high level of covariance with mostly positive correlation (Figure 26). With a value of 0.979, As and Cd have the highest calculated correlation coefficient. Cobalt and nickel also exhibited a high correlation coefficient of 0.94.

Concentration-depth profiles for selected elements exhibit high concentrations of As, Cd, Co, Cu, Ni, Pb, Sr, and Zn near the top of the stratigraphic section at 3.5 cm and 13 cm depth (Figure 27). These increases correspond to the RS2 – FD6 and RS2 – FD5 flood deposit units. At 9 cm and 19 cm in depth, the geochemical signature is characterized by a sharp decrease in As, Cd, Co, Cu, Ni, Pb, Sr, and Zn. These decreases correspond to eolian units within the section.

Concentrations of As, Cd, Co, Cu, Ni, Pb, and Zn increase steadily from 50 to 100 cm depth. The concentration of Sr also mostly increase from 50 cm to 100 cm

depth although there is a notable sharp decrease in Sr at 84 cm in depth. At the bottom of the stratigraphic section, concentrations of As, Cd, Co, Cu, Ni, Pb, and Zn are relatively low and trending lower. The concentrations of Cr and Sr are highest at the bottom of the section and trending higher.

Linear discriminant analysis (LDA) was performed on RS2 chemical samples from flood deposits FD1, FD2, FD3, and FD4 in an effort to differentiate flood units on the basis of their geochemical composition. Specifically, the analysis was based on concentrations of As, Cd, Co, Cr, Cu, Ni, Pb, Sr, and Zn. The analysis indicates samples cluster into 4 groups which are associated with specific flood deposits (Figure 28). Model performance using a 'leave one out' cross validation is poor (46.1% correctly classified) primarily due to the low number of overall samples and FD1 being comprised of only two samples.

Subsequently, a linear discriminant analysis was performed in which samples from RS1-FD9 were included. The RS1-FD9 samples were grouped with samples from RS2-FD3. Samples from RS1-FD9 and RS2-FD3 were expected to exhibit a similar geochemical signature as the two units exhibited similar (overlapping) radiocarbon ages, suggesting they were deposited during the same event. Figure 29 illustrates that four discernible groups remain although there is somewhat more spread to the FD3 group. One way to measure the increase in the spread of the group is the average Mahalanobis distance of the samples to the primary centroid of the cluster. The Mahalanobis distance is a measure of distance between a point and a distribution. In this case, the inclusion of the RS1-FD9 deposits into the RS2-FD3 group increases the average Mahalanobis distance from the primary centroid of the cluster from 1.42 to

2.18. For reference, the Mahalanobis distance from the centroid of the expanded group to other clusters ranges from 9.14 to 10.88.

Correlation of PD reach with RS reach

It was initially hypothesized that correlation of deposits in the different reaches would be possible if there were no additional inputs from another sediment source (i.e., the input of sediment from subbasins characterized by different geologic units) between reaches. Unfortunately, there exists such a drainage between the PD and RS reaches (Figure 30). Although this drainage was not conveying water during the period of field data collection, it is likely that the drainage would convey water during a flood event.

A Principal Component Analysis (PCA) of the concentrations of As, Cd, Co, Cr, Cu, Ni, Pb, Sr, and Zn for each individual site (PD1, PD2, RS1, and R2) reveals a similar geochemical signature between PD1 and PD2 and similarities between RS1 and RS2, however there is a difference in the chemical signature between the PD reach and RS reach (Figure 31).

Hydraulic Analysis

Hydraulic analysis using the HEC-RAS hydraulic computer model is performed to estimate discharges of paleofloods by generating water surface profiles from which the approximate magnitude of paleofloods responsible for depositing specific flood units can be determined.

The water surface profile at all discharges is typical of a subcritical flow regime (Figure 33). This reflects the absence of extremely narrow constrictions and cataracts within the RS reach. The modeled water surface elevations were calibrated by adjusting Manning's roughness coefficient. Elevations of the slackwater deposits at RS-1 more

closely matched the water surface elevations at the two sites where a Manning's n of 0.05 is applied to the channel (Figure 32). Thus, a Manning's n of 0.05 was used as the roughness coefficient. The estimated discharge of the lowest elevation paleoflood deposit (RS2-FD2) is $240 \text{ m}^3 \text{ s}^{-1}$ and for the highest elevation paleoflood unit (RS2-FD8) is $515 \text{ m}^3 \text{ s}^{-1}$.

Correlation of RS1 and RS2

Correlation of flood deposit units at RS1 and RS2 is made on the basis of radiocarbon age dating results, geochemical results, and water surface elevations as computed by the HEC-RAS model. Radiocarbon age dating indicates the RS1-FD9 ($390 \pm 30 \text{ BP}$) and RS2-FD3 ($350 \pm 30 \text{ BP}$) are of a similar age. Although the age results are not identical, the uncertainty associated with each age date indicates these flood deposits could be from the same event.

Correlation of RS1-FD9 and RS2-FD3 flood deposits is also suggested on the basis of the LDA procedure described above which geochemically classified RS2-FD3 samples with RS1-FD9 samples. The results of the hydraulic model also indicate that the elevations of RS1-FD9 and RS1-FD3 correspond to a water surface elevation profile of a flood event with a specific minimum discharge (Figure 33 and Figure 34).

RS Reach Flood Frequency Analysis

A total of 10 paleofloods were used in the flood frequency analysis. All of the flood deposits used in the flood frequency analysis were located at RS1 and RS2. These floods were selected because they were distinguishable from other floods based on the geochronology and stratigraphic relationships established by radiocarbon dating and cluster analysis of their geochemical composition. It is likely this results in an

underestimate of the number of significant paleofloods during the last ~375 years. Some paleofloods may not have left behind slackwater deposits and would not be accounted for. Similarly, some slackwater deposits of paleofloods may have been eroded and would not be accounted for. For slackwater deposits which are of unknown age, but whose age is constrained by stratigraphic position relative to a slackwater unit of known age, it is assumed that they are spaced evenly throughout the constrained time range. This approach is validated by the fact that the “number of floods per time period is more important in flood frequency analysis than the exact ages of the floods” (Greenbaum et al., 2014).

Flood frequency analysis using (a) the gaged record including the 2001 flood event and (b) the gaged record plus the 10 paleofloods was performed using PeakfqSA modeling software. PeakfqSA was designed to better incorporate historic and paleoflood data into flood frequency analyses. PeakfqSA employs a relatively general parameter-estimation method termed the Expected Moments Method (EMA). EMA can derive useful information from threshold data where the data fall into one of four categories: (a) floods of known magnitude, (b) floods of unknown magnitude that are less than a threshold, (c) floods of unknown magnitude that exceed some threshold, and (d) floods with magnitudes described by a range (England et al., 2003). The last category was used in this study, the lower bound is set as $200 \text{ m}^3 \text{ s}^{-1}$ and the upper bound is assumed to be infinite. This range was decided based on the fact the lowest preserved slackwater deposit corresponds to a discharge of $\sim 240 \text{ m}^3 \text{ s}^{-1}$, so we can roughly infer a discharge above $200 \text{ m}^3 \text{ s}^{-1}$ would have been “recorded” in the stratigraphy. The upper bound is set at infinite because there is a possibility the largest

flood which occurred between c. 1640 and 1990 was not “recorded” in the flood stratigraphy. More detailed information on PeakfloodSA and EMA can be found in Tim Cohn’s user manual for the software (Cohn, 2012).

Based on the age of deposits determined from radiocarbon dating and the relative age of deposits determined from stratigraphy, the paleoflood record consisted of 10 paleofloods during the last 375 ± 30 years. Two separate flood frequency analyses were conducted using the log-Pearson Type III method as described in the methods section (Figure 35). One utilized only data (1991-2015) from the upstream gaging station (at El Sifon) and the other data from the gaging station as well as the paleoflood records. Based on the gaged record only, the 100-year flood (with an annual exceedance probability, AEP = 0.01) is $856 \text{ m}^3 \text{ s}^{-1}$. By comparison, using the combination of gaged record and paleoflood data the 100-year flood is $429 \text{ m}^3 \text{ s}^{-1}$. The 500-year flood (AEP = 0.002) for the gaged record only is $2,225 \text{ m}^3 \text{ s}^{-1}$, in marked contrast to $997 \text{ m}^3 \text{ s}^{-1}$ for the paleoflood supplemented record. Using the gaged record only the 2001 flood has a recurrence interval of ~40 years (AEP = 0.025) versus a recurrence interval of ~100 years (AEP = 0.01) when using the combination gaged record and paleoflood data (Figure 35).

Paleofloods with computed discharges less than $490 \text{ m}^3 \text{ s}^{-1}$ plot above the flood frequency curve while paleofloods with discharges greater than $490 \text{ m}^3 \text{ s}^{-1}$ plot below the flood frequency curve. A poor fit for some of the gaged data is the result of censoring the left-hand tail of the observed data. This is a valid approach in an arid regions where it is likely there are many years when no rainfall occurs (Hussain, 2011). Comparison of the computed elevations of the 50- and 100-year floods to the FD-9

slackwater deposits at RS-1 indicates this deposit is the remnant of an older, larger flood event exceeding the 100-year flood event (Figure 36).



Figure 9. PD1 stratigraphic sections 1-4. The entire section is ~5 m in height. Note abundant vegetation which has helped preserve sediment from erosion during flooding.

Table 1. Description of Flood Deposit (FD) units at PD1.

FD1: Overlain by vegetated unit of fine loose silt and sand with abrupt boundary. Upper 20 cm crumbly to weak blocky structure with abundant roots. Very fine sediments brown in color. Slightly sticky texture. Lower 30 cm has cross-bedded structure with few roots. Abrupt, wavy lower boundary draped over roots and large rock clast.

FD2: Blocky and more indurated relative to overlying unit. Cross-bedding not present. Abundant roots. Contains a subangular rock clast which is roughly 20 cm in diameter and dips parallel to slope. Abrupt, wavy lower boundary.

FD3: Loose, cross-bedded fine to medium sand. Abrupt lower boundary. Erosional contact.

FD4: Upper portion contains calcium carbonate filaments and is light red to gray in color. Lower 42 cm has blocky, massive structure with faint appearance of cross-bedding. Abundant small roots. Texture is that of silt to fine sand. Color is dark brown. Abrupt lower boundary. Upper portion of unit may be buried soil.

FD5: Unit is of variable thickness; thickest in the upstream direction and pinching out in the downstream direction. Loose, well sorted medium sand. Cross-bedding present. Abrupt, distinct and straight lower boundary.

FD6: Well indurated, silt to fine sand. Units dips parallel to slope. Abrupt, straight lower boundary.

FD7: Massive fine sand. Crumbly to weak blocky structure. Sparse fine roots. Indistinct lower boundary.

FD8: Similar to above unit, but with more roots and more indurated. Massive, fine sand. Abrupt lower boundary

FD9: Loose, fine sand at top of unit. Cross-bedding present. Lighter in color than above units above. Slightly indurated and blocky structure toward bottom of unit. Abrupt boundary.

FD10: Upper 20-25 cm laminated parallel to upper boundary. Remainder of unit is loose, well sorted fine to medium sand. A few roots present. Abrupt, wavy lower boundary.

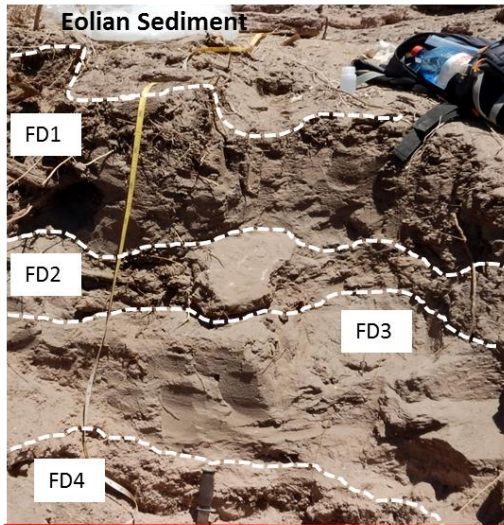
FD11: Indurated layer composed of silt. Millimeter scale cross-bedding apparent. Abrupt, wavy boundary.

FD12: Fine sand with faint cross-bedding. More massive relative to other predominantly sand units.

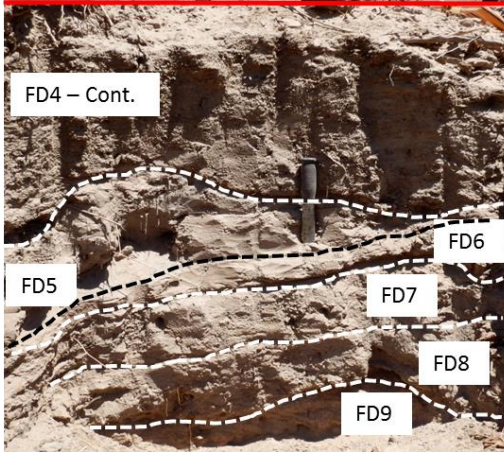
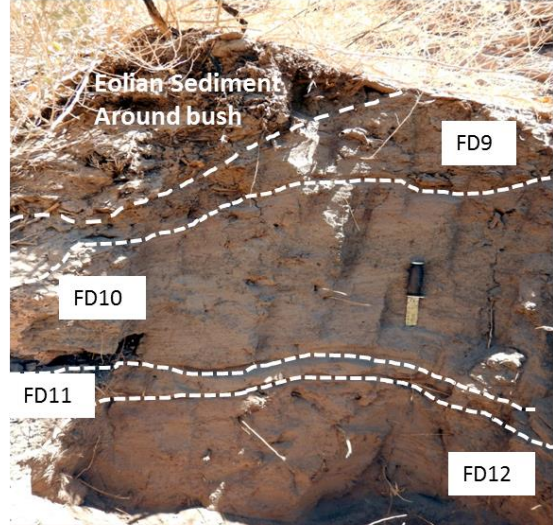
FD13: Loose, weakly laminated, very fine to fine sand. Silt layer toward bottom of section. Gradual, indistinct lower boundary.

FD14: Massive with a weakly blocky structure. Abundant roots. Local lenses of cross-bedded fine sand. Abrupt lower boundary.

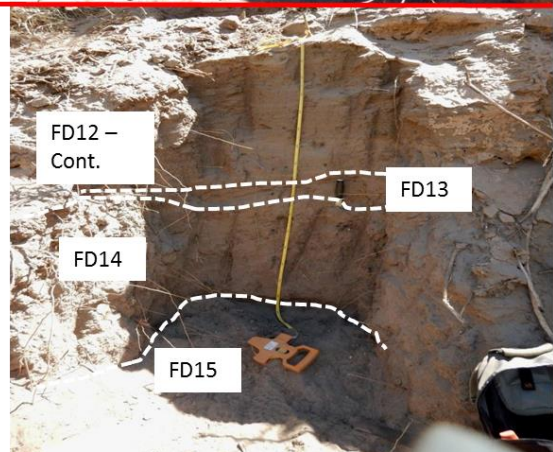
FD15: Loose fine sand. Massive structure. Section ends before lower boundary observed.



FD2 - Rock -
may be
colluvium
between
events



FD4 -
Possible
buried soil in
top of unit



PD1, Sections 1 & 2

PD1, Sections 3 & 4

Figure 10. PD1 Flood deposits. There a total of 15 flood deposits and 2 eolian deposits.

Table 2. Sample ID, section number, depth, and flood deposit ID for PD1 samples.

Chemical Sample ID	Section at Site	Depth (cm)	Deposit
PD1-1	Section 1	0-15	Eolian
PD1-2	Section 1	15-30	FD1
PD1-3	Section 1	30-45	FD1
PD1-4	Section 1	45-65	FD1
PD1-5	Section 1	65-75	FD2
PD1-6	Section 1	75-84	FD2
PD1-7	Section 1	84-94	FD3
PD1-8	Section 1	94-101	FD3
PD1-9	Section 1	101-124	FD4
PD1-10	Section 2	0-15	FD4
PD1-11	Section 2	15-30	FD4
PD1-12	Section 2	30-42	FD4
PD1-13	Section 2	42-46	FD5
PD1-14	Section 2	46-58	FD5
PD1-15	Section 2	58-66	FD6
PD1-16	Section 2	66-80	FD7
PD1-17	Section 2	80-90	FD8
PD1-18	Section 2	90-98	FD8
PD1-19	Section 2	98-108	FD9
PD1-20	Section 3	0-15	FD9
PD1-21	Section 3	15-30	FD9
PD1-22	Section 3	30-45	FD10
PD1-22b	Section 3	45-60	FD10
PD1-23	Section 3	60-75	FD10
PD1-24	Section 3	75-90	FD10
PD1-25	Section 3	90-104	FD10
PD1-26	Section 3	104-117	FD11
PD1-27	Section 3	117-132	FD12
PD1-28	Section 3	132-142	FD12
PD1-29	Section 3	142-150	FD12
PD1-30	Section 4	0-15	FD12
PD1-31	Section 4	15-30	FD12
PD1-32	Section 4	30-45	FD12
PD1-33	Section 4	45-60	FD12
PD1-34	Section 4	60-75	FD12
PD1-35	Section 4	75-87	FD13
PD1-36	Section 4	87-100	FD14

Table continued, Page 2 of 2

PD1-37	Section 4	100-115	FD14
PD1-38	Section 4	115-130	FD14
PD1-39	Section 4	130-145	FD14
PD1-40	Section 4	145-152	FD14
PD1-41	Section 4	152-160	FD15

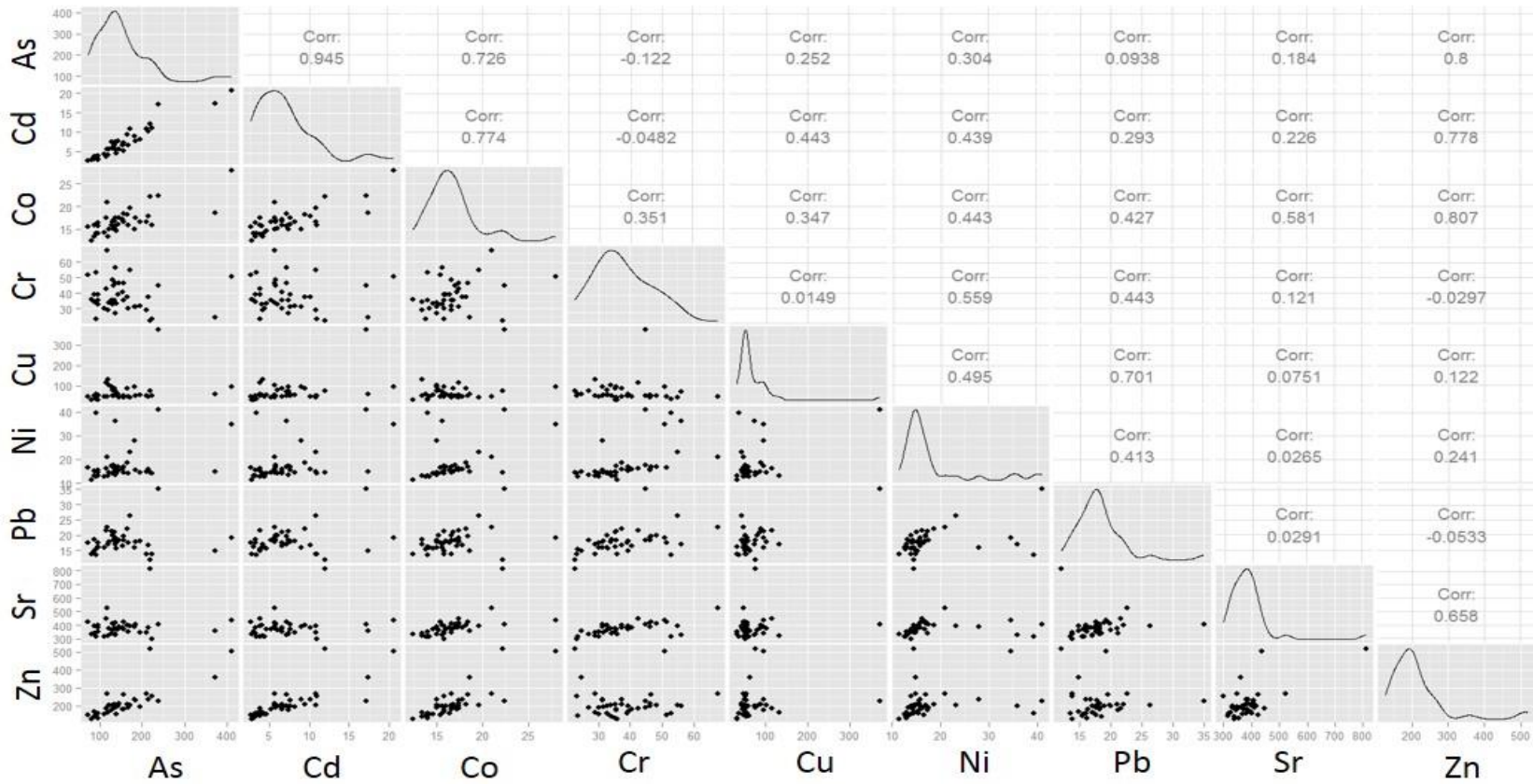


Figure 11. Scatterplot matrix of selected elemental concentrations for PD1. As and Cd have the highest correlation coefficient ($r = 0.945$). There are no pairs of elements which have a significant negative correlation.

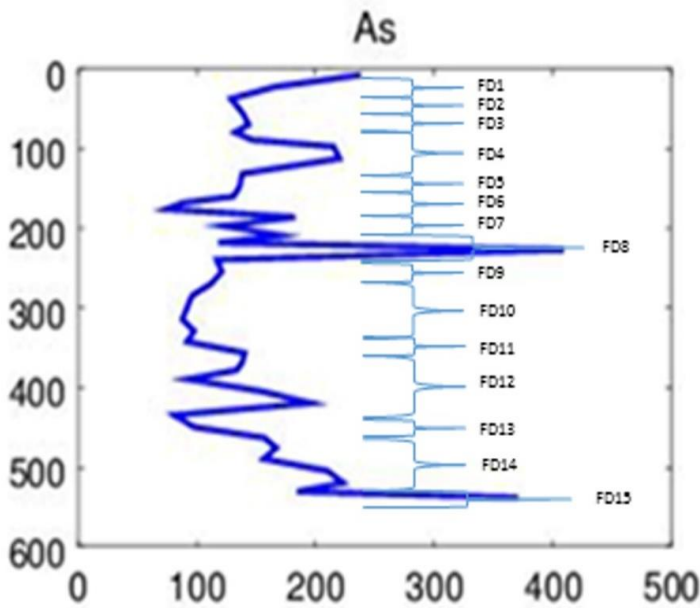
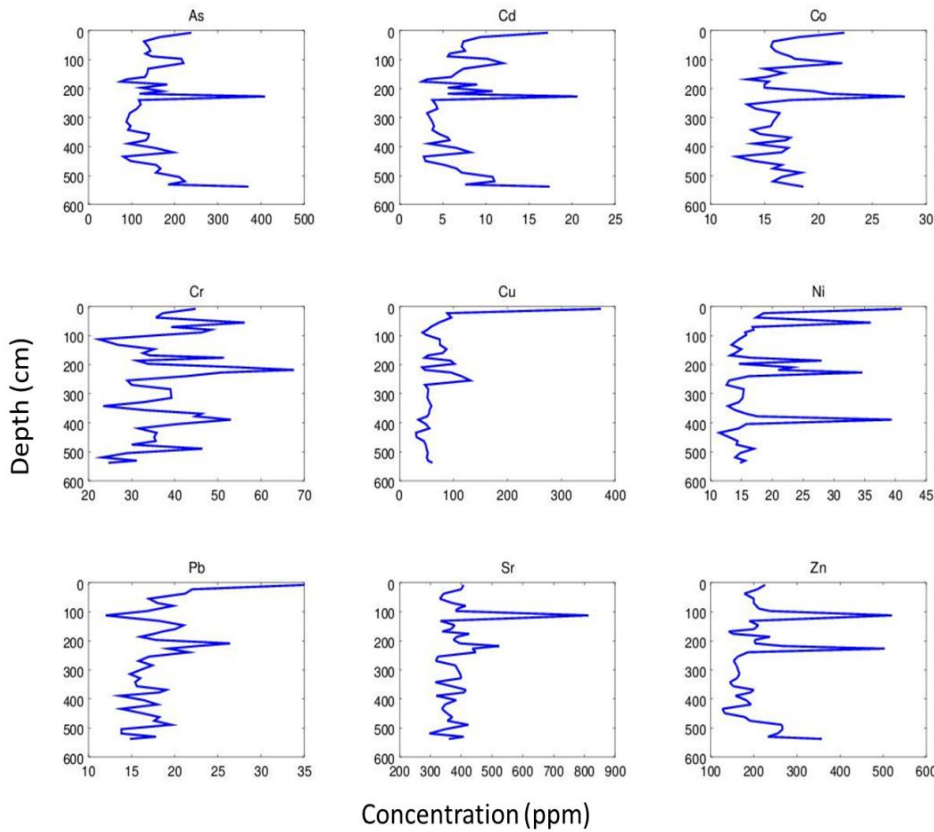


Figure 12. Concentration-depth profile of selected elements for PD1 samples. High concentrations of Cd, Co, Cu, Ni, and Pb at the top of the profile are associated with eolian deposits. At 100 cm there is a sharp increase in Sr and Zn and a sharp decrease in Cr and Pb. The blow up figure for As illustrates that for some flood deposits concentrations are relatively similar for the entire deposit (FD10). Other deposits have a wide range of concentrations (FD12).

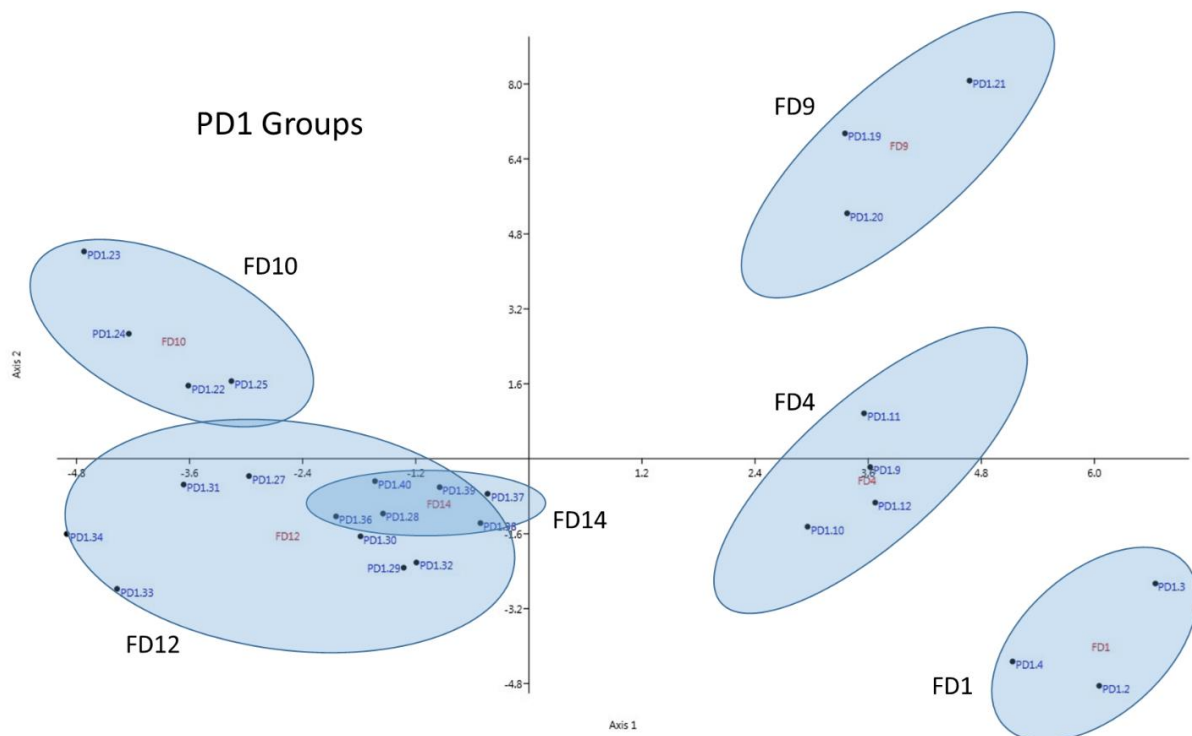


Figure 13. Plot of linear discriminant analysis results for PD1 samples representing FD1, FD4, FD9, FD10, FD12, and FD14. There are five distinct groups: FD1, FD4, FD9, FD10, and a group which contains both FD12 and FD14. Ellipses are used to indicate groupings rather than represent a specific confidence interval.



Figure 14. Stratigraphic section at PD2 measuring ~2m in height. These deposits are closer to the canyon rim than deposits at PD1.

Table 3. Description of Flood Deposit (FD) units at PD2.

FD1: Overlain by unit of loose medium sand with abundant roots and organic debris. Indistinct upper boundary. Loose, medium sand. Unit is distinguishable from overlying unit based primarily on variation in roots and organic debris.

FD2: Indurated, fine-grained, with blocky structure. Silt and fine sand with abrupt lower boundary.

FD3: Fine to medium sand. Few roots. Weakly laminated. Indistinct lower boundary.

FD4: Blocky structure. Fine to medium sand. Abrupt, distinct lower boundary. Unit slightly dipping in downstream direction.

FD5: Unit has a wedge-shaped geometry, with upper boundary dipping in downstream direction. Abundance of roots, particularly in upper portion of unit. Massive structure.

FD6: Fine to medium sand. Few roots present. Blocky structure with faint lamination.

FD7: Blocky, massive structure. Fine to medium sand. Some vertical roots present. Abrupt lower boundary.

FD8: Unit is more indurated relative to other units in section. Blocky structure. Noticeably finer sand. Some fine laminations approximately 0.5 cm in thickness.

FD9: Loose medium sand. Very few roots present. Abrupt lower boundary.

FD10: Indurated. Blocky, mostly massive structure. Some faint lamination present. Fine sand and silt.

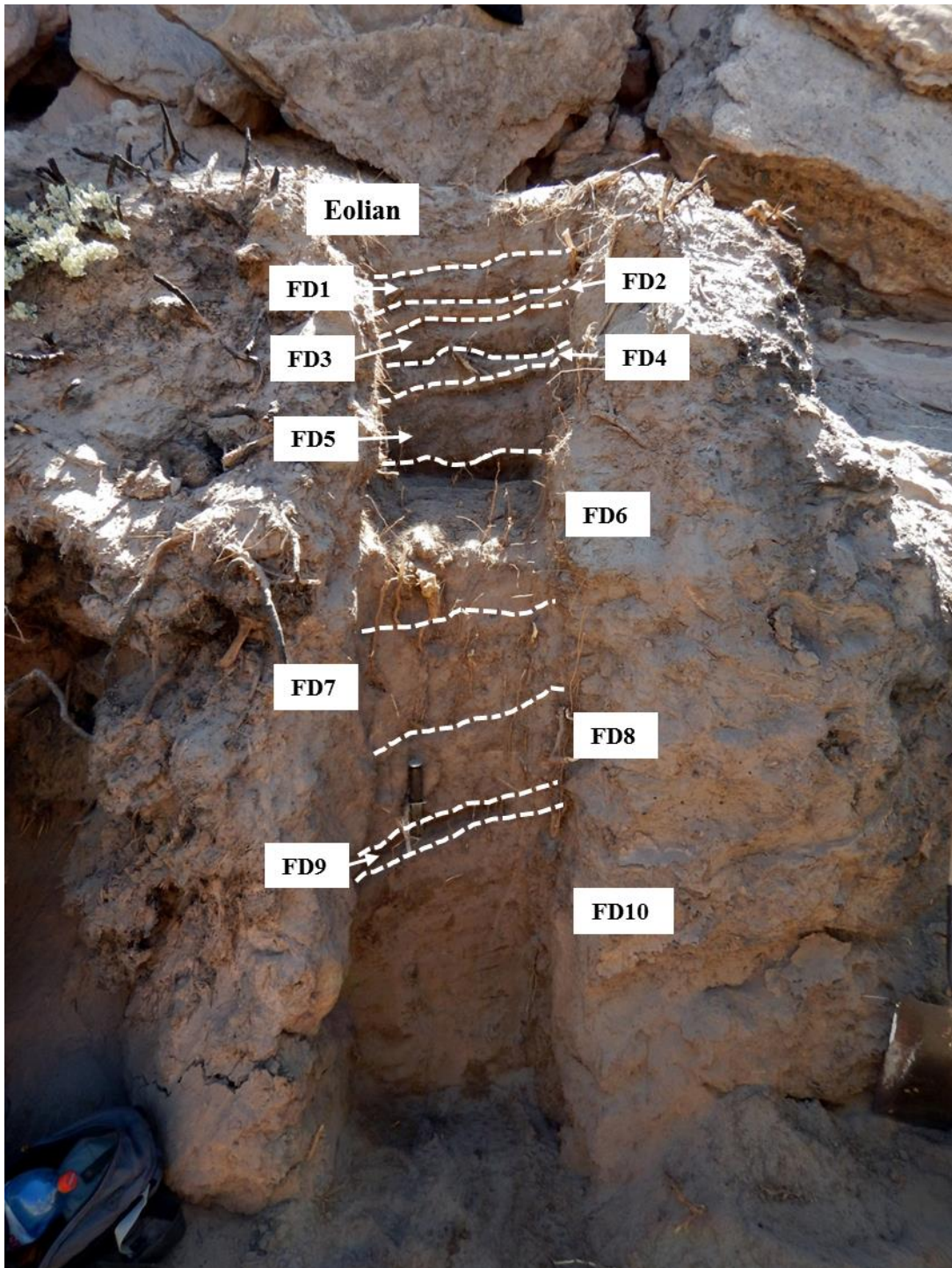


Figure 15. Flood deposits at PD2. There are a total of 10 flood deposits and 1 eolian deposit.

Table 4. Sample ID, section number, depth, and flood deposit ID for PD2 samples

Chemical Sample ID	Section at Site	Depth (cm)	Deposit
PD2-1	Section 1	0-10	Eolian 1
PD2-2	Section 1	10-21	Eolian 2
PD2-3	Section 1	21-30	FD1
PD2-4	Section 1	30-36	FD2
PD2-5	Section 1	36-44	FD3
PD2-6	Section 1	44-54	FD4
PD2-7	Section 1	54-64	FD5
PD2-8	Section 1	64-74	FD5
PD2-9	Section 1	74-80	FD6
PD2-10	Section 2	0-11	FD6
PD2-11	Section 2	11-22	FD6
PD2-12	Section 2	22-39	FD7
PD2-13	Section 2	39-50	FD8
PD2-14	Section 2	50-62	FD8
PD2-15	Section 2	62-67	FD9
PD2-16	Section 2	67-80	FD10
PD2-17	Section 2	80-95	FD10
PD2-18	Section 2	95-110	FD10
PD2-19	Section 2	110-130	FD10

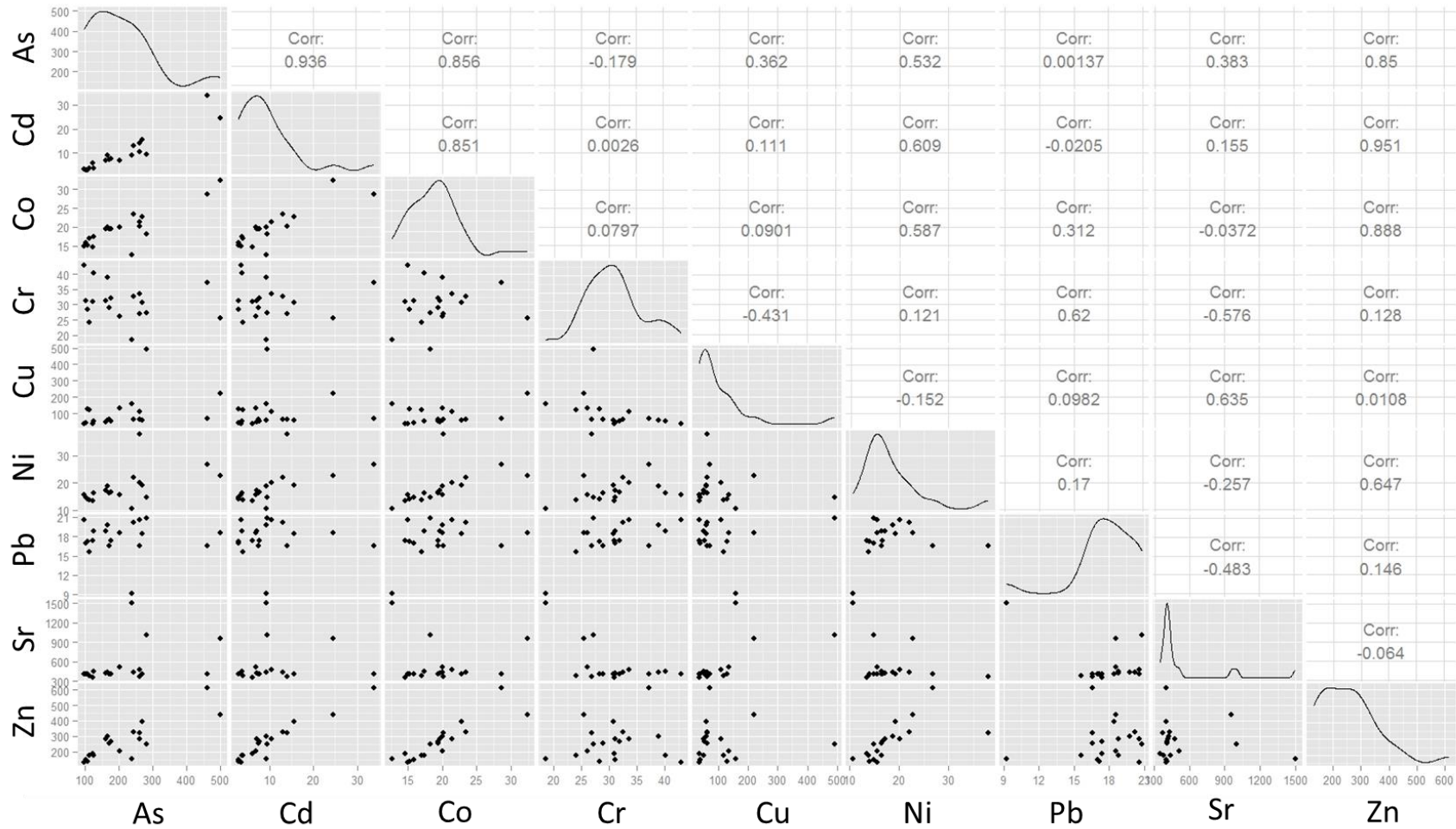


Figure 16. PD2 scatterplot matrix. Cd and Zn have the highest correlation coefficient ($r = 0.936$). There are no pairs of elements which have a significant negative correlation.

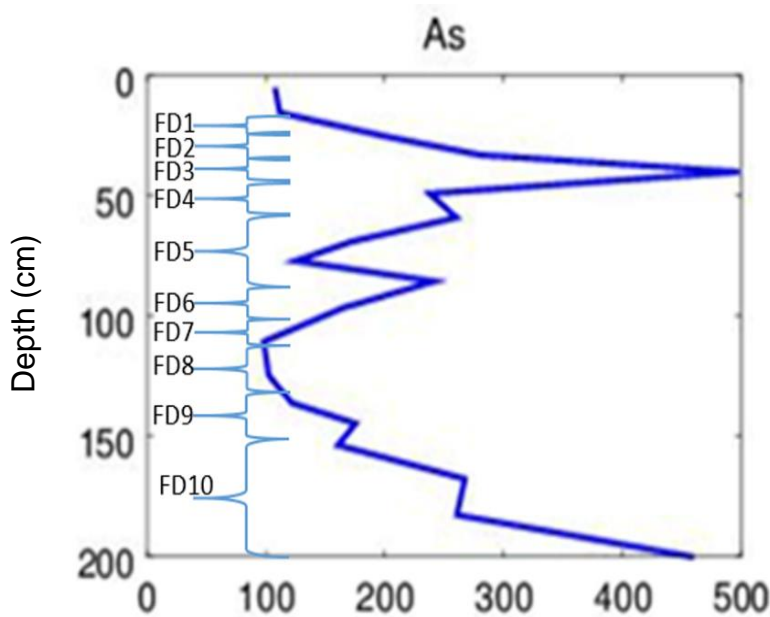
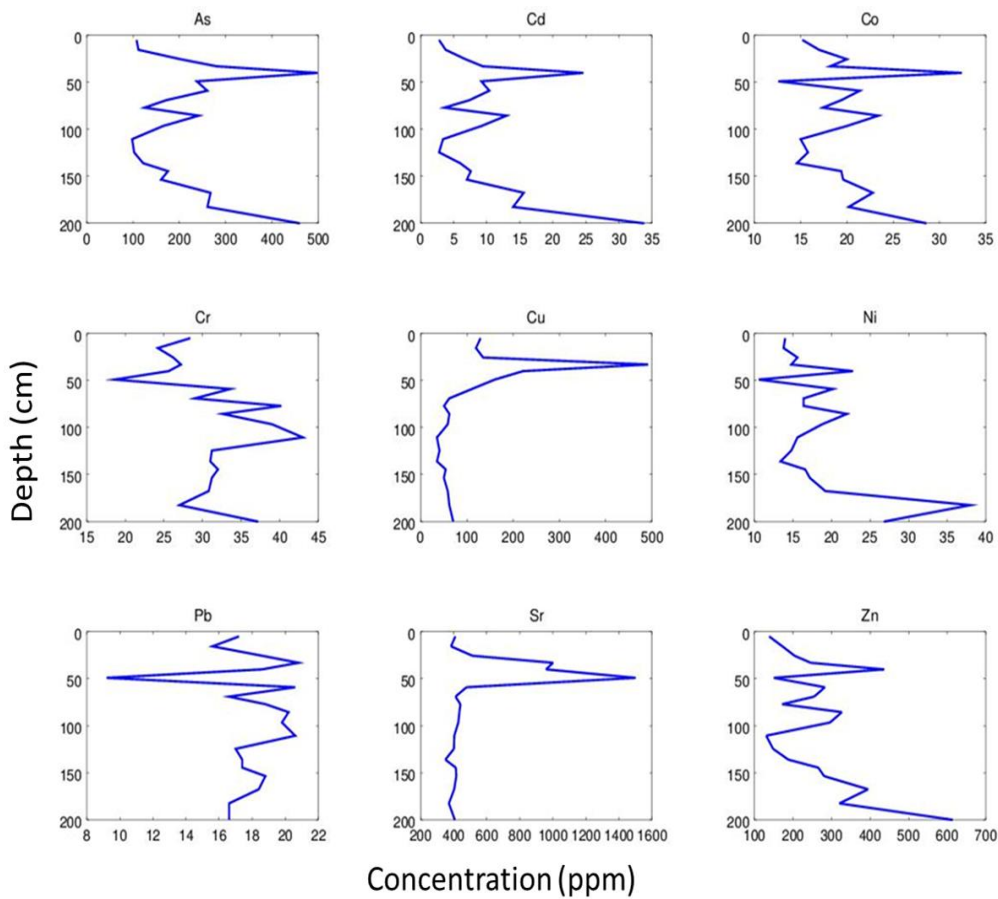


Figure 17. The concentration depth profile of PD2 deposits (above). There is a large “peak” at 40cm depth for As, Cd, Co, Cu, Sr, and Zn. This corresponds to FD3 as shown in the blow up of the As profile (left). Also note the overall shape for concentrations of As, Cd, Co, and Zn from 90cm to the bottom of the section. This corresponds to FD5 through FD12.

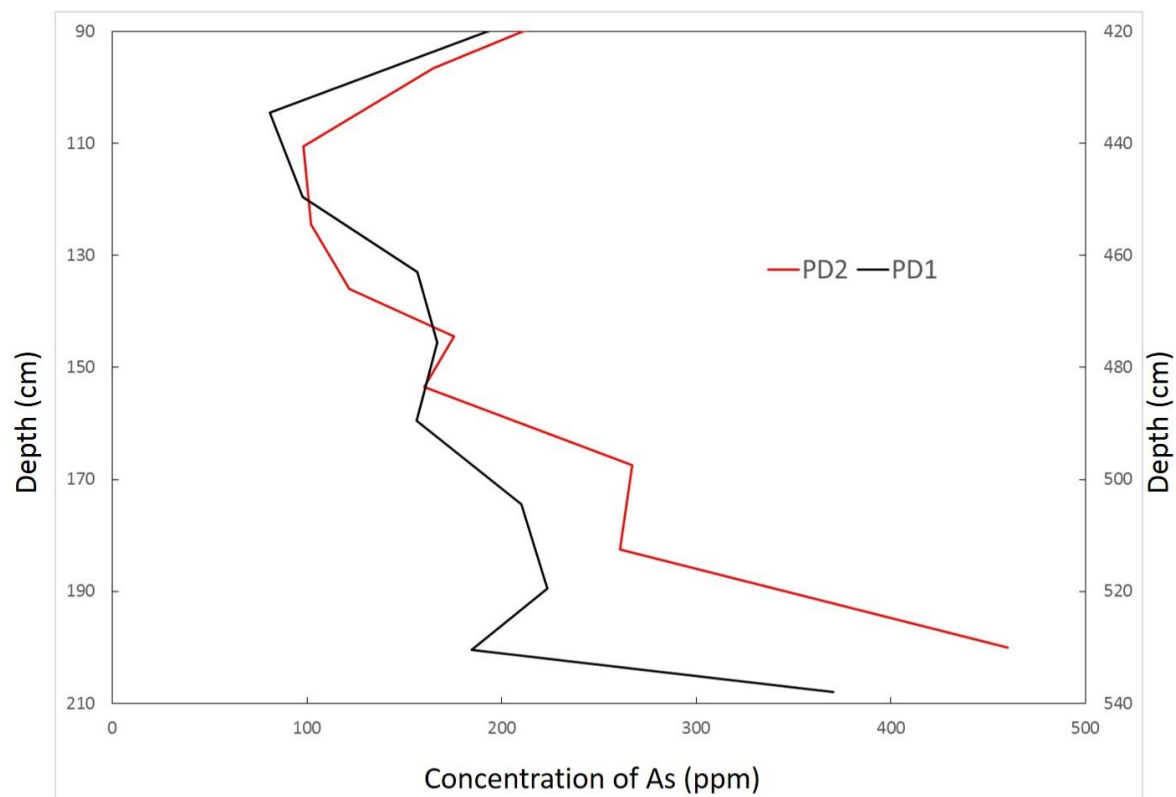
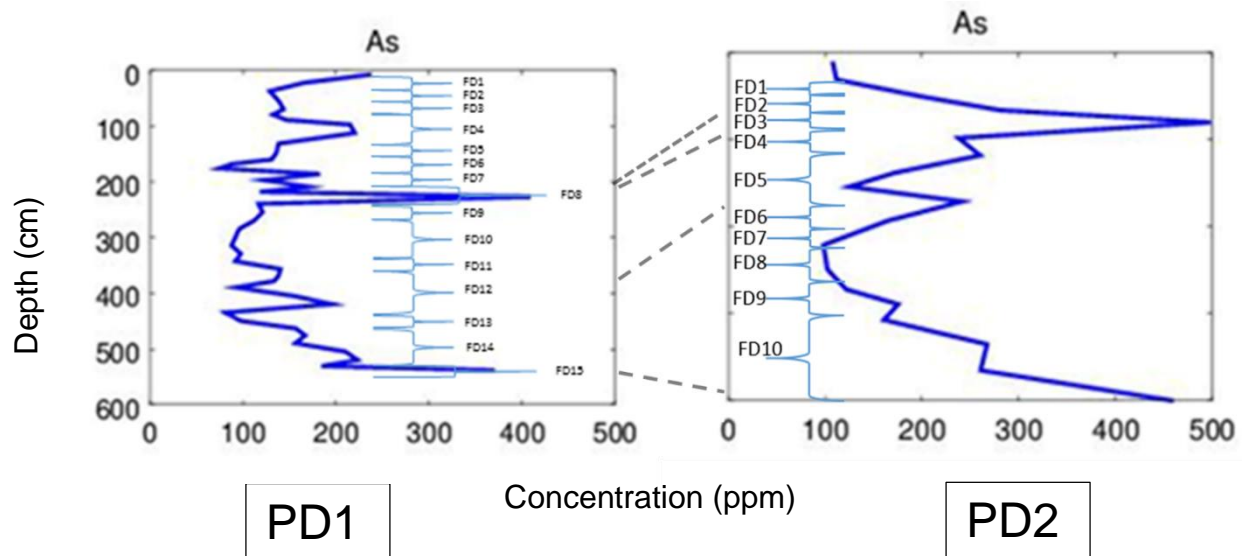


Figure 18. Flood deposits are correlated between PD1 and PD2. PD1-FD8 is correlated to PD2-FD3 on the basis of the peak for As (shown above), Cd, Co, Cu, Sr, and Zn. Similarities of As concentrations for the lower portions of the stratigraphic sections at PD1 and PD2 (Cd, Co, Cu, Sr, and Zn are similar though not shown). This results in the correlation of PD1-FD12 to PD2-FD5, PD1-FD-13 to PD2-FD9, and PD1-FD14 to PD2-FD10.

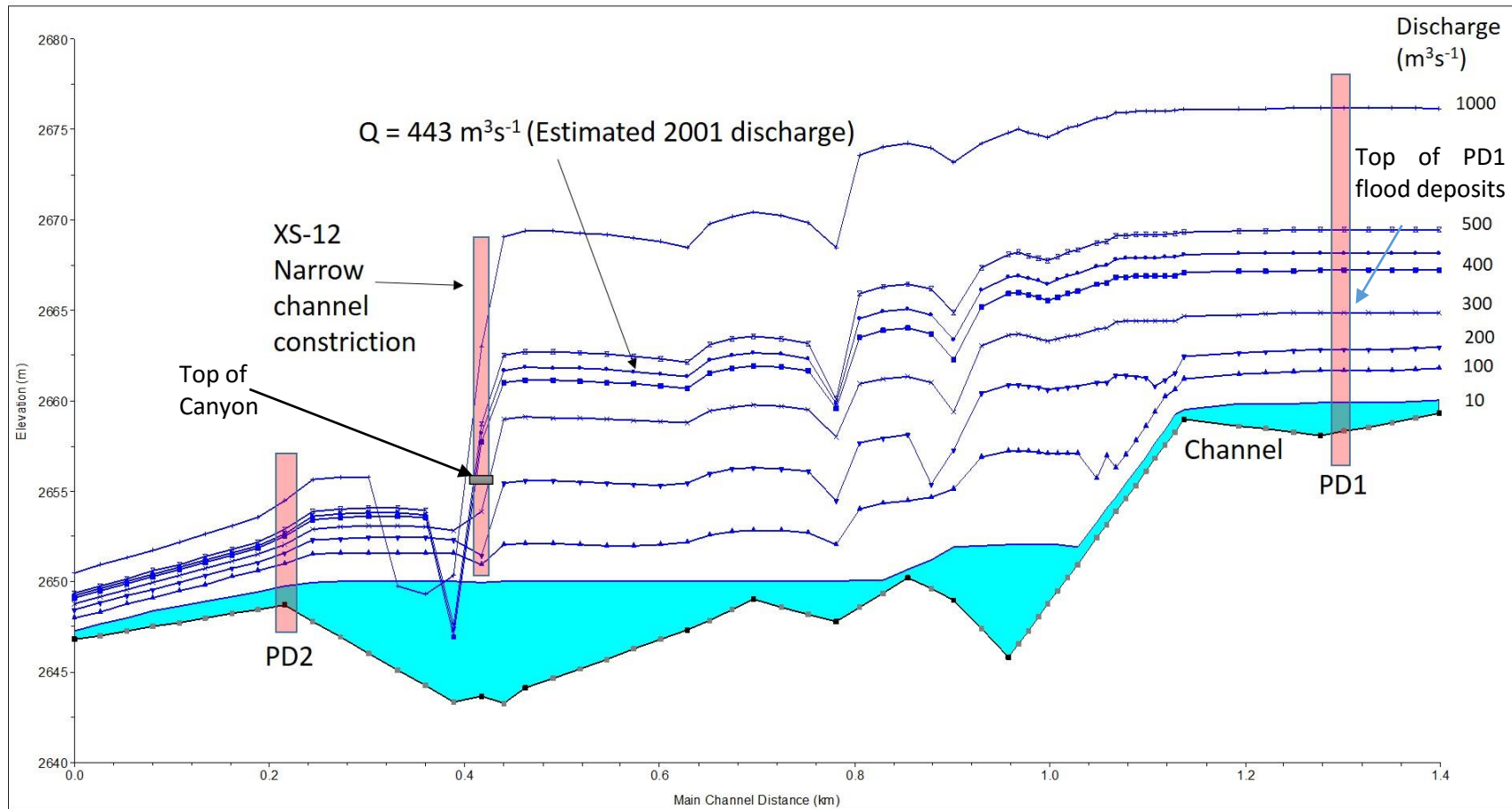


Figure 19. Water surface profiles at various discharges for PD reach. The elevation of the highest flood deposits at PD1 correspond to a discharge of $\sim 310 \text{ m}^3 \text{ s}^{-1}$. At XS-12 there is narrow constriction where wedged sediment is observed near the top of the canyon rim and overbank deposits are observed immediately upstream. The water surface profiles indicate the flow would overbank for a discharge of $443 \text{ m}^3 \text{ s}^{-1}$ (the estimated 2001 flood discharge).

Table 5. Description of Flood Deposit (FD) units at RS1.

- FD9: Continuous series of laminations. Very fine to fine sand. Abundant organic material including small sticks and leaves. Organic debris is parallel to laminae. Section terminates before a lower boundary is observed.
- FD8a: Continuous series of laminations with localized cross bedding. Fine sand with organic debris oriented parallel to laminae. Laminae strike ENE and parallel to tributary while dipping ~2-3° SSE toward valley wall. Abrupt lower boundary
- FD8: More indurated than adjacent units. Fine sand. Laminated with localized cross-bedding. Abrupt lower boundary.
- FD7: Fine sand. Laminated with organic material. Some organic material in top of unit; abundant organic material near bottom of unit.
- FD6: Laminated fine to medium sand. A few cross-beds. No organic material. Abrupt lower boundary.
- FD5: Loose, fine sand. Upper portion of unit is extensively cross-bedded; lower 2 cm of unit is laminated. Unit pinches out toward river. No organics present.
- FD4: Poorly laminated with abundant coarse organic material. Matrix is fine to medium sand. Unit pinches out toward river.
- FD3: Loose fine to medium sand with some laminations. Continuous unit, dipping toward river. A few lenticular granules and rounded pebbles present. Abrupt lower contact.
- FD2: Fine to medium laminated sand. Unit pinches out toward head of alcove and dips more steeply toward river relative to the overlying unit.
- FD1: Indurated, silt to fine sand. Matrix has massive structure with large (4-5 cm) rounded clasts along boundary.
-

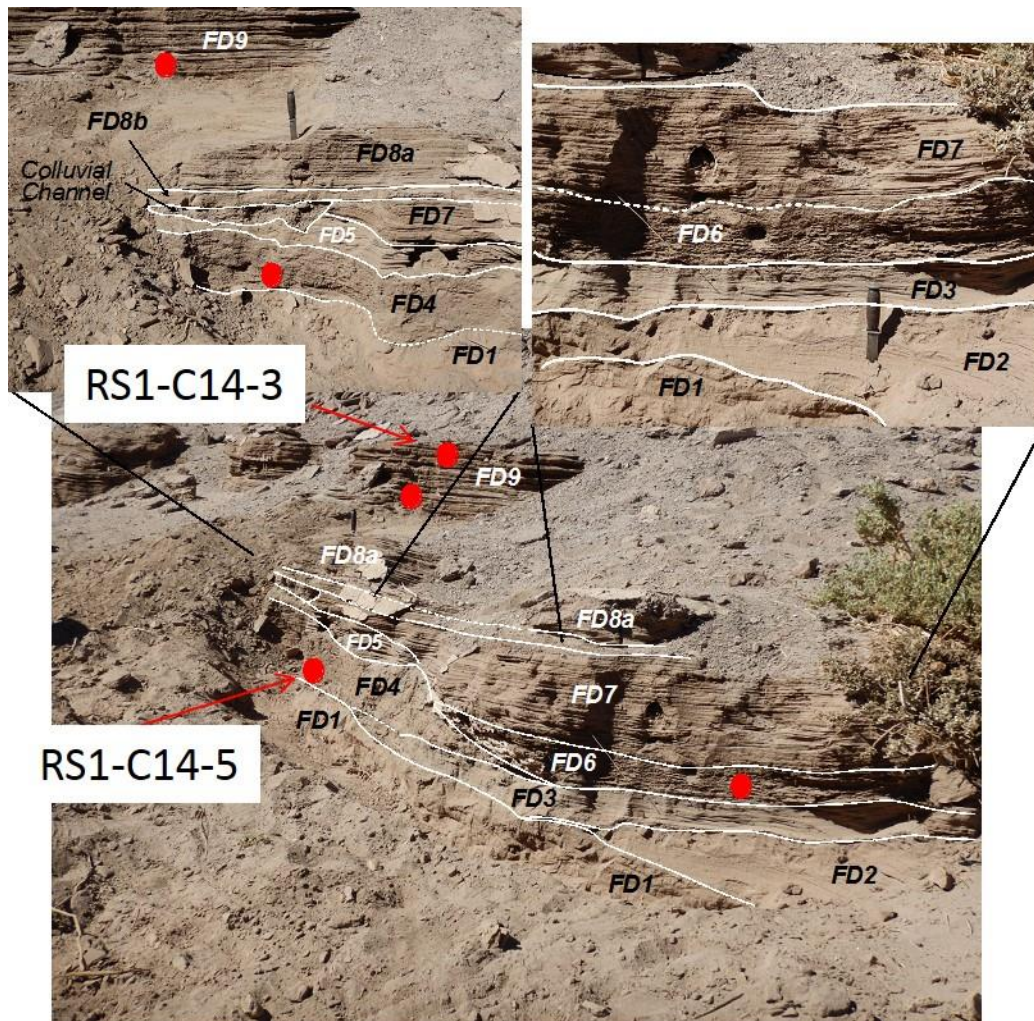


Figure 20. Flood deposit units and location of radiocarbon dating samples at RS1. The entire section measures ~1.2 m in thickness. A total of 10 flood deposits are identified.

Table 6. Radiocarbon age dating

Sample ID	Depth (cm)	Conventional Radiocarbon Age (Years)	2 Sigma calibrated result (95% probability)
RS1-C14-3	20-27	390 ± 30 BP	Cal AD 1455 to 1630 (Cal BP 495 to 320)
RS1-C14-5	46-57	210 ± 30 BP	Cal AD 1655 to 1710 (Cal BP 295 to 240) Cal AD 1720 to 1810 (Cal BP 230 to 140) Cal AD 1835 to 1845 (Cal BP 115 to 105) Cal AD 1855 to 1880 (Cal BP 95 to 70) Cal AD 1930 to Post 1950 (Cal BP 20 to Post 0)
RS2-C14-2	0-14	250 ± 30 BP	Cal AD 1640 to 1680 (Cal BP 310 to 270) Cal AD 1730 to 1800 (Cal BP 220 to 150)
RS2-C14-3	55-70	350 ± 30 BP	Cal AD 1485 to 1650 (Cal BP 465 to 300)

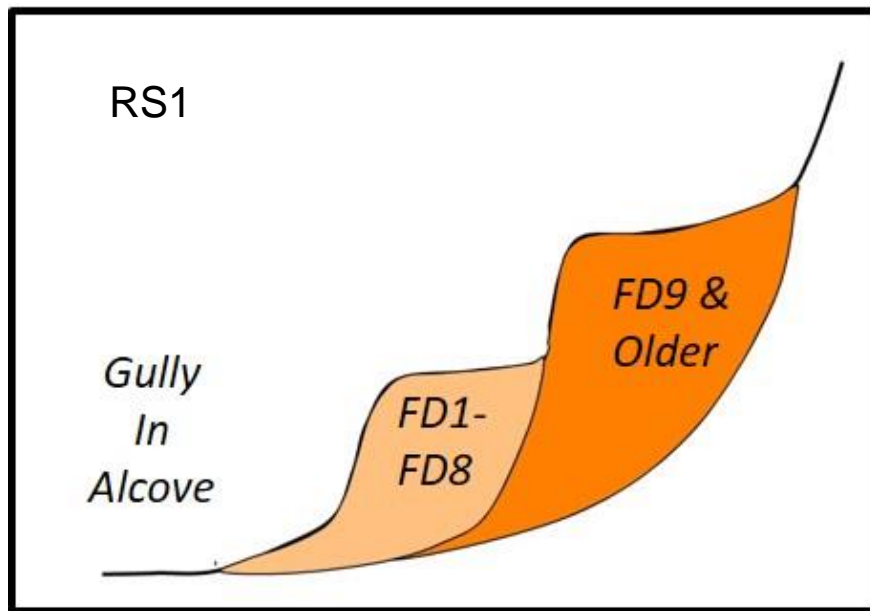


Figure 21. A cartoon depicting the stratigraphic relationship of deposits at RS1. FD1-FD8 are inset into FD9 and possibly older deposits.

Table 7. Sample ID, section number, depth, and flood deposit ID for RS1 samples

Sample ID	Section at Site	Depth (cm)	Deposit
RS1-5	Section 1	0-10	FD9
RS1-4	Section 1	0-20	FD9
RS1-3	Section 1	20-27	FD9
RS1-2	Section 1	27-37	FD9
RS1-1	Section 1	37-45	FD9
RS1-13	Section 2	0-10	FD8a
RS1-12	Section 2	10-18	FD8a
RS1-11	Section 2	18-23	FD8
RS1-10	Section 2	23-30	Colluvial fill
RS1-9	Section 2	30-36	FD5
RS1-8	Section 2	36-46	FD4
RS1-7	Section 2	46-57	FD4
RS1-6	Section 2	57-62	FD1
N/A	Section 3	0-47	FD7, Not sampled
RS1-14	Section 3	47-54	FD6
RS1-15	Section 3	54-60	FD3
N/A	Section 3	60+	FD1, Not sampled

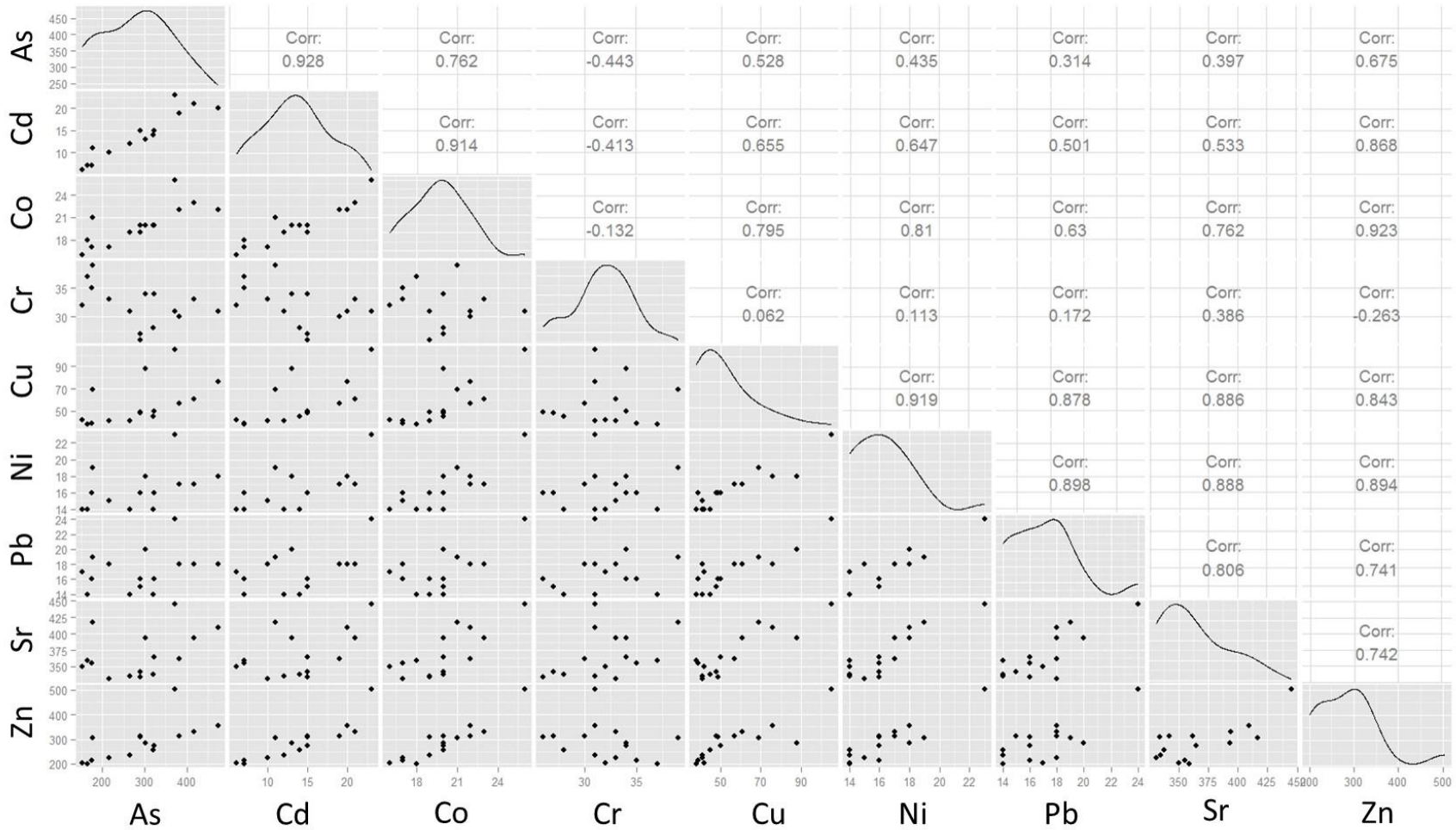


Figure 22. RS1 scatter plot matrix. As and Cd and Co and Zn have high correlation coefficients ($r = 0.928$ and $r = 0.923$).

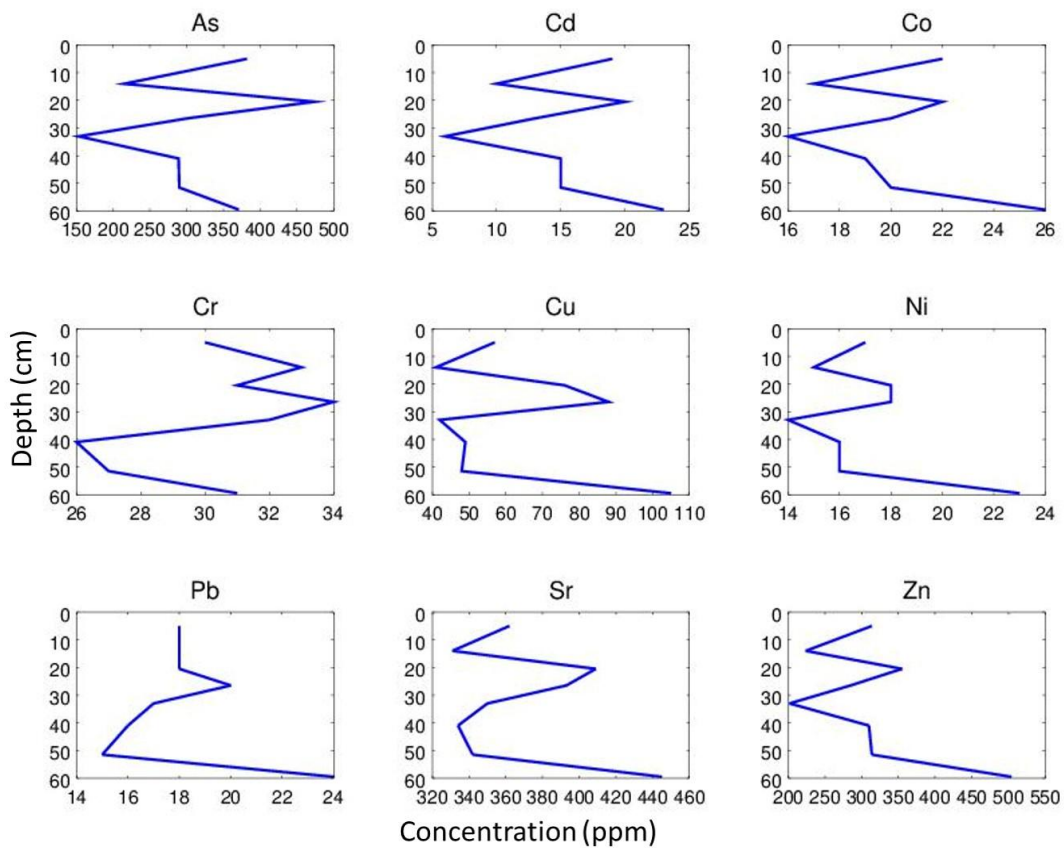


Figure 23. Concentration-depth profile for RS1. At ~14 cm depth there is a sharp decrease in As, Cd, Co, Cu, Ni, Sr, and Zn concentrations. Concentrations of all elements are relatively high at the bottom of the section.



Figure 24. Alcove feature at RS2. Inset of flood deposits units at RS2. The top of the highest deposit is ~14m from the top of the canyon rim.

Table 8. Description of Flood Deposit (FD) units at RS2

FD10: Loose, medium to coarse sand. Unit is continuous across width of alcove.

FD9: Lenticular, discontinuous unit. Laminated, medium sand.

FD8: Laminated, fine sand. Organic debris present and parallel to laminae. Laminae dip toward river. Appears to be small remnant of a larger unit with the remainder eroded. Abrupt lower boundary.

FD7: Loose, medium to coarse sand. Pebbles of 5 mm to 2 cm diameter present. Abrupt lower boundary.

FD6: Indurated, tabular shaped unit. Very thinly laminated. Very fine, well sorted sand. No organic debris present. Abrupt lower boundary.

FD5: Indurated. Laminated fine sand with small amount of organic debris. Abrupt lower boundary.

FD4: Distinctly laminated. Very fine to fine sand. Laminae dip toward river. Unit pinches out in NE direction. Distinct, abrupt lower boundary.

FD3: Laminated, fine sand. Abundant organic debris present. Organic debris is composed largely of leaves and occurs parallel to laminae. Laminae strike NE and dip ~10° NW toward head of alcove. Distinct lower boundary.

FD2: Laminated, fine sand. Laminations dip toward head of alcove. Abrupt lower boundary.

FD1: Loose, well sorted, medium sand. Heavily cross-bedded. Section terminates before observing lower boundary.

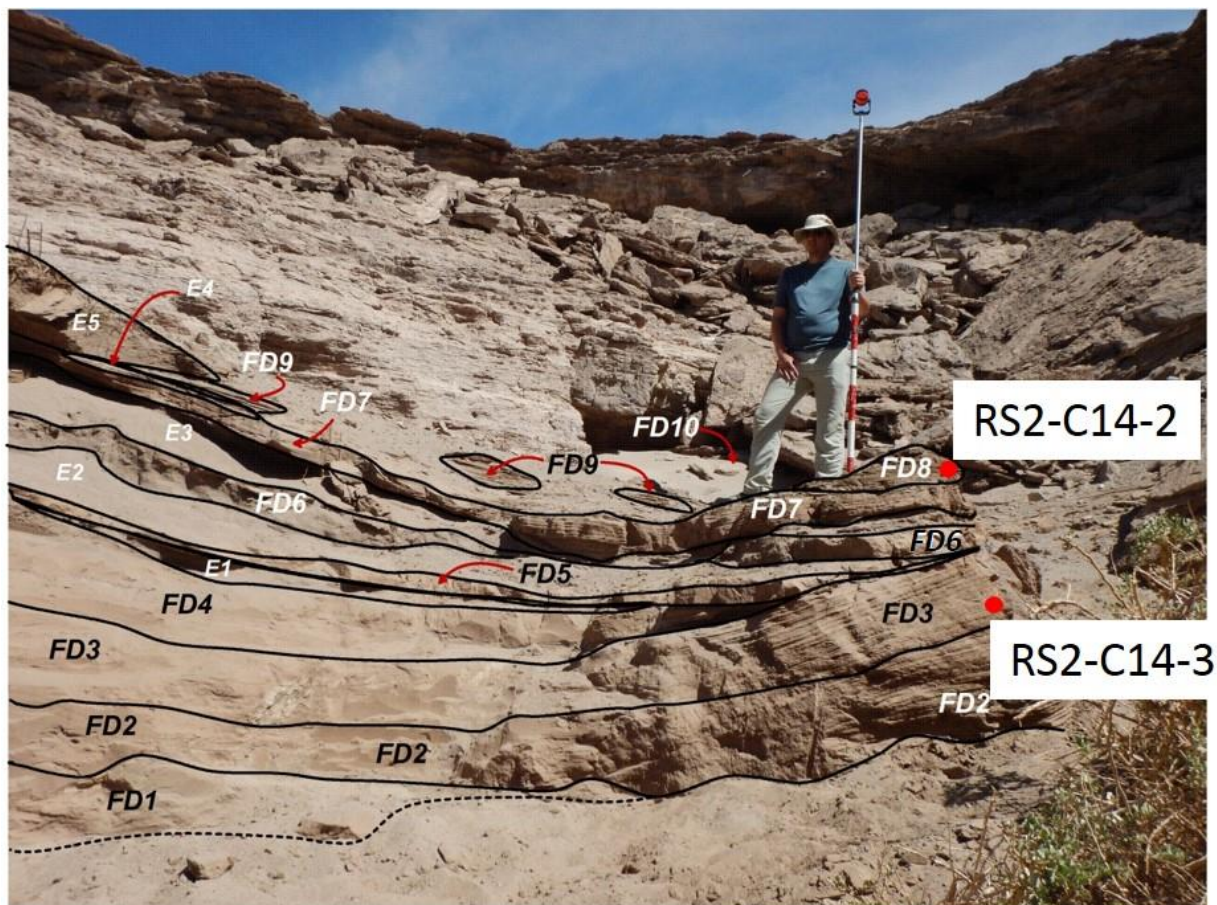


Figure 25. Flood deposits and location of radiocarbon samples at RS2. The section measures ~2 m in thickness. A total of 10 flood deposits and 5 eolian deposits were identified.

Table 9. Chemical sample ID, section, depth, and flood deposit unit for RS2.

Chemical Sample ID	Section at Site	Depth (cm)	Deposit
RS2-15	Section 1	0-7	FD7
RS2-14	Section 1	7-11	Eolian 3
RS2-13	Section 1	11-15	FD5
RS2-12	Section 1	15-22	Eolian 2
RS2-11	Section 1	22-39	FD4
RS2-10	Section 1	39-54	FD4
RS2-9	Section 1	54-69	FD4
RS2-8	Section 1	69-84	FD4
RS2-7	Section 1	84-94	FD3
RS2-6	Section 1	94-101	FD3
RS2-5	Section 1	101-116	FD2
RS2-4	Section 1	116-126	FD2
RS2-3	Section 1	126-134	FD2
RS2-2	Section 1	134-155	FD1
RS2-1	Section 1	155-175	FD1
RS2-21	Section 2	above 0	FD10
RS2-20	Section 2	0-14	FD8
RS2-19	Section 2	14-24	FD7
RS2-18	Section 2	24-34	FD6
RS2-17	Section 2	34-55	FD3
RS2-16	Section 2	55-70	FD3

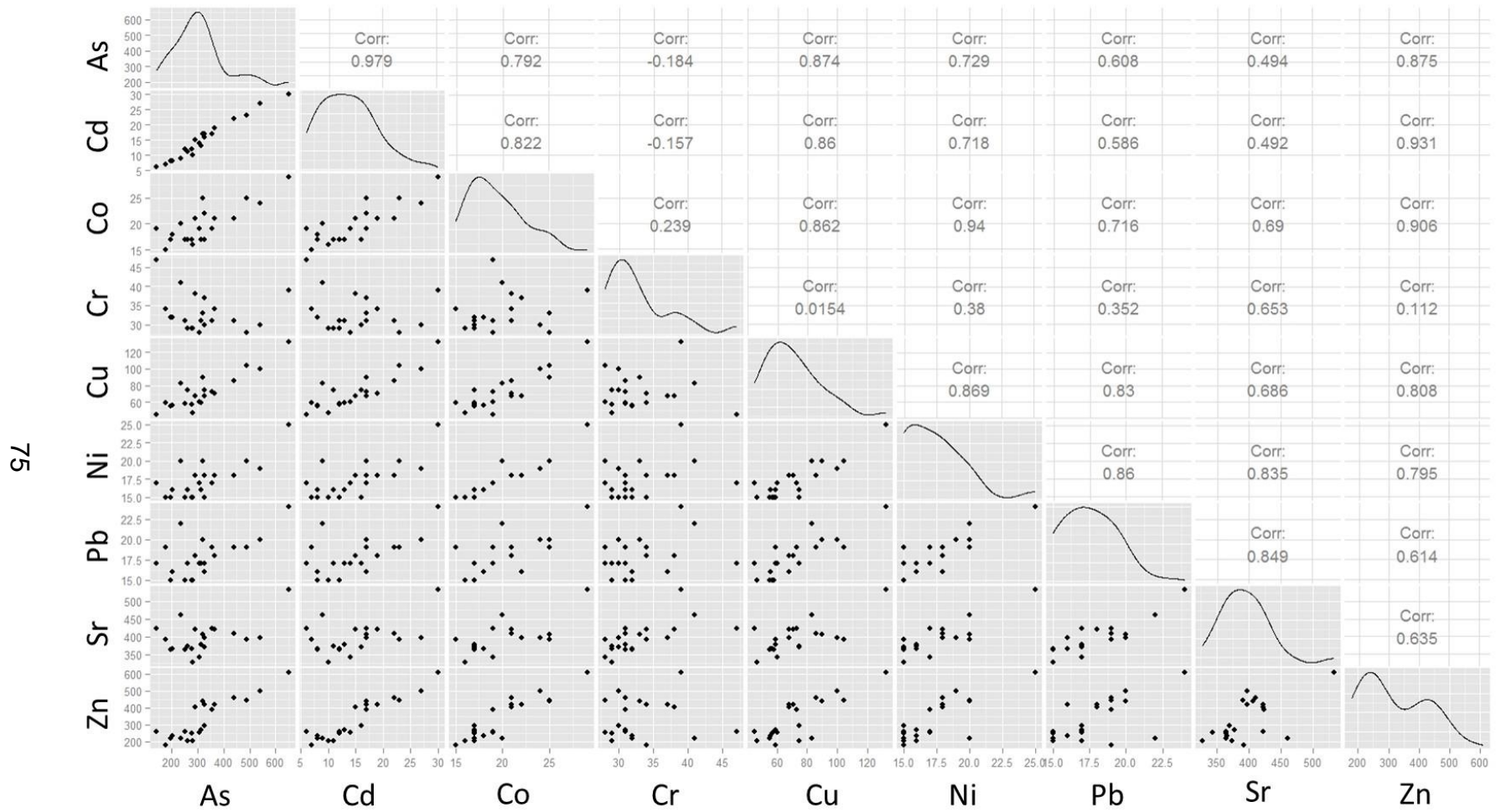


Figure 26. RS2 scatterplot matrix. As and Cd have the highest correlation coefficient ($r = 0.979$).

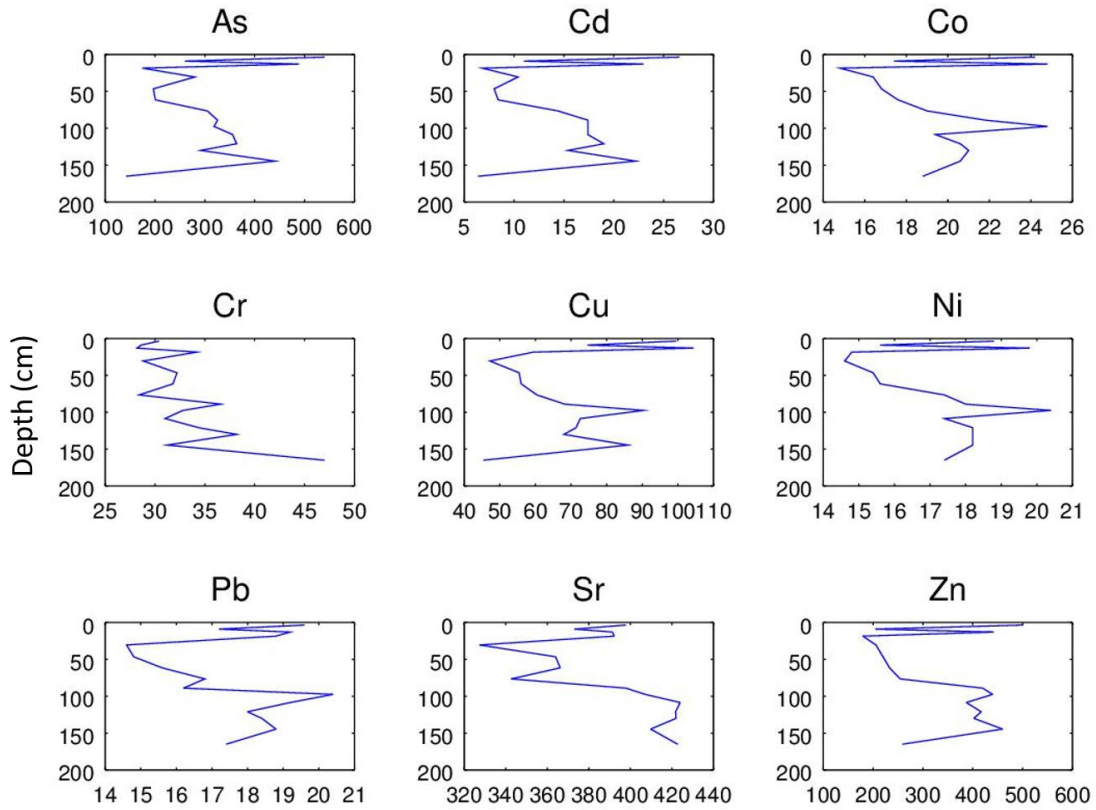


Figure 27. Concentration depth profile for RS2. Concentrations of all elements other than Cr are highest at the top of the profile and correspond to FD6.

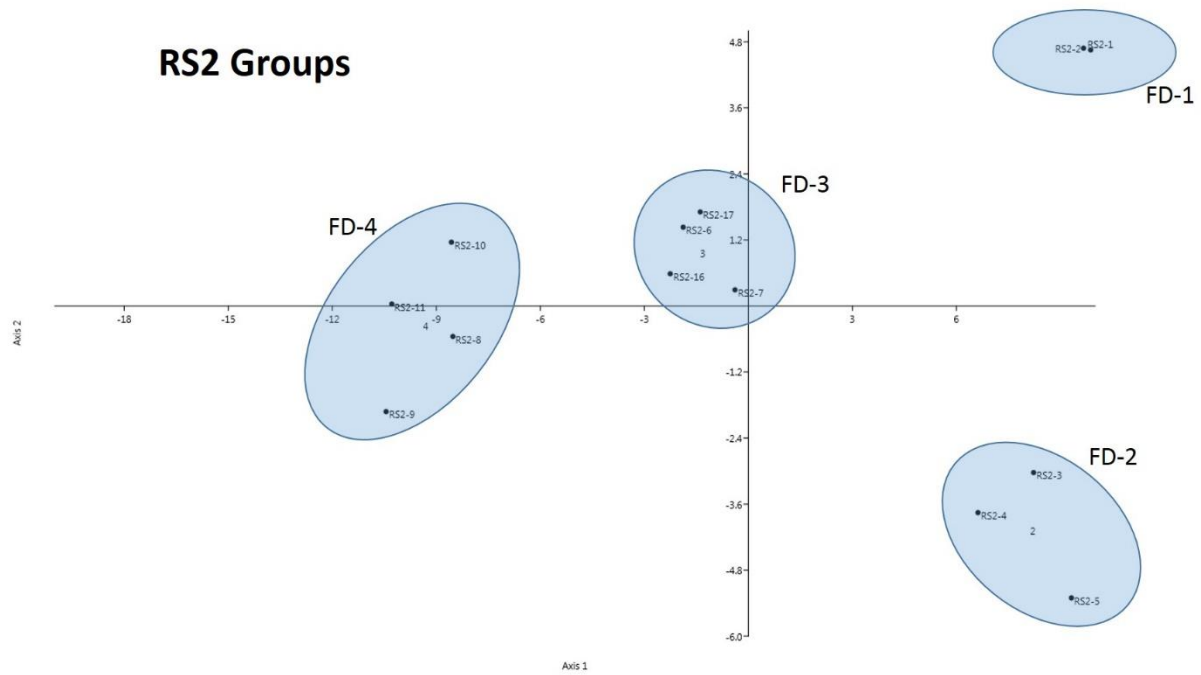


Figure 28. Bivariate plot representing the subspace created by linear discriminant analysis for selected elements and samples at RS2. Flood deposits FD-1 and FD-2 are separated best by the first discriminant function (Axis 1) while deposits FD-2, FD-3, FD-3 and FD-4 are all well separated by the second discriminant function (Axis 2). Ellipses are intended to provide an interpretation of groups rather than confidence intervals of the groupings.

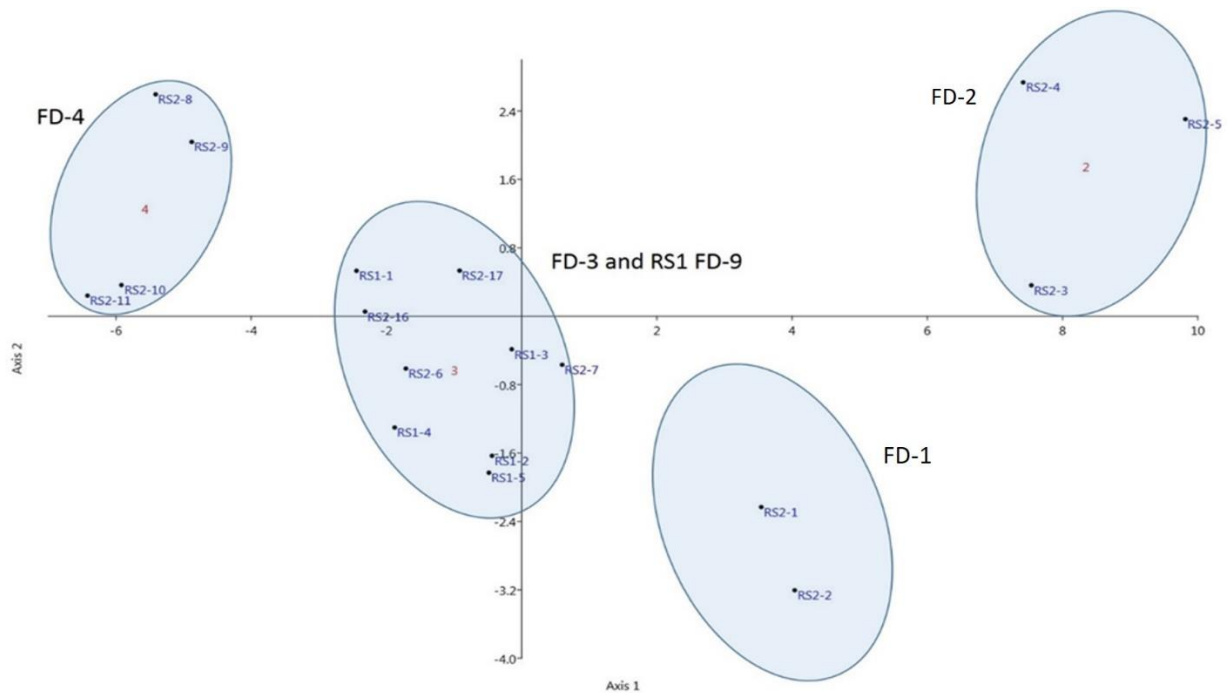


Figure 29. Bivariate plot representing the subspace created by linear discriminant analysis for selected elements and samples at RS2 and RS1 FD-9. RS1 FD-9 samples were assigned to the RS2 FD-3 group based on the results of correlation by radiocarbon dating. Groups are well separated and RS1 FD-9 deposits group into RS2 FD-3 reasonably well. Ellipses are intended to provide an interpretation of groups rather than confidence intervals of the groupings.



Figure 30. Mouth of the drainage between the PD reach and RS reach. This drainage has a different headwaters area which likely alters the geochemical signature between the two reaches. This prevents correlation of flood deposits between the two reaches based on chemistry.

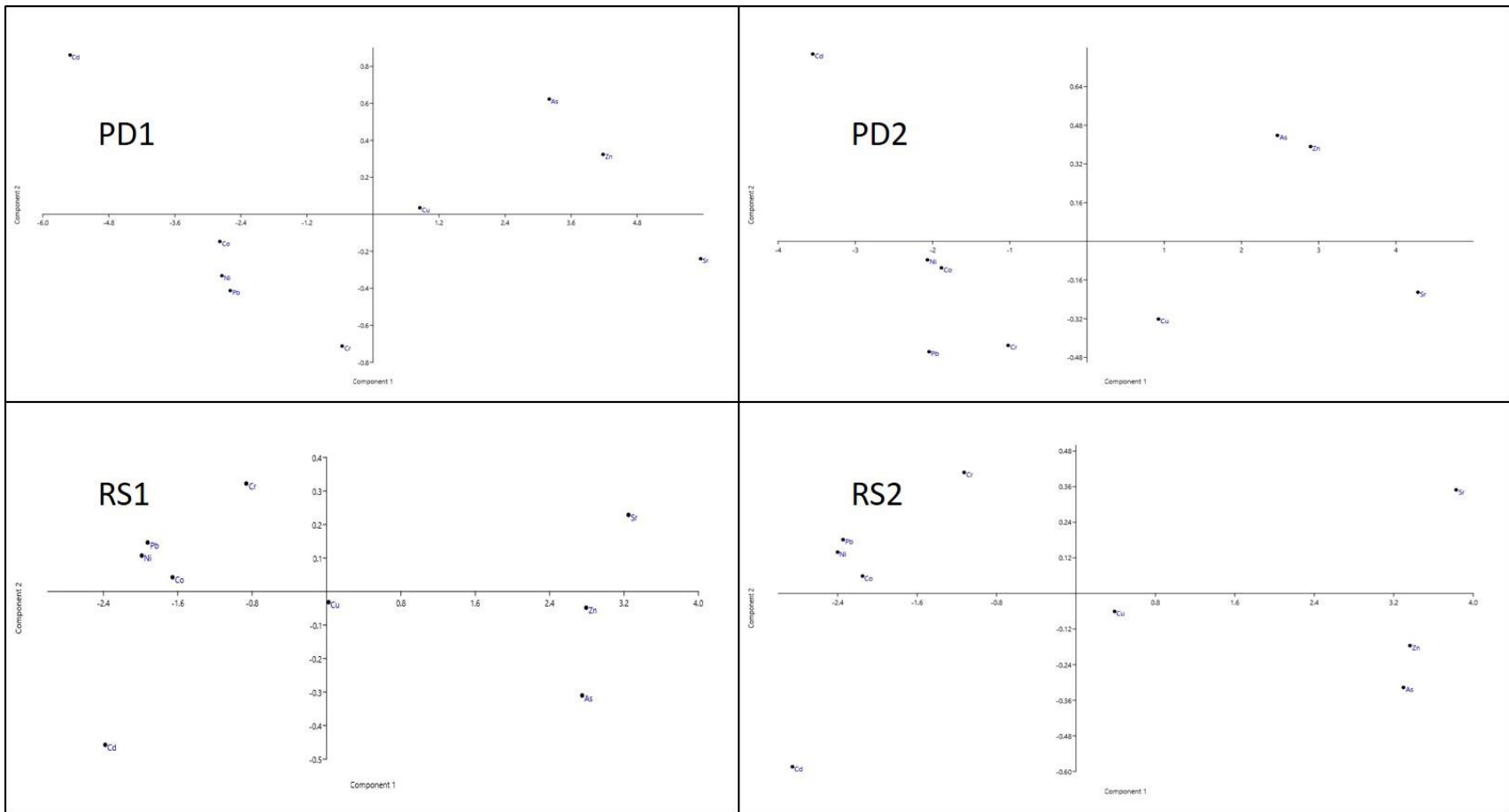


Figure 31. PCA analysis of elemental concentrations for selected elements for each of the individual sites (PD1, PD2, RS1, and RS2). PD1 and PD2 exhibit a similar geochemical signature. RS1 and RS2 also exhibit a similar geochemical signature. However, the geochemical signature between the two reaches appears to be different. This is a reflection of the input from the drainage between the two reaches which has a different headwaters area.

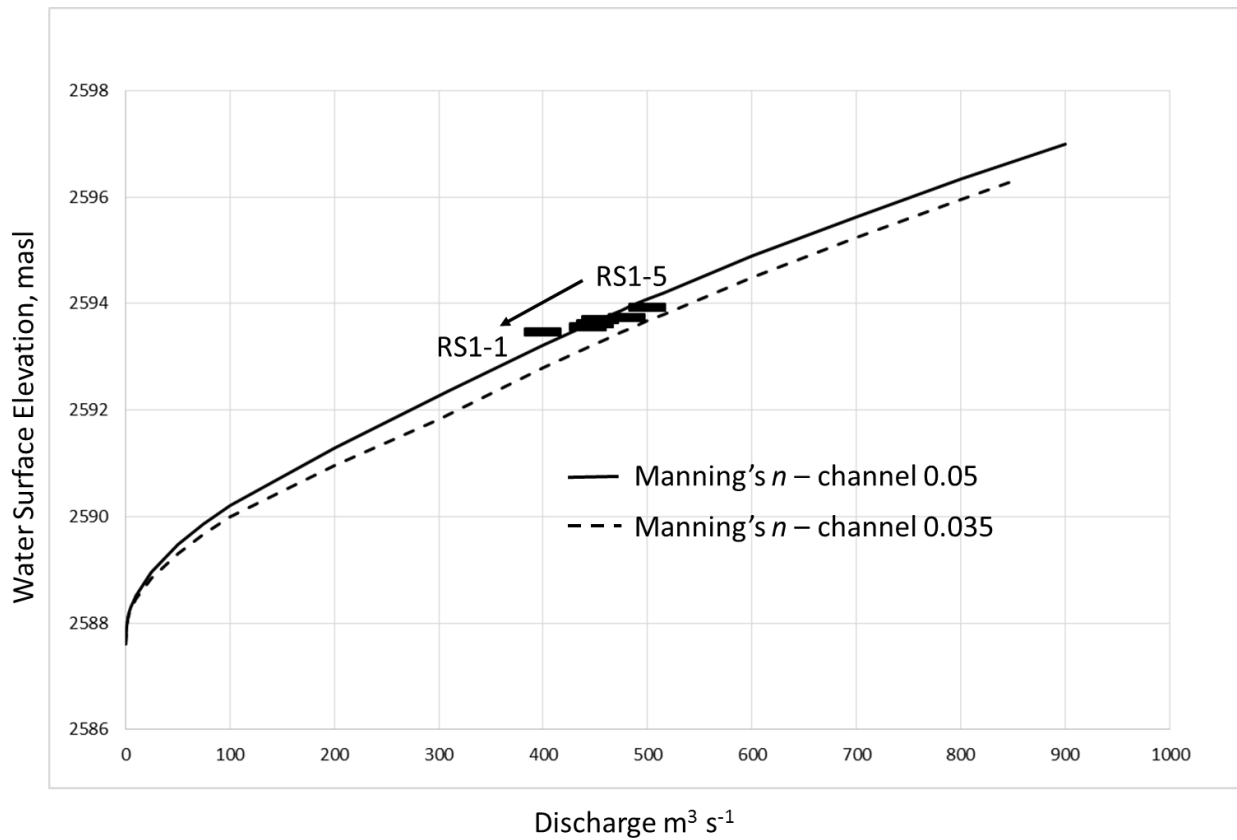


Figure 32. Rating curve for the cross section at RS1 calculated using Manning's n roughness coefficients of 0.05 (solid black line) and 0.035 (dashed black line) for comparison. Elevation and determined discharge for Samples RS1-1 through RS1-5 are depicted as black rectangles. The first scenario which uses a Manning's n of 0.05 fits the slackwater deposit data better.

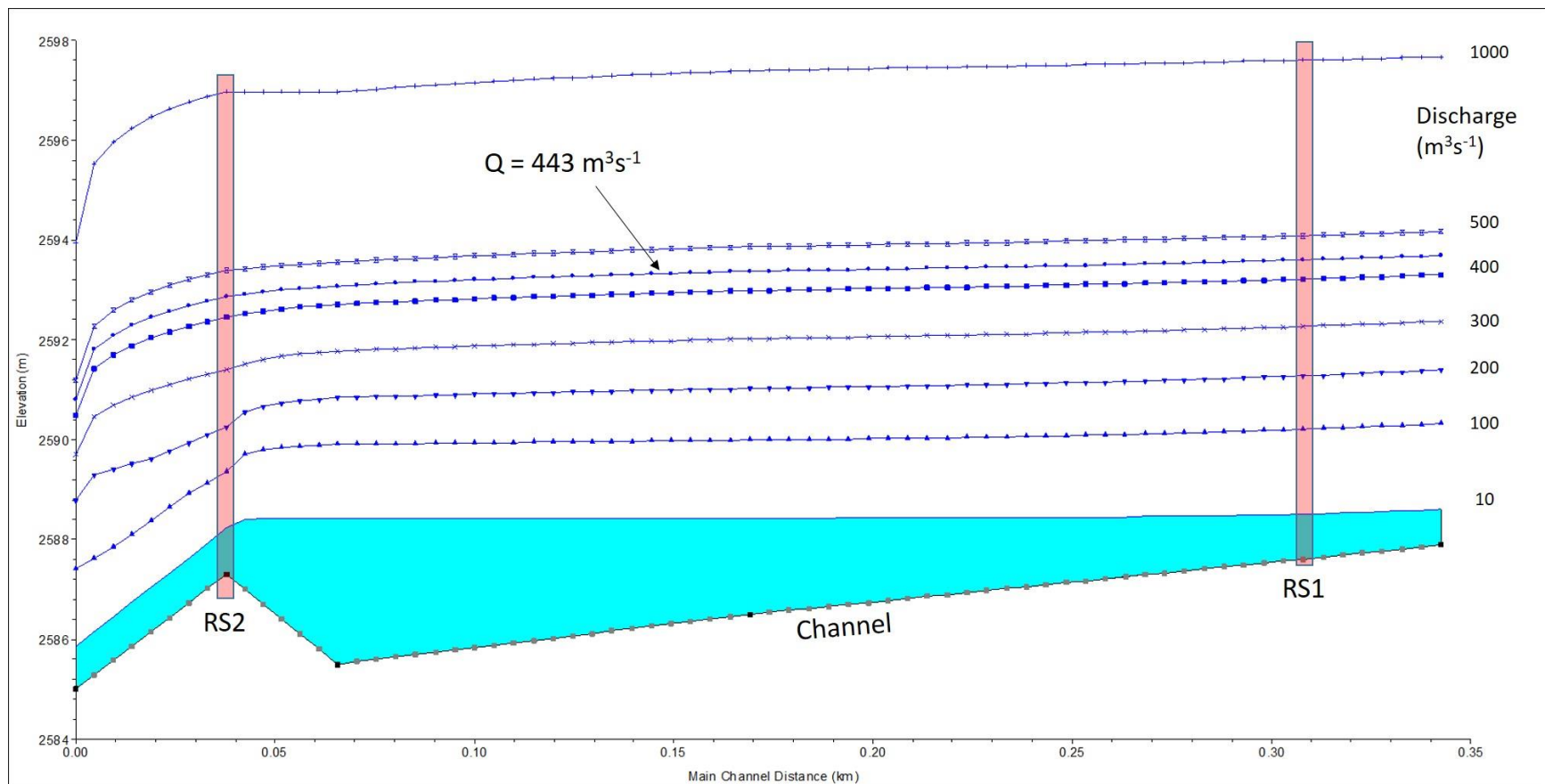


Figure 33. Water surface profiles for RS reach for varying discharge. The water surface profile is much smoother for this than the PD reach indicating the absence of critical flow and reflecting the relatively consistent width of the reach with no narrow constrictions in the channel. The water surface profile for the estimated flow of the 2001 flood ($443 \text{ m}^3\text{s}^{-1}$) is pointed out with an arrow.

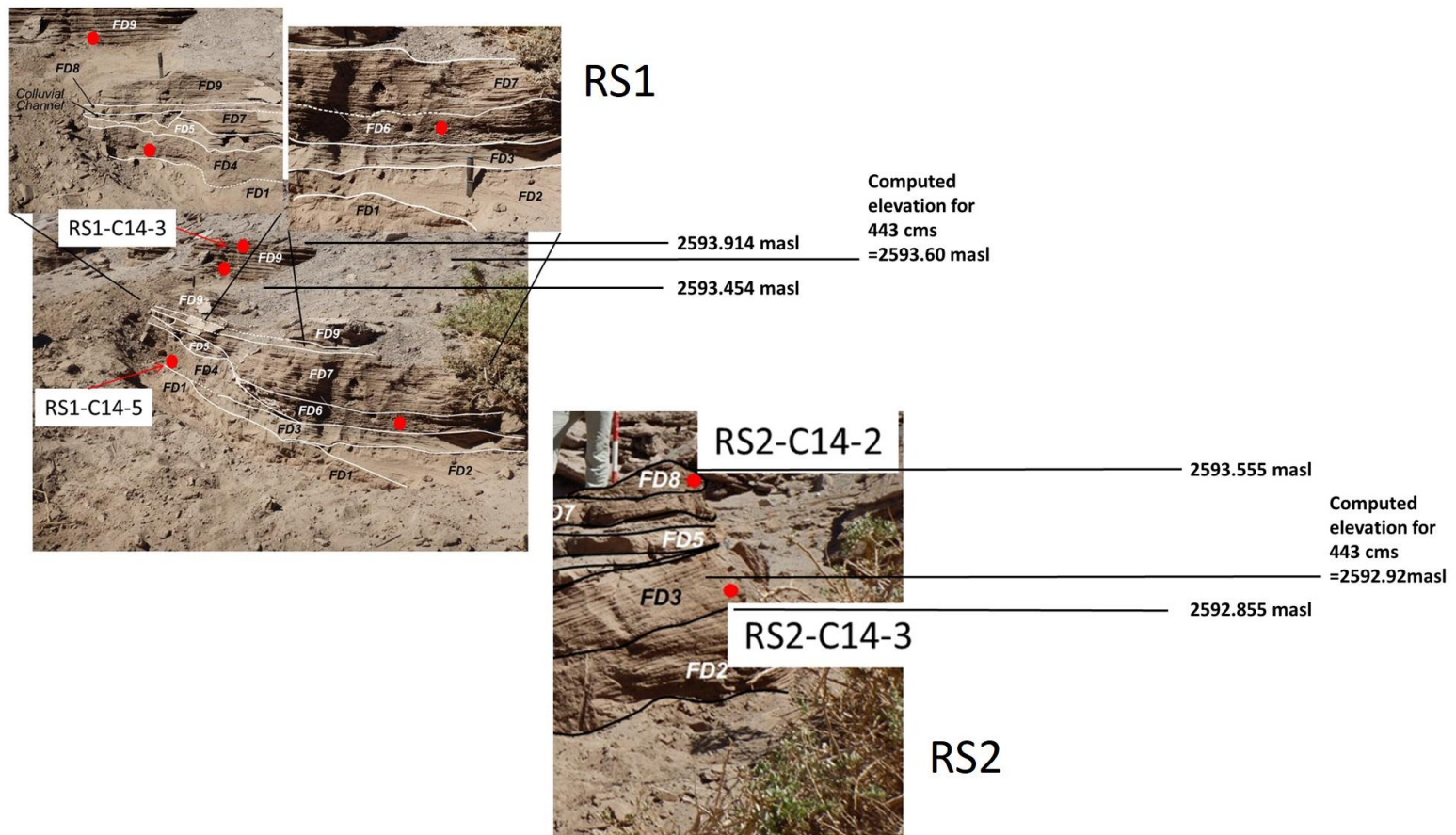


Figure 34. The computed elevation of the water surface profile for a discharge of $443 \text{ m}^3\text{s}^{-1}$ (the estimated 2001 flood discharge) is shown relative to the position of deposits at RS1 and RS2. The elevation is within the range of RS1-FD9 and RS2-FD3. These two flood deposits are correlated by both age dating and chemostratigraphic analysis. The computed water surface profile elevation also indicates these two deposits should be correlated.

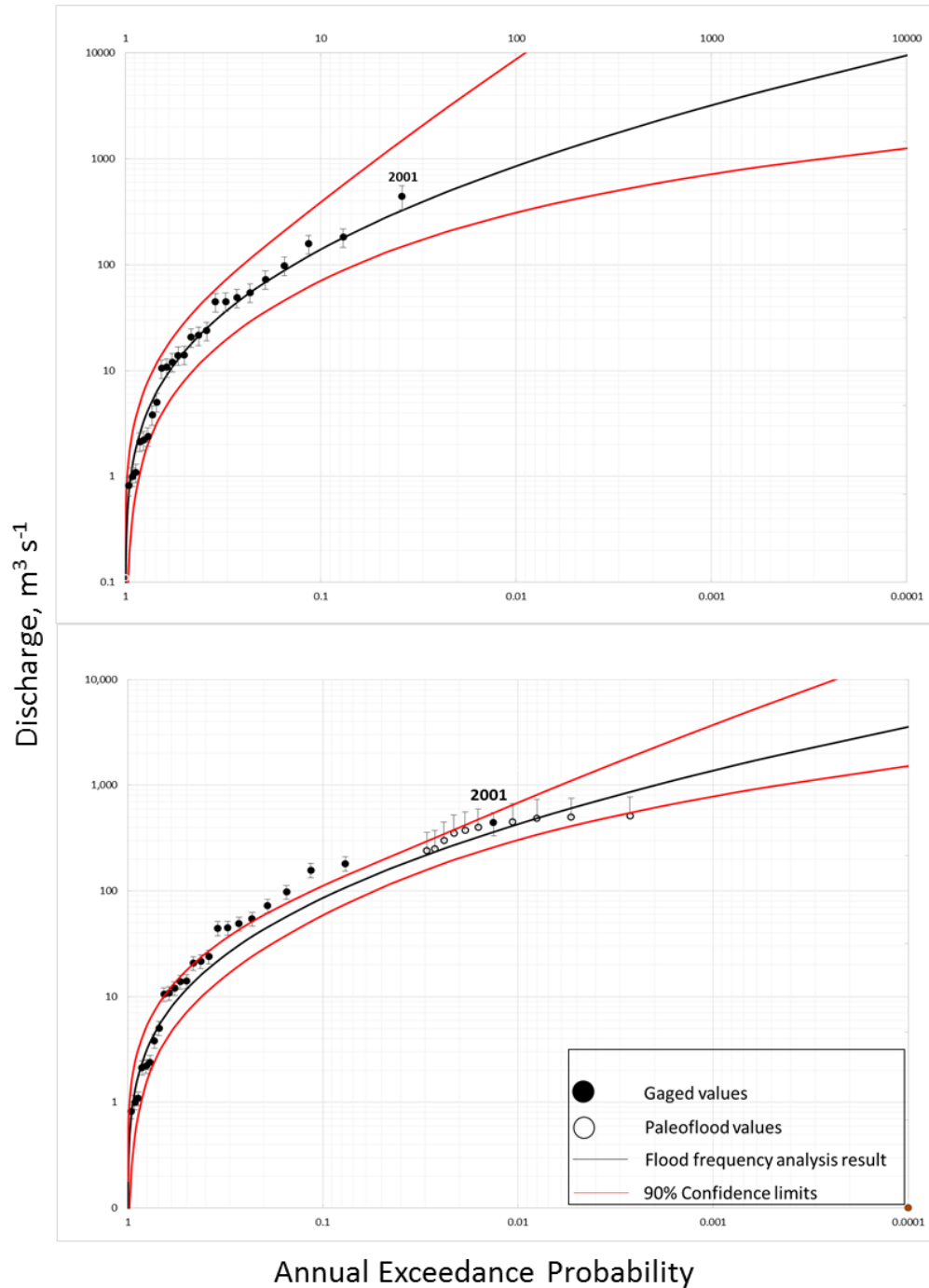


Figure 35. Flood frequency analysis results using the gaged record vs paleoflood and gaged record. The 2001 flood has a recurrence interval of ~40 years with the gaged record only but a recurrence interval of ~100 years when incorporating paleoflood data. Discharge values have an uncertainty of $\pm 25\%$ for the gaged record and an uncertainty of $+50\%$ for the paleoflood record. An annual exceedance probability of 0.01 is equal to a 100-year recurrence interval.

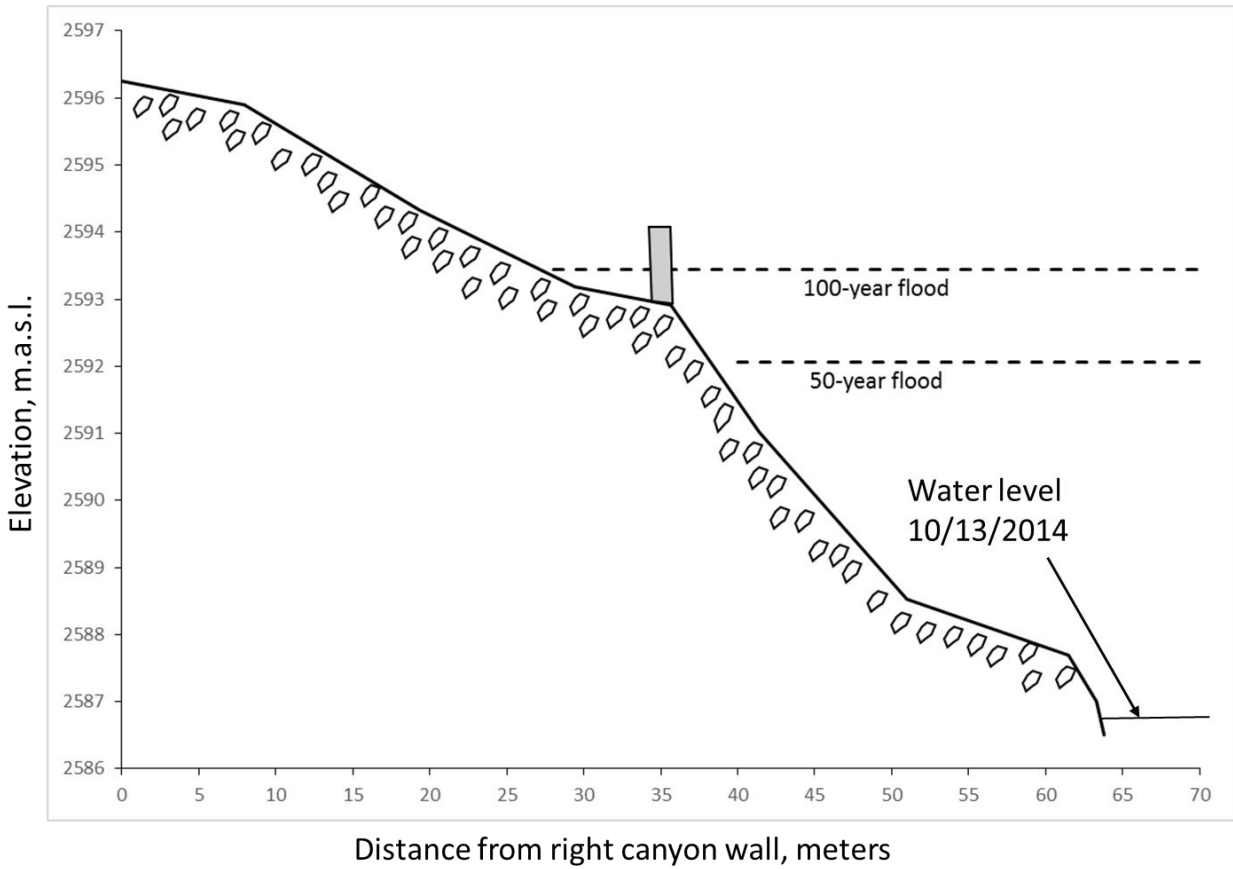


Figure 36. Partial cross section of computed water surface elevations for the 50-year recurrence interval (RI) and 100-year RI flood relative to RS-1 slackwater deposits. The 50-year RI flood discharge is $283 \text{ m}^3 \text{ s}^{-1}$ and the 100-year RI flood discharge is $429 \text{ m}^3 \text{ s}^{-1}$ while the difference in elevation of their water surface is 1.54 m.

CHAPTER FIVE: DISCUSSION

Utilization of Chemostratigraphic Methods

This study was designed to further understanding of hydrology of the Rio Salado through application of paleoflood analysis using slackwater deposits. The magnitude of an event was determined using water surface profiles generated by the commonly applied step-backwater method (Baker, 2008; O'Connor and Webb, 1988). To accurately determine the discharge that produced a geologically defined water surface profile, step-backwater methods require correlation of deposits or paleostage indicators within a reach. In other words, it is necessary to correlate paleoflood units deposited during a specific event between sites where they are preserved to determine the height of the water at that particular site along the reach.

Correlation of paleoflood deposits between sites is complicated by a number of factors, including differences in preservation along the channel. Deposits observed at one site may be missing from others due to variations in depositional settings or the erosion of sediments during subsequent events. Thus, the paleoflood record preserved at a given site often reflects only part of the river's entire flood history.

Correlation is generally based on deposit sedimentology and stratigraphic position, elevation of the deposit above the channel, and the age of the deposit. Of these parameters, flood deposit age is the most important and reliable parameter. Reliable age dating of deposits is not only an effective tool in determining the sequence of deposition, but is also key in flood frequency analysis and establishing recurrence intervals of floods (Thorndycraft et al., 2005).

Most studies to date have relied on radiocarbon dating techniques to determine the age of deposits (Baker, 1987). Radiocarbon dating is based on the amount of ^{14}C contained within a sample of organic material. ^{14}C is produced by the continual bombardment of ^{14}N in the atmosphere by cosmic rays. ^{14}C , however, is unstable and decays to ^{14}N at a constant rate described by its half-life, estimated to be 5730 ± 40 years. A certain amount of ^{14}C , along with ^{12}C , is incorporated in CO_2 , which allows both isotopes to be accumulated in plants until an equilibrium is reached with the atmosphere; animals also accumulate ^{14}C as they consume organic matter. Upon death ^{14}C replenishment ends and its levels within the organic materials decline as it decays to N. Thus, the time since the plant or animal died can be determined provided that the initial $^{14}\text{C}:^{12}\text{C}$ ratio and the decay rate are known. Interestingly, the true half-life of ^{14}C is not used to determine the age of an organic carbon bearing substance. Rather, the half-life of ^{14}C originally determined by William Libby of 5568 years is used by convention to keep all of the radiocarbon dates which have been determined since the 1950s consistent. For a larger number of studies, uncalibrated ages can be used, in which case the dates are reported in years before present (YBP) where the present is set at 1950 A.D. (again established by Libby).

The abundance of laminated organic material in many of the flood deposits found along the Rio Salado makes radiocarbon dating a viable age dating solution; however, complications can arise with the use of radiocarbon dating (both here and elsewhere). For example, it was originally assumed that the production of ^{14}C was a constant, but the radiocarbon dating of tree rings (the age of which is precisely known) showed that it was not. Variations in ^{14}C production can be caused by a range of factors including

changes in solar activity, the geomagnetic flux, fluctuations in CO₂ uptake by the oceans and human activity (Brown, 1997). As a result, the determination of age in terms of calendar dates requires a calibration process which is conducted on a regional basis using such factors as tree rings, dated marine sediments, and ¹⁴C/U-Th dated corals (Stuiver et al., 1998; Smol, 2002). For organic materials (and the deposits that they are contained in) less than about 200 years, a large amount of uncertainty is associated with the process of determining the calendar age of materials as the radiocarbon age (given in YBP) may intercept the calibration curve at multiple points (Haas and Doubrava, 1998). In other words, multiple ages are possible. For the present study, radiocarbon sample RS1-C14-5 which corresponds to the RS1-FD4 deposit has a measured radiocarbon age of 210 ± 30 YBP. However, converting the age of the unit into calendar years results in 4 possible dates because the measured ¹⁴C value intercepts the calibration curve at 4 points (Figure 37). As a result, multiple calendar ages ranging from 1655 AD to post 1950 AD are possible. Even in instances where the radiocarbon age intercepts the calibration curve at only one point radiocarbon dating methods have an uncertainty of ± 30 years or more. As a result, it is possible, if not likely, that the determined age of flood deposits dated between sites will overlap, making it difficult to effectively correlate units on the basis of age alone.

Radiocarbon age dating is considered most applicable for slackwater deposits between ca 300 and 55,000 years BP, radiocarbon dating may not be the best age dating option for these flood deposits (Dezileau et al., 2014). Prior to the results of the age dating, it was hypothesized that the majority of slackwater deposits along the Rio Salado would be on the order of 500 to 1000's of years old, which would have made

radiocarbon dating a better age dating solution. Other possible age dating techniques include Optically Stimulated Luminescence (OSL), ^{210}Pb , and ^{137}Cs . Although these methods are possibly better suited for dating more recent sediments, they are ultimately plagued by the same kind of age range uncertainty associated with radiocarbon dating. As a result, this study sought to explore the use of chemostratigraphic methods to correlate flood deposits.

The approach used here was to sample individual flood deposits identified in the field using stratigraphic methods and descriptions. The tested hypothesis was that sediments associated with a specific flood would exhibit a unique geochemical signature that differs from other previous or subsequent floods, and the signature of the deposited material would be similar along the channel. To test the hypothesis, differences in unit geochemistry were examined within a stratigraphic section, between sections of a given reach, and between reaches.

The analysis was hindered by the fact that multiple samples were not collected from some flood units. This shortcoming was the result of the time available to collect the samples and the costs involved in shipping samples. However, future analysis should ensure there are a sufficient number of samples collected from each unit to allow for detailed statistical analysis. One guideline which might be used is that the sample size of the smallest group should exceed the number of factors (elemental concentrations) used in the discriminant analysis. If 9 factors were retained (as was the case for this study), each flood deposit would need at least 10 samples collected from it. As an example, that would have required the collection, shipping, digestion, and ICP-OES analysis of ~450 samples. Because of the large number samples needed, a more

efficient method for elemental analysis of flood deposits used in this context would be analysis by portable x-ray fluorescence (pXRF). Using pXRF, samples could be analyzed in the field without the need for shipping or digestion. While pXRF has disadvantages in determining elemental concentrations relative to ICP-OES (Hunt and Speakman, 2015), the advantage of analyzing many more samples while in the field would be very useful for statistical methods which require a large number of samples.

In spite of the data limitations, it appears that within a stratigraphic section, chemical variations which describe individual flood units exist. Such differences are demonstrated within the concentration depth profiles for a stratigraphic section where distinct peaks (increasing or decreasing concentrations) are associated with individual flood deposits (i.e. the sharp peak in As, Cd, Co, Cu, Ni, Pb, Sr and Zn at ~50 cm depth in the PD1 profile is associated with PD1-FD8). Distinct geochemical signatures of individual flood units were also shown to exist more quantitatively using statistical methods. For example, flood deposits FD1, FD4, FD9, and FD10 at section PD1 are well characterized and distinguished from each other based on the results of the LDA analysis.

It also appears correlations between unique flood deposits preserved at different sites may exist within a reach. Take, for instance, the possible geochemical correlations of flood units that were made using concentration depth profiles at PD1 and PD2. Specifically, PD1-FD8 is likely correlated with PD2-FD3 based on the similarity of the unique elemental concentrations for those two flood deposits. Other potential correlations between PD1 and PD2 also were made on the basis of the concentration-depth profiles (see results section), and by means of statistical analyses. With regards

to the latter, correlation of flood deposits at RS1 and RS2 were made based on the LDA results which demonstrated that samples from RS2-FD3 group well with the samples from RS1-FD9.

Between reaches PD and RS correlations do not appear possible based on the results of the PCA. According to this analysis, PD1 and PD2 exhibit a similar geochemical signature. RS1 and RS2 also exhibit a similar geochemical signature, again showing that correlation within a reach is possible. However, the geochemical signature between the two reaches appears to be different. This is likely due to the large influx of sediment from a tributary between the two reaches. A broader implication of this finding is that in other field areas where such a tributaries do not exist, correlations of deposits may potentially be made over a very long distance. Conversely, correlation may not be possible even over short distances if there is influx of sediment from a different source area between stratigraphic sections. If the geochemistry of the source area that the tributary drains is similar to that of the source area of upstream deposits, we would not observe a change in the overall geochemistry between the reaches. This is true even in the case of highly localized rain events which may only produce flood flow in the tributary and downstream portions of the main channel.

Overall, the conclusion of this study is that chemostratigraphic correlation methods hold promise, and may significantly improve paleoslackwater analyses. This is exemplified along the Rio Salado by units RS1-FD9 and RS2-FD3 which exhibit overlapping radiocarbon ages. Correlation of RS1-FD9 and RS2-FD3 is also consistent with elevations of these slackwater deposits being matched with modeled water surface profiles for a specific discharge. However, the question remains as to whether these

deposits are from a single event, or two separate events of similar magnitude. Similarity in the geochemical characteristics of RD1-FD9 and RS2-FD3 suggest they were deposited by a single event in the early 1600s. Interestingly, an extreme event occurring in 1607 has been described in historical documents for the region (Magilligan et al. (2007), and identified in paleoflood deposits examined along the coast of Peru (Wells, 1990; Keefer et al., 2001) and along the northern Atacama of southern Peru (Magilligan et al., 2007).

This conclusion is consistent with other studies which have performed chemostratigraphic analysis on alluvial (non-flood) deposits. A study using LDA to identify and correlate sediments at the Cooper's Ferry archaeological site in Idaho, found that discriminant function analysis correctly classified 160 of 160 samples into 7 stratigraphic units (Holcomb, 2014). That same study also had success employing hierarchical cluster analysis to group sedimentary units. Although the sedimentary deposits in that study are not slackwater sediments, they are alluvial and eolian deposits which are similar in nature.

The approach described above assumes a well-established physical stratigraphic framework in which all individual flood deposits have been correctly identified in the field and all chemical samples correctly assigned to those flood deposits. However, indistinct boundaries between massive textured flood units composed of similar grain sizes, discontinuous lenses of sediment, and complex stratigraphic relationships whereby younger deposits can be inset into older ones can make it difficult to identify individual flood units. Sampling at a higher resolution could provide an alternative method which would make it possible to subdivide flood units that appear homogenous in the field into

additional units based on their geochemistry. As an example, chemical samples PD1-27 through PD1-34 were assigned to flood deposit PD1-FD12 and have a range of As concentrations from 81 ppm to 196 ppm (Figure 12). Although none of these concentrations is an outlier based on the definition of the interquartile range, it is possible that more than one flood deposit is represented by these samples. An increased number of chemical samples could make the use of unsupervised clustering techniques like hierarchical clustering possible, thereby aiding in identifying flood deposits on the basis of geochemistry.

Rio Salado Paleoflood History

An understanding of flood frequency and magnitude is a general requirement of designing bridges, culverts, irrigation networks, dams, and other infrastructure within a riverine environment. In the United States the determination of the 100-year flood is of particular importance as most design criteria is predicated on the magnitude and frequency of a flood with this recurrence interval. In addition, recent studies have suggested that large magnitude floods may have had a significant influence on the migration and behavior of ancient societies within the Atacama region by impacting their irrigation and agricultural systems (Manners et al., 2007). Previous studies in arid environments have shown that rare, large magnitude floods also are of particular importance in controlling channel and valley form and in transporting sediment along the river. Furthermore, determining the frequency of large floods within the Rio Loa basin is important because these floods are the primary means by which contaminated sediments are redistributed along the river.

Flood frequency and magnitude relationships are typically determined using gaging station data. Previous studies have demonstrated that such analyses may contain considerable uncertainty when records are less than 100 years in length (Kochel and Baker, 1982). This is particularly true in arid environments where the hydrologic flow regimes are skewed; large magnitude, geomorphically important events have long recurrence intervals (Baker, 1977). Paleoflood reconstruction of past events can be used to extend the length of the flood record and overcome the problem that short term gaging data presents.

There is an exceptional record of flood deposits along the Rio Salado. These deposits have been well preserved and contain an abundance of organic material making them suitable for radiocarbon dating. These deposits allowed for the construction of a preliminary paleoflood record which was used to refine the flood magnitude-frequency relationships determined using gaging station data alone.

Flood frequency analysis was based on 10 paleoflood deposits at RS1 and RS2; the oldest dates to the early 1600's and the youngest has a radiocarbon date of 210 ± 30 YBP, but might be much more recent (post 1950 AD) (the radiocarbon age intercepts the calibration curve at multiple points). The smallest paleoflood had a discharge of $240 \text{ m}^3\text{s}^{-1}$ and the largest paleoflood had a discharge of $515 \text{ m}^3\text{s}^{-1}$. By comparison, the 2001 flood event (the largest during the recent past) had a discharge of $443 \text{ m}^3\text{s}^{-1}$ based on a previous estimate by Houston (2006) and adjusted for increased contributing area.

The flood frequency analysis using the paleoflood data results in flood magnitude and frequency values that are substantially different than those generated using only the gaging station data. For example, using only gaging data, the 100 year flood event

has a discharge of $856 \text{ m}^3\text{s}^{-1}$. The gaging data plus paleoflood data indicates the discharge of the 100 year flood event is $429 \text{ m}^3\text{s}^{-1}$, a reduction of about 50 %. The recurrence interval of the 2001 flood changes from ~40 years based on gaging data only to ~100 years using the gaging data plus the paleoflood data. Houston (2006) had previously estimated the recurrence interval of the 2001 flood to be in the range of 100 to 200 years. This study indicates the 2001 flood is on the lowest end of that estimate. A seemingly obvious implication of this paleoflood analysis is that floods similar in magnitude to the 2001 flood event are likely to have occurred more frequently in the past than previously believed. This does not necessarily mean that these flood events are more likely to occur in the future. Paleoflood analysis is a reconstruction of what has actually occurred in the past and demonstrates what can occur within the system. In order to predict what may occur in the future and to refine design criteria based on potential future flooding, climatic regime processes and the linked hydrology would need to be better understood. This is an interesting and needed area of future work but is beyond the scope of this study.

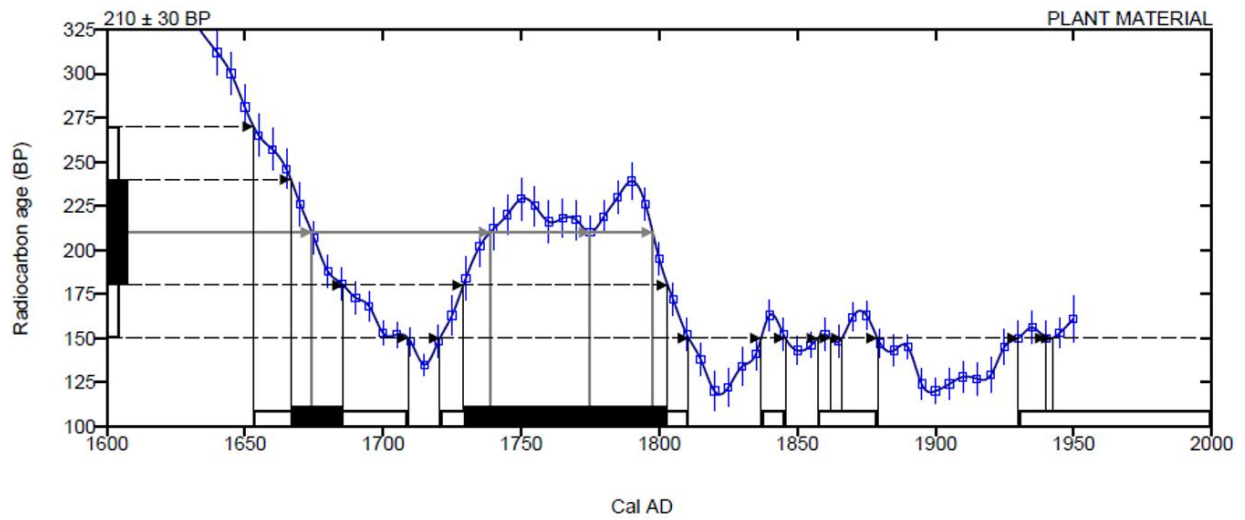


Figure 37. The interception of the radiocarbon age with multiple points along the calibration curve results in a wide range of possible calendar ages for sample RS1-C14-5 which was sampled from flood deposit RS1-FD4. The possible calendar age ranges from 1655 AD to post 1950 AD.

CHAPTER SIX: CONCLUSION

The goal of this research was to apply methods of chemostratigraphy to slackwater deposits along the Rio Salado, Chile in order to enhance paleoflood reconstruction. Furthermore, paleoflood reconstruction and subsequent paleoflood data were used in a flood frequency analysis. This study has shown that chemostratigraphy is capable of interpreting stratigraphy in terms of individual flood deposits and correlating flood deposits along the Rio Salado. Additionally, the paleoflood enhanced flood frequency analysis indicates a flood with a 100 year recurrence interval has a discharge of $429 \text{ m}^3\text{s}^{-1}$, which is about 50% of the discharge calculated using only the gaged record. Also, the recurrence interval for a flood of the magnitude of the 2001 Atacama flood is ~ 110 years.

Through chemostratigraphy, this study was able to potentially correlate four flood deposits at site PD1 with flood deposits at PD2; PD2 is 0.67 km downstream of PD1. Through a combination of radiocarbon dating and chemostratigraphy along a 0.34 km reach of the Rio Salado, this study successfully correlated a flood deposit at RS1 with a flood deposit at RS2. Calibration of the flow model based on this correlation indicates these sediments were deposited by a flood with a discharge of $443 \text{ m}^3\text{s}^{-1}$. A different geochemical signature of slackwater deposits between the PD reach and RS reach was identified by analysis of concentration – depth profiles and principal component analysis. The differing geochemical signature is attributed to a tributary between the two reaches. This tributary was dry at the time of the field work conducted for this study but likely contributes a significant amount of flow and sediment during flood events.

The oldest flood deposit analyzed in this study had a radiocarbon age of 390 ± 30 YBP, while the youngest deposit dated to 210 ± 30 YBP (but is potentially much younger). If, however, the oldest radiocarbon age is correct it would indicate an unusually high number of large floods occurred within a relatively short period of time. Although beyond the scope of this study, this is would be an interesting topic for future research.

Future Work

Perhaps the most important recommendation for future work in this area of study is that more samples be collected from each flood deposit identified in the field. Additional samples from each flood deposit would permit a more rigorous multivariate statistical analysis, including outlier removal and normality testing. A proposed means for collecting more samples from each flood deposit is the use of pXRF for elemental analysis. By using pXRF, samples could be analyzed in the field eliminating the need for expensive shipping of samples and time consuming digestion of samples. This type of analysis could aid in identifying stratigraphy which has been misinterpreted using standard, in-field stratigraphic methods. Once a reliable chemostratigraphic framework has been established, pXRF could also provide a rapid in-field assessment of how new samples fit into the existing framework. This would include the ability to correlate newly discovered flood deposits with known deposits on the basis of which previously established group they are classified with by a predictive model.

BIBLIOGRAPHY

- Baker, V. R., 1977 Stream-channel response to floods, with examples from central Texas. *Geol. Soc. Am. Bull.* 88, 1057-1071. doi: 10.1130/0016-7606(1977)88<1057:SRTFWE>2.0.CO;2
- Baker, V. R., Kochel, R. C., Patton, P. C. & Pickup, G., 1983 Palaeohydrologic analysis of Holocene flood sediments. *Spec. Publ. Int. Assoc. Sediment.* no. 6, 229-239. DOI: 10.1002/9781444303773.ch18
- Baker, V.R., 1987. Paleoflood hydrology and extraordinary flood events. *J. Hydrol.* 96, 79–99. doi:10.1016/0022-1694(87)90145-4
- Baker, V.R., 2008. Paleoflood hydrology: Origin, progress, prospects. *Geomorphology* 101, 1–13. doi:10.1016/j.geomorph.2008.05.016
- Chillrud, S.N., Hemming, S., Shuster, E.L., Simpson, H.J., Bopp, R.F., Ross, J.M., Pederson, D.C., Chaky, D. a., Tolley, L.-R., Estabrooks, F., 2003. Stable lead isotopes, contaminant metals and radionuclides in upper Hudson River sediment cores: implications for improved time stratigraphy and transport processes. *Chem. Geol.* 199, 53–70. doi:10.1016/S0009-2541(03)00055-X
- Chow, V.T., 1959. *Open Channel Hydraulics*. McGraw-Hill, New York.
- Cohn, T., 2012. *User Manual for Program PeakfqSA Flood-Frequency Analysis with the Expected Moments Algorithm*.
- Cudworth Jr., A.G., 1989. *Flood Hydrology Manual*. Denver, Colorado.
- Dalrymple, T., 1960. *Flood-Frequency Analyses* 80.
- Dezileau, L., Terrier, B., Berger, J.F., Blanchemanche, P., Latapie, a., Freydier, R., Bremond, L., Paquier, a., Lang, M., Delgado, J.L., 2014. A multidating approach applied to historical slackwater flood deposits of the Gardon River, SE France. *Geomorphology* 214, 56–68. doi:10.1016/j.geomorph.2014.03.017
- Drew, L.J., Grunsky, E.C., Sutphin, D.M., Woodruff, L.G., 2010. Multivariate analysis of the geochemistry and mineralogy of soils along two continental-scale transects in North America. *Sci. Total Environ.* 409, 218–27. doi:10.1016/j.scitotenv.2010.08.004
- England, J.F., Salas, J.D., Jarrett, R.D., 2003. Comparisons of two moments-based estimators that utilize historical and paleoflood data for the log Pearson type III distribution. *Water Resour. Res.* 39, n/a–n/a. doi:10.1029/2002WR001791
- Faure, G., 1986. *Principles of Isotope Geology*. Wiley.
- Fenske, J., 2003. *Application of paleohydrology to corps flood frequency analysis*. Res. Doc. US Army Corps Eng.
- Greenbaum, N., Harden, T.M., Baker, V.R., Weisheit, J., Cline, M.L., Porat, N., Halevi, R., Dohrenwend, J., 2014. A 2000 year natural record of magnitudes and frequencies for the largest Upper Colorado River floods near Moab, Utah. *Water Resour. Res.* 50, 5249–5269. doi:10.1002/2013WR014835
- Haas, H., Doubrava, M.R., 1998. Chronologies Onto Absolute Time Scales. *Radiocarbon* 40, 561–569.
- Holcomb, J.A., 2014. *Expanding the Chemostratigraphic Framework of the Cooper's Ferry Site (10IH73) Using Portable X-Ray Fluorescence Spectrometry*. Oregon State University.

- Houston, J., 2006. The great Atacama flood of 2001 and its implications for Andean hydrology. *Hydrol. Process.* 20, 591–610. doi:10.1002/hyp.5926
- Houston, J., Hartley, A.J., 2003. The central Andean west-slope rainshadow and its potential contribution to the origin of hyper-aridity in the Atacama Desert. *Int. J. Climatol.* 23, 1453–1464. doi:10.1002/joc.938
- Hunt, A.M.W., Speakman, R.J., 2015. Portable XRF analysis of archaeological sediments and ceramics. *J. Archaeol. Sci.* 53, 626–638. doi:10.1016/j.jas.2014.11.031
- Hussain, Z., 2011. Application of the Regional Flood Frequency Analysis to the Upper and Lower Basins of the Indus River , Pakistan 2797–2822. doi:10.1007/s11269-011-9839-5
- Jones, A.F., Macklin, M.G., Brewer, P. a., 2012. A geochemical record of flooding on the upper River Severn, UK, during the last 3750years. *Geomorphology* 179, 89–105. doi:10.1016/j.geomorph.2012.08.003
- Kachigan, S.K., 1991. *Multivariate Statistical Analysis: A Conceptual Introduction*. Radius Press.
- Kochel, R.C., Baker, V.R., 1982. Paleoflood hydrology. *Science* 215, 353–61. doi:10.1126/science.215.4531.353
- Latorre, C., Betancourt, J.L., Arroyo, M.T.K., 2006. Late Quaternary vegetation and climate history of a perennial river canyon in the Río Salado basin (22°S) of Northern Chile. *Quat. Res.* 65, 450–466. doi:10.1016/j.yqres.2006.02.002
- Liebens, J., 2001. Heavy metal contamination of sediments in stormwater management systems: the effect of land use, particle size, and age. *Environ. Geol.* 41, 341–351. doi:10.1007/s002540100392
- Magilligan, F.J., Goldstein, P.S., Fisher, G.B., Bostick, B.C., Manners, R.B., 2008. Late Quaternary hydroclimatology of a hyper-arid Andean watershed: Climate change, floods, and hydrologic responses to the El Niño-Southern Oscillation in the Atacama Desert. *Geomorphology* 101, 14–32. doi:10.1016/j.geomorph.2008.05.025
- Manners, R.B., Magilligan, F.J., Goldstein, P.S., 2007. Floodplain Development, El Niño, and Cultural Consequences in a Hyperarid Andean Environment. *Ann. Assoc. Am. Geogr.* 97, 229–249. doi:10.1111/j.1467-8306.2007.00533.x
- Martinez, A.M., Kak, A.C., 2001. PCA versus LDA. *IEEE Trans. Pattern Anal. Mach. Intell.* 23, 228–233. doi:10.1109/34.908974
- Miller, J.R., Lechler, P.J., Desilets, M., 1998. The role of geomorphic processes in the transport and fate of mercury in the Carson River basin, west-central Nevada. *Environ. Geol.* 33, 249–262. doi:10.1007/s002540050244
- Miller, J.R., Mackin, G., Orbock Miller, S.M., 2015. *Application of Geochemical Tracers to Fluvial Sediment*, SpringerBriefs in Earth Sciences. Springer International Publishing, Cham. doi:10.1007/978-3-319-13221-1
- Mukundan, R., Radcliff, D.E., Ars, J.C.R.U., Risse, L.M., 2010. Sediment Fingerprinting to Determine the Source of Suspended Sediment in a Southern Piedmont Stream. *J. Environ. Qual.* 39, 1328–1337. doi:10.2134/jeq2009.0405
- National Research Council, 1988. *Estimating Probabilities of Extreme Floods: Methods and Recommended Research*. National Academies Press.
- National Research Council, 1999. *Improving American River Flood Frequency Analyses*. National Academies Press.
- O'Connor, J., Webb, R., 1988. Hydraulic modeling for paleoflood analysis. *Flood*

- Geomorphology, John Wiley & Sons, New York, 383–402.
- Racey, A., Love, M.A., Bobolecki, R.M., Walsh, J.N., 1995. The use of chemical element analyses in the study of biostratigraphically barren sequences: an example from the Triassic of the central North Sea (UKCS). *Geol. Soc. London, Spec. Publ.* 89, 69–105. doi:10.1144/GSL.SP.1995.089.01.06
- Ramkumar, M., Berner, Z., Stüben, D., 2010. Hierarchical delineation and multivariate statistical discrimination of chemozones of the Cauvery Basin, south India: Implications on spatio-temporal scales of stratigraphic correlation. *Pet. Sci.* 7, 435–447. doi:10.1007/s12182-010-0091-z
- Ratcliffe, K.T., Wilson, A., Flint, S.S., Payenberg, T., Rittersbacher, A., Hildred, G. V., 2014. PROCEEDINGS, INDONESIAN PETROLEUM ASSOCIATION Thirty-Eighth Annual Convention & Exhibition, May 2014 GROUND TRUTHING CHEMOSTRATIGRAPHIC CORRELATIONS IN FLUVIAL SYSTEMS.
- Rech, J. a., Currie, B.S., Michalski, G., Cowan, A.M., 2006. Neogene climate change and uplift in the Atacama Desert, Chile. *Geology* 34, 761–764. doi:10.1130/G22444.1
- Taylor, M.P., Hudson-Edwards, K. a, 2008. The dispersal and storage of sediment-associated metals in an arid river system: the Leichhardt River, Mount Isa, Queensland, Australia. *Environ. Pollut.* 152, 193–204. doi:10.1016/j.envpol.2007.05.011
- Thorndycraft, V.R., Benito, G., Rico, M., Sopeña, A., Sánchez-Moya, Y., Casas, A., 2005. A long-term flood discharge record derived from slackwater flood deposits of the Llobregat River, NE Spain. *J. Hydrol.* 313, 16–31. doi:10.1016/j.jhydrol.2005.02.003
- Tinkler, K.J., Wohl, E., 1998. *Rivers Over Rock: Fluvial Processes in Bedrock Channels.* American Geophysical Union.
- U.S. Water Resources Council, 1982. *Guidelines for Determining Flood Flow Frequency.* Bull. 17B Reston, Virginia, Hydrol. Subcomm. Off. Water Data Coord. U.S. Geol. Surv. 182.
- Webb, R., Jarrett, R., 2002. *One-Dimensional Estimation Techniques for Discharges of Paleofloods and Historical Floods.* Anc. Floods, Mod. Hazards.
- Webb, R., O'Connor, J., Baker, V., 1988. Paleohydrologic reconstruction of flood frequency on the Escalante River, South-Central Utah. *Flood Geomorphol.* John Wiley Sons New
- WHO, 2011. *Guidelines for Drinking-Water Quality, fourth edition,*. doi:10.1016/S1462-0758(00)00006-6
- Wilson, L.R., 2011. Determination of trace element provenance, Rio Loa basin, northern Chile. Master's Thesis.
- Wohl, E.E., 1998. Uncertainty in flood estimates associated with roughness coefficient. *J. Hydraul. Eng.* 124, 219–223.

APPENDICES

Appendix A: ICP-OES readings

Table A1. Elemental concentrations for samples as determined by ICP-OES (ppm)

Sample ID	As	Cd	Co	Cr	Cu	Ni	Pb	Sr	Zn
PD1-1	107.4	2.8	15.2	28.4	129.4	14.0	17.2	410.2	138.8
PD1-2	111.6	3.8	17.0	24.2	119.8	13.8	15.6	384.4	173.0
PD1-3	202.6	6.8	20.0	26.2	135.0	15.6	18.6	513.4	204.4
PD1-4	280.4	9.4	18.2	27.2	491.2	14.8	20.8	1001. 2	246.6
PD1-5	498.2	24.6	32.4	25.6	221.4	22.8	18.6	958.4	436.4
PD1-6	237.6	9.2	12.6	18.6	160.2	10.6	9.2	1499. 0	151.0
PD1-7	260.2	10.4	21.4	33.6	111.0	20.2	20.6	477.8	283.0
PD1-8	171.8	7.4	19.4	29.0	62.0	16.4	16.6	411.2	255.0
PD1-9	124.8	3.6	17.4	40.2	50.8	16.4	18.8	441.2	172.6
PD1-10	241.6	13.0	23.4	32.6	62.2	22.0	20.2	435.0	327.0
PD1-11	164.8	9.2	20.0	39.0	58.8	18.8	19.8	428.6	296.2
PD1-12	98.0	3.4	15.0	43.0	35.4	15.6	20.6	404.0	131.0
PD1-13	102.2	2.8	15.8	31.2	41.0	14.8	17.0	402.0	148.8
PD1-14	121.6	6.0	14.6	31.0	35.6	13.4	17.4	350.0	188.4
PD1-15	175.4	7.6	19.4	32.0	54.4	16.6	17.4	413.6	266.0
PD1-16	160.4	7.0	19.6	31.2	50.4	17.2	18.8	416.2	281.0
PD1-17	267.2	15.6	22.8	30.8	58.8	19.2	18.4	403.6	395.0
PD1-18	260.6	14.0	20.2	27.0	62.2	38.0	16.6	371.4	320.8
PD1-19	460.0	33.8	28.6	37.2	70.6	26.8	16.6	407.4	614.2
PD1-20	238.0	17.2	22.4	44.8	373.0	41.0	35.0	407.4	226.4
PD1-21	165.4	9.4	18.2	37.2	88.4	18.6	22.0	400.4	208.4
PD1-22	128.6	7.4	15.8	35.6	96.0	17.4	21.2	343.4	178.2
PD1-23	138.4	7.2	15.6	56.2	72.8	36.0	17.0	330.6	200.6
PD1-24	143.6	7.6	16.0	39.2	57.8	16.8	18.0	371.2	199.8

Table A1. Elemental concentrations for samples as determined by ICP-OES (ppm)

Sample ID	As	Cd	Co	Cr	Cu	Ni	Pb	Sr	Zn
PD1-25	132.0	5.8	16.6	48.4	51.8	17.0	19.8	414.2	206.2
PD1-26	146.4	5.6	17.4	46.2	42.4	15.6	18.2	388.8	211.6
PD1-27	215.2	10.2	17.8	37.2	49.6	15.8	16.8	382.0	238.2
PD1-28	220.0	12.0	22.2	22.4	74.6	14.6	12.0	812.0	519.4
PD1-29	138.0	7.4	15.0	26.8	75.0	13.4	18.2	333.2	190.0
PD1-30	136.2	6.6	16.8	35.2	87.2	15.0	21.0	379.4	210.6
PD1-31	131.0	6.0	15.2	32.6	80.0	14.0	20.0	366.8	200.8
PD1-32	88.4	3.2	13.4	34.2	52.8	13.2	18.6	339.0	142.2
PD1-33	74.2	2.6	15.4	51.4	46.4	16.6	17.6	425.2	152.2
PD1-34	182.6	9.0	15.0	31.2	94.6	28.0	16.0	386.4	237.4
PD1-35	122.4	5.6	15.0	33.8	101.8	14.6	17.8	374.6	202.6
PD1-36	170.8	10.8	19.6	55.0	42.0	23.2	26.4	396.0	202.8
PD1-37	118.2	5.6	21.0	67.6	47.2	21.0	22.6	523.0	268.0
PD1-38	409.2	20.6	28.0	50.8	95.6	34.6	19.2	436.2	503.0
PD1-39	116.6	3.8	17.4	42.6	114.8	16.2	21.6	447.6	186.4
PD1-40	121.0	4.2	13.4	29.0	131.4	13.0	17.0	324.2	162.8
PD1-41	112.0	4.4	14.2	30.0	47.0	12.6	15.8	317.6	153.4
PD2-1	107.4	2.8	15.2	28.4	129.4	14.0	17.2	410.2	138.8
PD2-2	111.6	3.8	17.0	24.2	119.8	13.8	15.6	384.4	173.0
PD2-3	202.6	6.8	20.0	26.2	135.0	15.6	18.6	513.4	204.4
PD2-4	280.4	9.4	18.2	27.2	491.2	14.8	20.8	1001.2	246.6
PD2-5	498.2	24.6	32.4	25.6	221.4	22.8	18.6	958.4	436.4
PD2-6	237.6	9.2	12.6	18.6	160.2	10.6	9.2	1499.0	151.0
PD2-7	260.2	10.4	21.4	33.6	111.0	20.2	20.6	477.8	283.0
PD2-8	171.8	7.4	19.4	29.0	62.0	16.4	16.6	411.2	255.0
PD2-9	124.8	3.6	17.4	40.2	50.8	16.4	18.8	441.2	172.6
PD2-10	241.6	13.0	23.4	32.6	62.2	22.0	20.2	435.0	327.0

Table A1. Elemental concentrations for samples as determined by ICP-OES (ppm)

Sample ID	As	Cd	Co	Cr	Cu	Ni	Pb	Sr	Zn
PD2-11	164.8	9.2	20.0	39.0	58.8	18.8	19.8	428.6	296.2
PD2-12	98.0	3.4	15.0	43.0	35.4	15.6	20.6	404.0	131.0
PD2-13	102.2	2.8	15.8	31.2	41.0	14.8	17.0	402.0	148.8
PD2-14	121.6	6.0	14.6	31.0	35.6	13.4	17.4	350.0	188.4
PD2-15	175.4	7.6	19.4	32.0	54.4	16.6	17.4	413.6	266.0
PD2-16	160.4	7.0	19.6	31.2	50.4	17.2	18.8	416.2	281.0
PD2-17	267.2	15.6	22.8	30.8	58.8	19.2	18.4	403.6	395.0
PD2-18	260.6	14.0	20.2	27.0	62.2	38.0	16.6	371.4	320.8
PD2-19	460.0	33.8	28.6	37.2	70.6	26.8	16.6	407.4	614.2
RS1-1	319.8	14.0	20.0	28.2	44.6	14.0	14.4	337.6	257.0
RS1-2	165.0	6.6	18.2	36.8	38.2	14.4	14.4	358.6	199.8
RS1-3	265.8	11.8	19.4	31.0	40.8	14.0	13.8	335.2	235.0
RS1-4	323.0	15.0	20.4	34.0	50.0	16.0	16.2	364.6	273.4
RS1-5	418.0	21.4	22.8	33.0	60.8	17.4	17.6	394.2	329.6
RS1-6	371.2	22.6	26.4	30.6	104.8	23.4	23.6	445.2	504.4
RS1-7	290.2	15.0	19.6	27.2	48.4	16.4	15.2	342.0	313.6
RS1-8	288.6	15.2	19.2	25.6	48.8	15.6	15.8	334.4	309.8
RS1-9	152.6	6.2	16.4	32.4	41.6	14.2	16.8	349.8	201.8
RS1-10	301.0	13.0	19.6	33.8	88.2	17.6	19.6	392.8	285.0
RS1-11	474.4	20.4	21.8	30.8	76.4	17.6	18.0	409.4	355.0
RS1-12	214.6	10.4	17.2	33.0	41.2	15.0	17.8	330.6	224.0
RS1-13	381.6	19.0	22.2	30.4	56.6	17.0	18.4	361.8	313.8
RS1-14	174.0	7.2	17.0	35.0	39.2	15.6	16.4	355.4	213.6
RS1-15	177.0	11.2	21.2	39.4	68.6	19.2	19.4	417.4	305.8
RS2-1	141.8	6.4	18.8	47	45.4	17.4	17.4	422.8	258.8
RS2-2	441	22.2	20.6	31.2	86	18.2	18.8	409.8	460
RS2-3	291.4	15.4	21	38.2	68	18.2	18.4	422	402.2
RS2-4	363.8	19	20.6	34.4	71.4	18.2	18	421.8	416.8

Table A1. Elemental concentrations for samples as determined by ICP-OES (ppm)

Sample ID	As	Cd	Co	Cr	Cu	Ni	Pb	Sr	Zn
RS2-5	355.6	17.4	19.4	31	72.6	17.4	19.2	424	387
RS2-6	318.4	17.4	24.8	32.8	90.4	20.4	20.4	407.2	439.8
RS2-7	325.4	17.4	21.8	36.6	68.2	18	16.2	397.8	419.8
RS2-8	305	14.4	19	28.4	60.4	17.4	16.8	342.6	254.2
RS2-9	200.8	8.4	17.6	31.8	56	15.6	15.6	366.2	233
RS2-10	196.6	8	16.8	32.2	55.4	15.4	14.8	364	219.8
RS2-11	279.8	10.4	16.4	28.8	47.2	14.6	14.6	327.4	205.6
RS2-12	174.6	6.8	14.8	34.2	59.4	14.8	18.8	392.2	179.4
RS2-13	489	23	24.8	28.2	104.4	19.8	19.2	391.4	441.6
RS2-14	259.8	11	17.4	28.6	74.6	15.6	17.2	373.2	205.4
RS2-15	540	26.6	24.2	30.4	99.6	18.8	19.6	397.8	500.4

Appendix B: Radiocarbon dating results

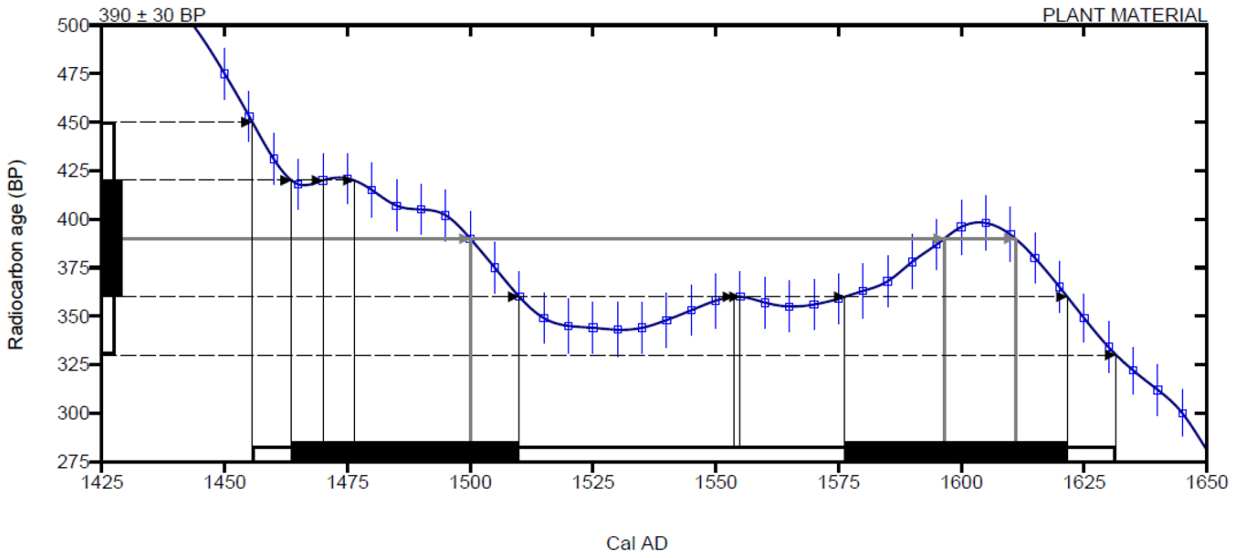


Figure B1. Interception of radiocarbon age with calibration curve for RS1-C14-3 which corresponds to flood deposit RS1-FD9.

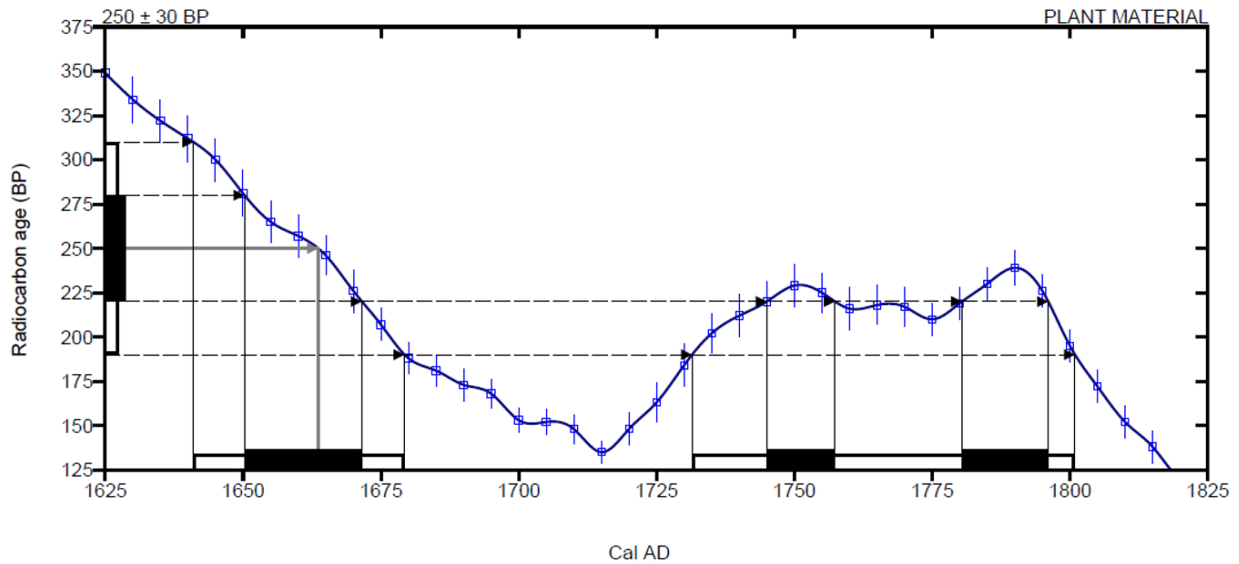


Figure B2. Interception of radiocarbon age with calibration curve for RS2-C14-2 which corresponds to flood deposit RS2-FD8

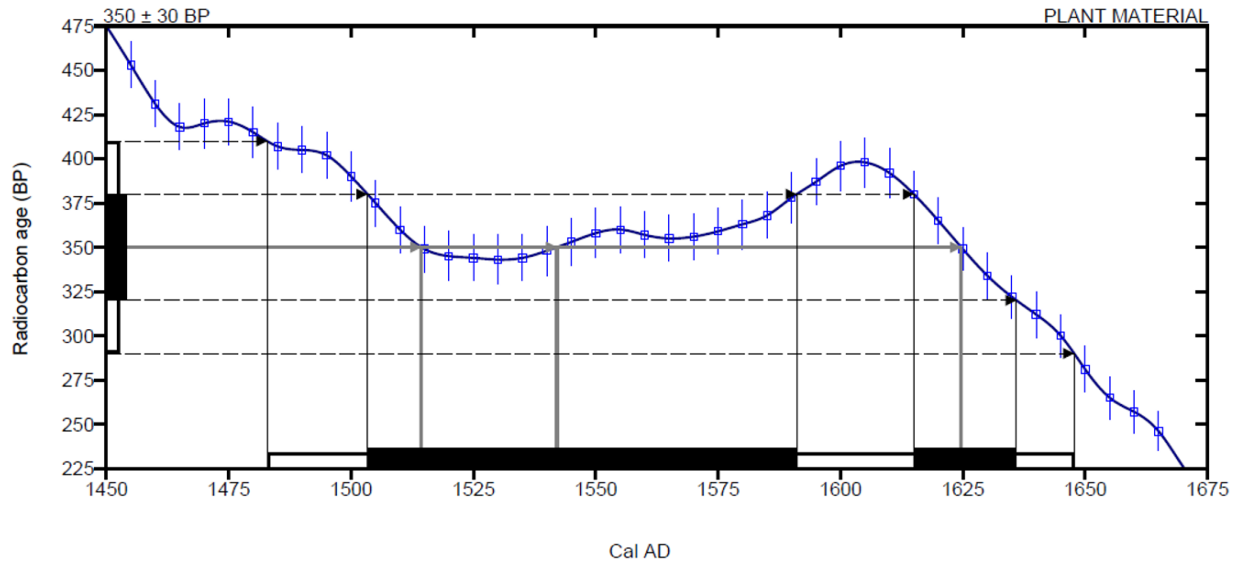


Figure 2. Interception of radiocarbon age with calibration curve for RS2-C14-3 which corresponds to flood deposit RS2-FD8